In vitro characterization of cyanoacrylate embolic glues used for vascular embolization

Yongjiang Li

Par **Yongjiang LI**

In vitro characterization of cyanoacrylate embolic glues used for *vascular embolization*

Thèse présentée
pour l'obtention du grade
de Docteur de l'UTC

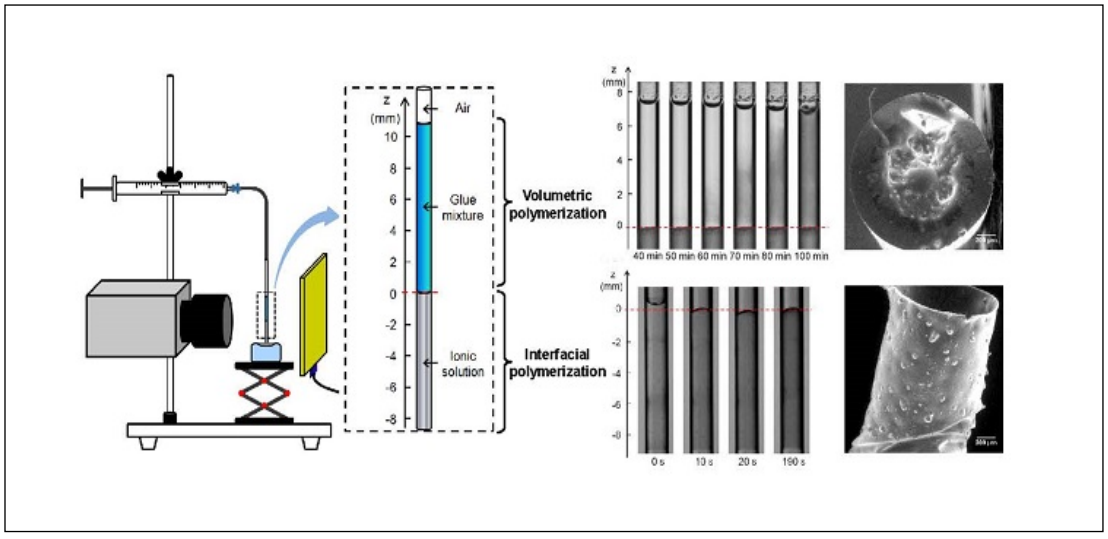

Soutenue le 18 avril 2017
Spécialité : Biomechanics and Bioengineering : Unité de Recherche Biomécanique et Bio-ingénierie (UMR-7338)

D2351

In vitro characterization of cyanoacrylate embolic glues used for vascular embolization

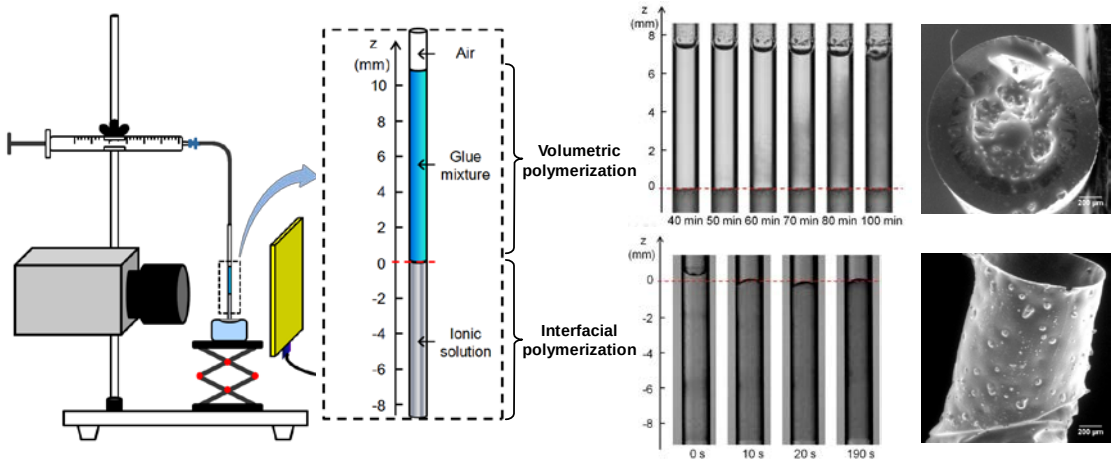

Yongjiang LI

Biomechanics and Bioengineering Laboratory (UMR CNRS 7338)
Université de Technologie de Compiègne, Sorbonne Universités

Supervisors :

- **Anne-Virginie Salsac, Université de Technologie de Compiègne**
- **Dominique Barthès-Biesel, Université de Technologie de Compiègne**

This dissertation is submitted for the degree of
Doctor of Biomechanics and Bioengineering

18 April 2017

Acknowledgements

This thesis represents not only my work during the past three years and a half, it is the results of work by many people who I wish to thank. This thesis is also the result of many experiences I have encountered at Université de technologie de Compiègne (UTC) from dozens of remarkable individuals who I also wish to acknowledge.

First and foremost I wish to express my sincere gratitude to my supervisors: **Anne-Virginie Salsac** and **Dominique Barthès-Biesel**, for their patience, motivation, enthusiasm, and immense knowledge. During the past three years and a half, they helped me come up with the thesis topic and encouraged me in all the time of research. They supported me both academically and emotionally through the rough road to finish this thesis. Thanks to them I had the great honor to be one of their PhD students.

I would like to thank the rest of my thesis committee: **Christine Vauthier, Alba Marcellan, Emmanuel Houdart, Carlo Gonzato** and **Myriam Bernaudin**, for their warm encouragement, insightful comments, and profound questions. I am particularly grateful for the assistance given by **Luminita Duma, Elise Prost** and **Carlo Gonzato** for their sincere suggestions and guidance. I would like to offer my special thanks to **Océane Lançon** and **Mihai-Cristinel Sandulache** for their previous works which have laid foundation of my thesis. I also thank **Audrey Fohlen** and **Thomas Delpech** for their contribution to the characterization of the polymerization kinetics, and **Frédéric Nadaud** for the SEM pictures. In addition, I would like to thank the companies: **GEM S.r.l**, **Aspide** and **Guerbet** for having provided Glubran 2 and Lipiodol samples. I would also like to express my gratitude to the Chinese Scholarship Council (CSC) for their financial support.

I thank my colleagues in the Biomechanics and Bioengineering Laboratory (BMBI, UMR CNRS 7338): Anne Le-Goff, Angxiao Fan, Badr Kaoui, Barbara Dupont, Benjamin Sévénié, Bruno Sarkis, Bruno Ramaël, Carlos Quesada-Granja, Claire Dupont, Doriane Vesperini, Elodie Colaco, Giorgio Davico, Ilyesse Bihi, Isabelle Claude, Neeraj Maheshwari, Quan Yuan, Risa-Nurin Baiti, Sagnik Datta and Vittoria Pandolfi. Also I thank my friends at UTC: Caiyun Liu, Chen Zheng, Chunfeng Lian, Dingfu Zhou, Hongjuan Bai, Hongliang Liu, Huiling Lu, Mingming Yang, Jingjing Xu, Kang Yang, Nan Li, Shanggui Cai, Wenxiang

Zhang, Xuhong Li and Yunchao Peng. In particular, I am grateful to Lei Lei, Liang Meng and Changjie Yin for accompanying me when I wrote my thesis.

Last but not the least, I would like to thank my family: my parents and my sister, for supporting me spiritually throughout my life.

Abstract

Vascular embolization is a minimally invasive treatment used to selectively eliminate or stop the vascular supply to specific body areas. One technique consists of navigating a microcatheter into the targeted blood vessel and injecting an embolic agent which reacts in contact with blood. Cyanoacrylate-based embolic glues are the main liquid adhesives used for vascular embolization owing to their low viscosity, good penetration ability and low tissue toxicity. To enable its detection once injected, the glue is mixed with a radio-opaque contrast agent such as the Lipiodol® iodized oil. Although the technique is commonly used, there is very little information on the dynamics of the injection process in complex blood flows or on the polymerization kinetics of the glue-Lipiodol mixture. Consequently, safe occlusion is difficult to achieve, even in the hands of experienced radiologists.

The main objective of the thesis is to quantitatively investigate the physical properties and polymerization kinetics of cyanoacrylate glues mixed with Lipiodol in different proportions. We have designed a new experimental setup to characterize the polymerization process of a glue/Lipiodol mixture on contact with an ionic or proteinaceous solution. We find that there is a fast polymerization process at the interface between the glue and the substrate, followed by the propagation of a polymerization front in the glue mixture volume. The time constants of the processes depend on the solution and glue mixture compositions. Another objective is to analyze the dynamic embolization process. An *in vitro* model of the injection process is used to first investigate the drop formation between two non-reacting immiscible flows. The injection of a glue mixture into a flowing ionic solution is then performed to show the joint influence of polymerization and hydrodynamics.

It is the first time that such comprehensive characterization of cyanoacrylate-based embolic glues is acquired. The results can provide crucial information to interventional radiologists, that will help them understand and control the glue behavior after injection to achieve a safe and permanent obliteration of the vessels.

Table of contents

List of figures

List of tables

Chapter 1

Introduction

1.1 Vascular embolization

1.1.1 Definition and history

Interventional radiology, which emerged in the 1960s, developed from diagnostic angiography and from the innovative minds and technical skills of many angiographers. Its conceiver Charles Dotter who first put forward the concept of Interventional radiology: "The angiographic catheter can be more than a tool for passive means for diagnostic observation; used with imagination, it can become an important surgical instrument." Since then interventional radiology has become a valuable alternative to surgical management (Rösch et al., 2003).

The pioneers of interventional radiology may date back to the early 20th century. Dawbarn [22] was the first to report on embolization of head and neck cancers in 1904. The first embolization of carotid-cavernous fistula was performed in the 1930s using muscle fat or fascia as embolic agents [10]. In the 1960s, the first embolization of arteriovenous malformation (AVM) was reported by Luessenhop and Spence [60] who introduced silastic beads through a surgically exposed common carotid artery. In 1968, Doppman [27] first used autologous clots as an embolic agent to occlude a spinal arteriovenous malformation. This technique was quickly adopted for use in gastrointestinal bleeding [78] and hemorrhage from pelvic fractures [61]. In the 1970s, a series of embolic agents (e.g. coils, Gelfoam, isobutyl-2-cyanoacrylate, polyvinyl alcohol, n-butyl cyanoacrylate(nBCA) ...) were innovated and introduced to the field of interventional radiology. Interestingly, some of these materials, or their derivatives, continue to be employed today. Besides embolic agents, many embolization techniques have been developed thanks to the contribution of schools and institutions of interventional neuroradiology (INR). The French and American schools, both leading the INR in the 1970s, highlighted the need for selectivity and superselectivity in endovascular

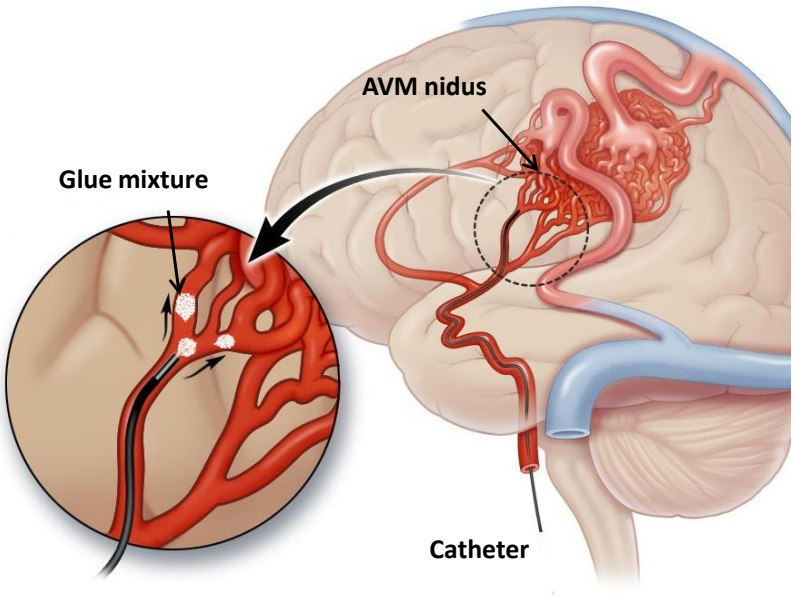

Fig. 1.1 Schematic of embolization of brain arteriovenous malformations. (from *www.taafonline.org/am_treatment.html*)

procedures. Djindjian et al. [25] in France and Kricheff et al. [50] in the USA demonstrated a novel approach using the transfemoral route for catheter embolization in the 1970s, which replaced the carotid artery direct puncture as a common approach. Berenstein introduced the first use of flow-controlled embolization with a detachable balloon. Flow control was achieved by manipulation of the balloon in a proximal artery, permitting the distribution of embolic agents to desired sites in distal arteries. These techniques are still employed in current vascular embolization procedures. In the wake of developments in catheterization, medical imaging and interventional techniques, vascular embolization has been considerably improved to be a more accurate and less invasive treatment. It has become one of the mainstays of interventional radiology.

Vascular embolization (VE) is a minimally invasive surgical procedure used to selectively reduce or stop the blood supply to specific parts of the body. It is carried out under medical imaging guidance by navigating a guidewire and a micro-catheter into the targeted blood vessels, through which embolic agents are delivered into the circulation (Figure 1.1). This technique has been widely used for various surgical purposes: to occlude vessels or vascular abnormalities (either arterial or venous); to arrest or prevent hemorrhages; to devitalize a structure such as a tumor; to reduce blood flow to an arteriovenous malformation; to remodel a vascular wall or to redirect the blood flow [15].

VE can be performed either as a definitive treatment or as an adjunctive therapy to subsequent surgical management (microsurgical resection or radiotherapy) [5]. In some cases, it is an emergency means of controlling bleeding. Vascular embolization is usually conducted prior to surgical resection, which helps to reduce the size of lesions by reducing the blood flow, and/or closing deep feeding blood vessels that may be difficult to gain access to during surgery. Vascular embolization allows not only vessel occlusion but also in situ administration of various therapeutic agents, particularly drugs. In addition, it is no longer restricted to symptomatic indications (e.g., hemostasis embolization) but more and more as a curative technique for instance for the definitive treatment of aneurysms, arteriovenous malformations (AVMs) and arteriovenous fistulas (AVFs) [13, 68].

The indications of vascular embolization are constantly broadening. The most remote anatomical areas are today within reach and a wider number of clinical conditions are nowadays treated. Medical conditions treated with vascular embolization can be grouped as follows: 1. vascular anomalies, such as occlusion of AVM, AVF, venous malformation, lymphatic malformation and hemangioma; 2. hemorrhage, such as upon trauma, pseudo-aneurysms rupture, epistaxis, hemoptysis and bleeding of gastrointestinal (GI) tract; 3. other conditions, including tumors, varicoceles, redistribution of blood flow and organ ablation [15]. New applications regularly appear in medical practice along with recent developments in embolic agents and catheterization techniques.

1.1.2 Embolic materials

During the last 30 years, there have been phenomenal advances in the development and availability of embolic materials. Interventional radiologists now have a large array of embolic materials suited for the treatment of aneurysms, AVMs and AVFs, tumors and trauma [24]. To achieve a safe and effective vascular embolization, interventional radiologists should be familiar with the physical properties and specific delivery considerations of the various embolic agents.

Classification of embolic agents

Different kinds of embolic agents are used in clinical applications, such as coils, detachable balloons, polyvinyl alcohal (PVA), microspheres, gelatin sponges, gelatin particles, cyanoacrylate glues and ethanol. These agents can be classified on the basis of their physical state (solid or liquid), mechanism of action (mechanical or chemical), durability of occlusion (temporary or permanent) and origin (natural or synthetic). In clinical practice, a more useful way of classification is according to the duration of occlusion. Table 1.1 lists some widely

Duration of occlusion	Embolic agents		
Temporary	Gelatin sponge, oxidized cellulose, microfibrillar collegen		
Permanent	Solid agents	Mechanical devices	Coils, detachable Balloons
		Particulate agents	PVA, TAGMs, microsphere
	Liquid agents	Adhesives	nBCA glue
		Non-adhesive agents	Onyx
		Sclerosing agents	Ethanol

Table 1.1 Classification of widely used embolic agents. TAGMs: tris-acryl gelatin microspheres.

used embolic agents in clinical practice, with a classification based on both the duration of occlusion and the physical state. While both solid and liquid agents have specific utilities, no single embolic agent is suitable for all indications. For each case, one must choose the one that is the most appropriate for the patient at stake among all available agents. The choice of embolic agents depends on the size of the vessel to be occluded, the blood flow velocity through the vessel, the characteristics of the obstruction (e.g. distal or proximal) and the duration of occlusion desired (temporary or permanent). Embilization of large vessels usually requires mechanical devices such as coils or detachable balloons [15, 58], but they are generally no used for the embolization of complex AVMs. Particulate or liquid agents are typically used for small vessels [59]. Coils, balloons, Gelfoam and other mechanical devices lead to a mechanical obliteration of the vessel associated with flow deceleration and subsequent thrombosis. They have little or no use in the management of lesions [80]. Particles and microspheres (50–2000 μm) could theoretically penetrate and occlude the nidus of AVMs if perfectly sized, but in reality this is rarely achieved. Determination of the appropriate particle size is problematic, too small particles can lead to the risk of paradoxic embolization to the lungs [77]. Particles are mostly used for the preoperative embolization of highly vascularized tumors to diminish the perioperative bleeding risk and induce tumor necrosis. They are also used to induce thrombosis in a vessel secondary to partial success of an earlier endovascular embolization procedure. Compared to solid embolic agents, liquid embolic agents have good penetration ability, which allows a vascular area to be homogeneously filled. This means that a recanalization of the embolized area will barely take place [7]. This is the reason why liquid embolic agents are preferred clinically and thus appropriate for the treatment of complex vascular anomalies such as AVMs.

Liquid embolic agents

Liquid embolic agents can be classified into two categories: sclerosing agents and occlusive casting agents. Absolute alcohol (Ethanol) is the most commonly used sclerosing agent for permanent occlusion. Embolization with absolute alcohol has a direct toxic effect on the endothelium that activates the coagulation system and causes the aggregation of red blood cells, which results in the occlusion of vessels. The injection of this agent should therefore be carefully controlled to avoid serious complications. Balloon occlusion catheters are often used in the embolization with absolute alcohol. The balloon is inflated upstream of the injection site to temporarily stop the blood flow. This process reduces the convection of absolute alcohol, which promotes a local toxic effect on the endothelium and protects non-targeted healthy tissues. Low viscosity of ethanol allows its injection via small catheters. Additionally, it can be mixed with a contrast medium (e.g. an iodized oil). These two advantages ensure a highly selective embolization performed under fluoroscopic guidance. However, absolute alcohol carries significant risks. It damages capillary beds of healthy tissue (e.g., skin) and is usually associated with significant soft tissue swelling, permanent nerve injury and pain upon injection [80, 66]. The amount of ethanol injected during a single embolization session is limited to reduce its toxic effects. Most other commonly used sclerosants are alcohol derivatives, such as sodium tetradecyl sulfate (Sotradecol) and ethanolamine oleate. These agents are both less painful and less toxic than absolute alcohol. As a result, some lesions can be treated without general anesthesia.

The occlusive casting agents mainly include two types: adhesive and non-adhesive. Onyx® (non-adhesive) and cyanoacrylate-based glues (adhesive) are two typical occlusive casting agents used for vascular embolization. They are preferred clinically because of their low recanalization rates and are thus appropriate for permanent vessel occlusion (e.g., as in treatment of AVMs). Onyx® (ev3, Irvine, USA) is a nonadhesive, liquid, opaque embolic agent used for the embolization of vasular malformations. It gained Food and Drug Administration (FDA) approval in 2005. Onyx® is comprised of ethylene-vinyl alcohol copolymer (EVOH) dissolved in dimethyl sulfoxide (DMSO) at various concentrations, which are marketed as Onyx 18 (6% EVOH and 94% DMSO), Onyx 20 (6.5% EVOH and 93.5% DMSO) and Onyx 34 (8% EVOH and 92% DMSO). Tantalum powder is added for opacity. When it comes into contact with an aqueous solution, like blood, its solvent DMSO rapidly dissolves into the solution, causing its main component EVOH to precipitate and form a flexible permanent spongy polymer cast. The precipitation progress starts from the outer surface inward, forming a skin with a liquid center that continues to flow (like lava) as the solidification continues [66]. Onyx® is thought to be a more manageable agent than nBCA as it solidifies slowly from outside to inside while the DMSO solvent diffuses, reducing the

Name	Manufacturer	Component	Sold as	Poly. rate	Cost/vial (€)	Available area
Histoacryl	B.Braun	nBCA	0.5-ml/vial	Faster	25	—
TruFill	Cordis	nBCA	1.0 g/vial	Faster	—	US
Glubran 2	GEM	nBCA+MS	1.0-ml/vial	Slow	150	Europe
Purefill	Fimed	nHCA	1.0-ml/vial	Slow	—	Europe
Fuaile	Fuaile	nBCA+nOCA	1.0-ml/vial	Slower	60	China

Table 1.2 Commercially available cyanoacrylate-based embolic glues.

risk of microcatheter entrapment. In the case of AVM treatments, prolonged and repeated Onyx® injections within a same pedicle are possible and allow Onyx® to be pushed more distally toward and within the nidus. As Onyx® is not absorbable, it is capable of producing permanent vascular occlusion although recanalization is possible [7]. The disadvantages of Onyx® include its solvent DMSO, which can potentially be angiotoxic with rapid injections. DMSO volume and injection time need to be monitored closely to achieve safe embolization. The safe injection rate is less than 0.25 ml/90 s [66].The need for slow injection results in a longer procedure with relatively increased radiation exposure for both the patient and surgeon. In addition, only catheters that are DMSO-compatible can be used with Onyx® [41].

Cyanoacrylate (CA) monomers, generally known as super glues or instant adhesives, were first synthesized in 1942 by Harry Coover. They were used as incisional wound closures or emergency sealants for hemorrhage during the Vietnam War. Since then CA has evoked considerable medical interests. Various properties of CA monomers have been explored and improved for biomedical purposes such as tissue adhesives, hemostatic and embolic agents. The principal features of CA glues are their low viscosity, rapid polymerization rate and good penetration ability. These characteristics are particularly useful in the embolization of vascular abnormalities, especially for large, high-flow lesions such as AVMs. Initially, only isobutyl 2-cyanoacrylate (IBCA) was used extensively for the endovascular therapy of AVMs. Since 1980s, n-butyl cyanoacrylate (nBCA) replaced IBCA as a substitute in interventional neuroradiology [11]. Several commercially available CA glues currently exist: n-butyl cyanoacrylate (Histoacryl®, TruFill® and Glubran®2), n-octyl cyanoacrylate (Dermabond® and Fuaile®) and n-hexyl cyanoacrylate (Purefill®).

Table 1.2 lists the commonly used commercially available cyanoacrylate-based glues. Histoacryl® and Histoacryl Blue® (B.Braun, Melsungen, Germany) are sterile liquid topical skin adhesives composed of nBCA monomer (Figure 1.2a). The two products are different in only one respect: Histoacryl® is a colorless liquid, and Histoacryl Blue® is colored with

the dye D&C Violet #2 with intent to ease visualization of the device during application. Histoacryl® and Histoacryl Blue® have been the only available glues for external use in Europe for many years, but they are still not approved for intravascular use by the European Community (EC). Nevertheless, they have been used for embolization of cerebral vascular diseases for more than 20 year on patients [33, 46, 40]. In recent years, the fact that Histoacryl has no official recognition attracts attention and its intravascular use is thus prohibited. TruFill (Cordis, Miami Lakes, USA) is a similar agent to Histoacryl approved for cerebral AVM embolization by FDA in 2000. It is supplied as one or two 1-g tubes of nBCA, 10 ml of ethiodized oil and 1 g of tantalum powder, which are mixed together just before use [100]. New generation of embolic glues have been developed in the past decade, typically Glubran®2. Glubran®2 (GEM, Viareggio, Italy) is a class III medical-surgical glue authorized for surgical use and for endovascular use in neuroradiology [52, 53], which fulfills the requirements of the European Directive on Medical Devices 93/42/EEC. Glubran®2 is not same as other CA glues (e.g. Histoacryl® or TruFill®) which are simple monomers. The composition of Glubran®2 is a mixture of two monomers: nBCA and metacryloxysulpholane (MS). nBCA is a cyanoacrylate monomer common to Histoacryl® (Figure 1.2a). MS is a monomer produced by the manufacturer (Figure 1.2b). The addition of MS allows to lower the polymerization temperature to about 45 °C and to prolong the polymerization time. MS reduces the inflammatory effect of Glubran®2. Glubran®2 does not produce bubbles and seems to diffuse more homogeneously and in a more predictable way than Histoacryl® [52]. According to these characteristics, Glubran®2 has received CE certification for internal and endovascular use. In addition to Glubran®2, Purefill® (FIMED, Quincié-en-Beaujolais, France) is another new liquid embolic agent with the CE trademark, which is described as an arterial and venous embolization product due to its haemostatic action. Purefill® is a sterile,translucent, liquid embolic agent comprised of n-hexyl cyanoacrylate (nHCA) monomers. It is also a class III implantable medical device, which is applicable in the field of neuroradiology and interventional radiology. Additionally, newly developed embolic agents continue to appear in the worldwide market. Fuaile (Fuaile, Beijing, China), for instance, is the third generation of medical adhesive composed of 2-octyl cyanoacrylate (OCA) and nBCA. It has been used in the vascular embolization owing to its good diffusion properties, low polymerization heat and desirable polymer toughness [42].

Cyanoacrylate glues undergoes rapid exothermic polymerization catalyzed by nucleophiles found in blood or on the vascular endothelium. Modification of the polymerization process is required to allow safe injection through a microcatheter. The fact that cyanoacrylate-based embolic glues lack radiopacity obliges to mix them with a radio-opaque contrast agent. To enable its follow-up after injection in the vessels, cyanoacrylate glues are usually mixed

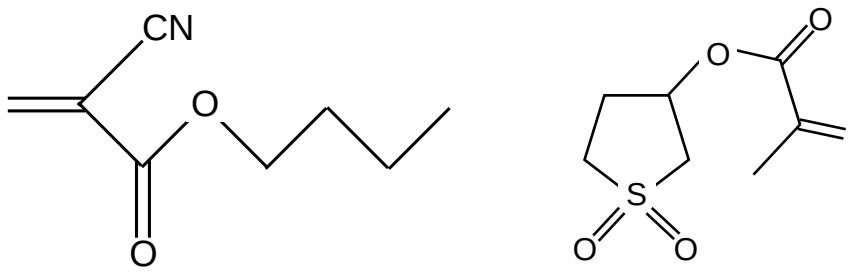

(a) (b)

Fig. 1.2 Chemical structure of (a) n-butyl cyanoacrylate (nBCA) and (b) metacryloxysulpholane (MS).

with an iodized poppy seed oil marketed as Lipiodol (Laboratoire Guerbet, Aulnay-sous-Bois, France). Lipiodol is an iodized oily contrast medium that is usually used to outline structures during radiological investigations. Lipiodol consists of a mixture of long-chain (C16 and C18) di-iodinated ethyl esters of fatty acids from poppy seed (Papaver somniferum var. nigrum) oil, which contains 98% unsaturated fatty acids. The predominant fatty acid is linoleic acid (70%). Lipiodol is a pale yellow to amber, clear liquid, containing 37% (w/w) iodine (i.e. an iodine concentration of 480 mg/mL) [39]. Lipiodol was called Ethiodol® in the USA until 2012. Mixing cyanoacrylate glues with Lipiodol slows the rate of solidification, thereby facilitating endoscopic administration via needle injection and reducing the risk of inadvertent adherence to catheters and endoscopes. The volume ratio of CA glue to Lipiodol is usually varied between 1:1 and 1:5 depending on the vessel diameter, desired penetration distance and blood velocity. Lipiodol is used not only for its radio-opacity property, but also for its drug delivery and tumour-seeking properties and its ability to induce plastic (adapted to the size of vessels) and transient embolization of the microcirculation [39].

Onyx® and nBCA glues are permanent embolic agents preferred clinically in the treatment of vascular malformations. Both agents have their own advantages and disadvantages. nBCA glues may be preferred to Onyx® in some fistulous AV shunts, perforating arteries, leptomeningeal collaterals, en passant feeders, and when the catheter position is away from the nidus. Reflux may be less likely with nBCA glues than Onyx® [66]. Mean fluoroscopy time and procedure time are higher for Onyx® embolizations compared with nBCA embolizations [102]. But nBCA glue is generally considered less predictable than Onyx®, even in experienced hands. Compared to nBCA glues, the use of Onyx® leads to less inflammation and an easier surgical manipulation, but the toxic effects of DMSO results in vasospasm, angionecrosis, arterial thrombosis and vascular rupture. DMSO-compatible microcatheters and syringes need to be used for injection. Tantalum may cause sparking with bipolar cautery during surgery [66]. There is no current consensus in the literature as to which one is ideal

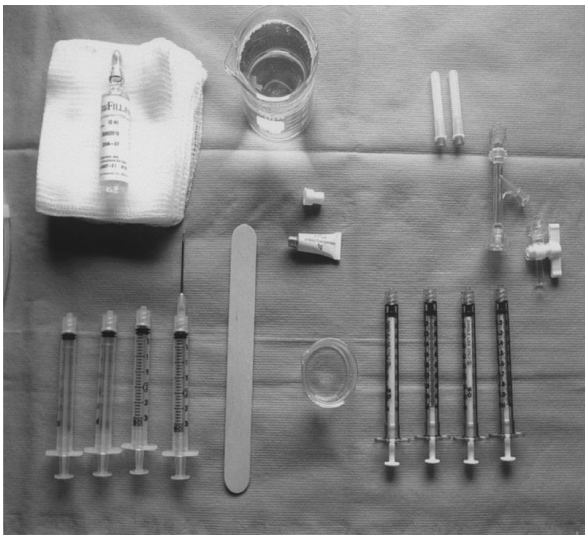

Fig. 1.3 Sterile table with requirements for the preparation of glue mixtures [80].

for a given clinical situation. The choice is largely determined by specific preferences and local expertise in practice.

1.1.3 Techniques of embolization

Embolization to block blood vessels is a very high-risk procedure. It should be performed by physicians with training in the interventional neuroradiology or peripheral interventional radiology and in-depth knowledge of angiographic and embolization techniques. The technique of embolic glue used for vascular embolization is a combination of art and science. There are several variables in the process, including the mixture of components, the delivery system used, the volume and speed of injection, and the nature of the vascular bed that is being embolized [80].

The primary measure usually taken is to mix embolic glue with Lipiodol before injection, which results in slowing down the rate of polymerization and allows visualization of the injected mixture. Various ratios of glue to Lipiodol are used, generally in the range of 1:1 up to 5:1. As the glue polymerizes immediately on contact with any ionic medium, the preparation of glue mixtures must be made in a separate nonionic environment, generally a separate sterile table (Figure 1.3) away from the regular tables. New gloves should be worn and all components required for the glue preparation (syringes, beakers, sponges, etc.) should be kept away from the standard angiographic supplies. To avoid the contact of glue with ions, catheters are flushed with a nonionic solution, typically 5% dextrose in water. The glue mixture is prepared just prior to use.

Fig. 1.4 Closed flush system with adapter, contrast pump connection and saline flush [66].

The delivery system is another key component of embolization with CA glues. Generally vascular embolization is performed using coaxial microcatheter systems through the common femoral artery (CFA) groin approach (Figure 1.5). After gaining access to the (right) common femoral artery, a short sheath, selective catheters and the closed flush system (Figure 1.4) are assembled for catheter flushing and the later injection process. Regular flushing of the catheter with 5% dextrose (approx 3–5 ml according to dead space of the microcatheter) is essential to prevent clot formation and a possible embolic complication in the catheter. Meticulous examination of these closed flush systems is required to ensure that the system is free of air. Selective catheterization of the target vessel is carried out using the coaxial microcatheter system, which has the advantage of permitting the removal of the inner catheter without losing access. The microcatheter is usually placed close to or within the branch being embolized. Once the catheter is in its expected final position, a selective angiogram through the catheter should be performed to ensure that the position is appropriate [5].

After selective catheterization of the target vessel, the injection process is performed with one of the two general techniques: sandwich technique (meniscus-to-meniscus technique) and continuous column technique. The sandwich technique consists of injecting a small volume of mixture followed by an injection of 5% dextrose in sterile water, which expels the mixture from the microcatheter and flushes it forward into the circulation. The average volume of mixture injected on each deposition ranges from 0.2 ml to 0.5 ml. Although this volume of glue sounds quite small, especially relative to a large AVM, a small amount of mixture creates a much larger cast because of the incorporation of blood elements. The total volume of the injected mixture depends on the size of nidus, which is often less than 2 ml. The advantages of the sandwich technique include good penetration of the nidus, and

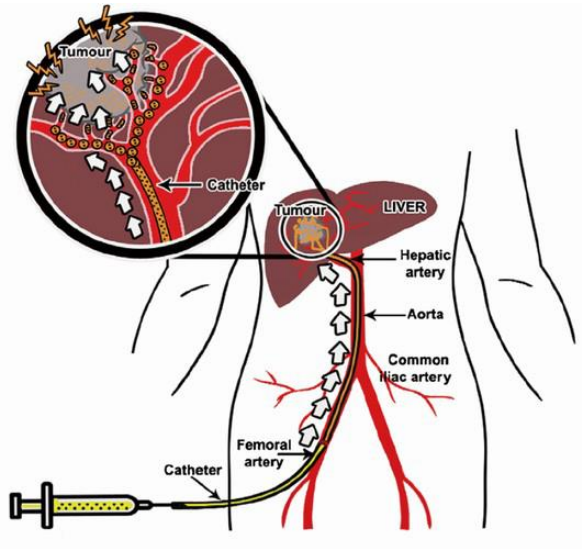

Fig. 1.5 Common femoral artery groin approach used for vascular embolization [39].

reduction of the likelihood of glue adhering to the catheter tip. The primary disadvantage is the limit volume of adhesive delivered on each deposition. The continuous column technique consists of filling a syringe with adhesive and injecting continuously as the agent exits the catheter and forms a cast. The advantage of this technique is that larger volumes of glue can be used to make a more complete cast of the malformation. However this technique is more difficult to control in practice. It often produces a proximal cast with reflux of the adhesive, resulting in increased potential of nontarget embolization [80]. At the end of the injection, operators must aspirate back the glue and rapidly pull the microcatheter inside the guiding catheter [23].

Embolization with cyanoacrylate-based glue has long been advocated in the management of vascular abnormalities, especially AVMs. Nevertheless, cyanoacrylate-based glues are technically more difficult to control, less predictable and less manageable than other embolic agents, making them more hazardous in less experienced hands and hence contraindicated for presurgical procedures [85]. Despite all this, embolization with cyanoacrylate glues still plays an irreplaceable role in interventional radiology owing to its particular characteristics. An in-depth knowledge of physics and chemistry of the embolization process is thus required to improve embolization techniques for a safe and permanent embolization of the vessels.

1.2 *In vitro* characterization of glue embolization

In vitro characterization of glue embolization focuses on the two primary physical phenomena during the embolization process: one is the dynamics of the injection process in complex

blood flow, the other is the polymerization kinetics of the glue-Lipiodol mixture. Various studies have characterized the dynamics of the injection process through a co-flow injection system by neglecting the polymerization reaction of glue. There are also many studies carried out to investigate the polymerization mechanisms of pure CA glue or to characterize the polymerization rate of glue mixtures used for vascular embolization. All these research studies have laid the foundation of *in vitro* characterization of glue embolization.

1.2.1 Drop formation of co-flow injections

Co-flow injection systems have been employed to investigate the drop formation process used in many industrial applications: ink jet printing, production of spherical particles and micro-capsules, etc [90]. When a liquid injected through an orifice into a second immiscible liquid, drops form through one of two mechanisms: at low injection velocities, drops form, grow and ultimately detach themselves from the tip of the orifice which is referred to as the dripping regime; at higher injection velocity, the injected liquid forms a fluid stream that breaks up downstream into drops due to the Rayleigh-Plateau instability [72, 76], which is known as the jetting regime. Over the past decades, the mechanism of drop formation and prediction of drop size in the co-flow injection system have received considerable attention. The drop formation process has been investigated extensively both experimentally and numerically.

Dripping regime

Various studies have focused on the formation of drops in unconfined environments with an external fluid at rest. Early experimental studies have focused on the effects of the different control parameters on drop sizes. They showed that the size of drops, which form in the dripping regime, increases with the diameter of the injection tube, the interfacial tension and viscosity of the external liquid or when decreasing the flow rate ratio and density ratio of the two liquids. When dimensionless numbers are used to characterize the drop formation process, it has been indicated that the behavior is mainly influenced by the capillary number of the outer flow Ca_o and the Weber number of of the inner fluid We_i. These parameters describe, respectively, the ratio of viscous forces from the outer fluid and the inertial forces from the inner fluid to the surface tension forces. The other non-dimensional numbers that play an important role are the Bond number Bo, which compares gravitational to surface tension forces and the Reynolds number Re, which measures the inertial to viscous forces. Dripping occurs when both Ca_o and We_i are small. Increase in either Ca_o or We_i will leads to the transition from dripping to jetting.

Jetting regime

The formation of drops in the jetting regime, has also received great attentions since its first observation by Savart [84]. Plateau [73] showed that the cylindrical jet becomes unstable when its length exceeds its circumference. The size of the drops formed is controlled by the perturbations, which result from the interface instability. Tyler [97] was the first to apply Rayleigh's linear stability analysis [75] to predict the drop size. He postulated that the drop emerged from a cylindrical jet detaches with the same volume as the portion of the jet of length equal to the disturbance wavelength on the jet surface. But this model can only predict the drop size from liquid jets into air [97]. The first study of the instability of a liquid jet into another immiscible liquid was carried out by Tomotika [95]. Since then numerous theoretical and experimental studies used Tomotika's theory to predict the jet length and the drop size when a jet is injected into an immiscible liquid at rest [62–64, 9, 21]. Kitamura et al. [48] found experimentally that Tomotika's theory gives a good prediction for the drop size when the outer liquid flows at the same speed as the jet, while drops formed from jets injected into quiescent liquids are much larger than the prediction.

Dripping-to-jetting transition

Previous studies have highlighted the governing mechanisms of the dripping-to-jetting transition. Stability studies have concluded that the transition from drop generation to jet formation is, in general, due to a transition from absolute to convective instability [35–37], even though cylindrical jets may occasionally break up due to an absolute instability [98]. Some experimental studies have been performed to investigate the transition from dripping to jetting in the liquid-liquid system. Cramer *et al*. [19] concluded that the dripping-to-jetting transition is favored by any parameter that enhances the drag force of the outer phase and increases the momentum of the dispersed inner phase. A more general framework was provided by Utada *et al*. [99] based on a microfluidic injection. They have conducted the injection with a micrometric capillary tube into a millimetric tube (no confinement effect) and have observed a dripping to jetting transition when viscous or inertial forces become comparable to interfacial tension. They have shown two distinct types of transition from dripping to jetting. The first one is driven by the flow rate of the outer flow. A transition to narrowing jets occurs when the interfacial tension is overcome by the viscous drag exerted by the outer fluid on the liquid interface, where the capillary number of the outer fluid $Ca_o \gtrsim 1$; The second one is driven by the flow rate of the inner flow. A transition to widening jets takes place when the inertial forces of the inner fluid overcome the interfacial tension, where the Weber number of the inner fluid $We_i \gtrsim 1$. This study was followed by several that considered

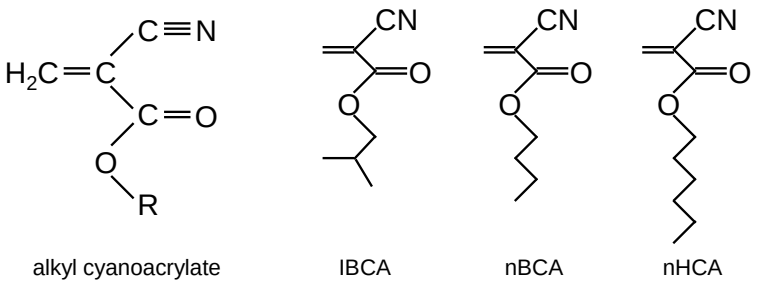

Fig. 1.6 Structure of alkyl cyanoacrylates, R represents an alkyl group. Isobutyl cyanoacrylate (IBCA), n-butyl cyanoacrylate (nBCA) and n-hexyl cyanoacrylate (nHCA).

the case of a highly confined jet on the microfluidic scale [35, 16]. Guillot *et al.* [35] have observed that the transition in this case is ruled by the capillary number *Ca*, whose critical value depends on the value of the confinement.

In summary, despite the fact that a great deal of research on co-flowing injections has been carried out over the past century, there is still little information that can be directly applied to understand the injection process during the vascular embolization. To well understand and control the technique of embolization with glue, an experimental study of the co-flow injection in a confined environment is required. It is also necessary to characterize the flow topology of injection process in conditions similar to the physiological conditions, which are essential to explain the injection process during embolization, to predict drop size and to optimize the embolization procedure.

1.2.2 Polymerization kinetics of alkyl cyanoacrylates

The main surgical glues used in the procedure of vascular embolization are based on cyanoacrylates, typically nBCA. nBCA is a monomer of the alkyl cyanoacrylate family. The general monomeric structure of alkyl cyanoacrylate (Figure 1.6) consists of a double-carbon ethylene group with two reactive electro-withdrawing functions: cyano (-CN) and ester (-COOR). The ester can have various hydrocarbons attached to the R position such as methyl, ethyl or butyl. The hydrocarbon in this position also contributes to the denomination of the cyanoacrylate [74], for instance, isobutyl cyanoacrylate (IBCA), n-butyl cyanoacrylate (nBCA) and n-hexyl cyanoacrylate (nHCA). Alkyl cyanoacrylate polymerizes immediately in contact with ionic solutions, such as blood plasma and saline solutions. The polymerization is initiated by nucleophiles present in the blood or on the vascular endothelium. The rapid polymerization rate of alkyl cyanoacrylate contributes to the presence of two strong electro-withdrawing functions (-CN and -COOR) at the vinyl function, which exhibit a remarkable reactivity towards nucleophiles. Even water and traces of weak bases are suffi-

cient to initiate the polymerization. This explains why alkyl cyanoacrylates are extremely difficult to maintain stable in pure form when free from the acid stabilizers (SO_2, sulfonic acid, ...). Normally a small amount of acid stabilizers is necessary to prevent spontaneous polymerization. Changes in the length and isomeric configuration of the hydrocarbon R also modulate the physical and chemical properties of cyanoacrylate molecules: a longer chain results in a shower polymerization rate, lower heat release during polymerization and lower histotoxicity [96, 20]. That is why long alkyl chain cyanoacrylates have been widely developed for biomedical purposes.

Extensive investigations have been accomplished to understand the polymerization mechanisms of alkyl cyanoacrylates. According to the different types of nucleophiles, cyanoacrylate monomers undergo three distinct types of polymerization mechanisms: anionic polymerization initiated by simple anions (acetate, hydroxide, cyanide, iodide, bromide ...); zwitterionic polymerization initiated by covalent organic bases (triethylamine, benzyl dimethylamine or pyridine) [26]; radical polymerization initiated by radicals [67]. In practice, anionic and zwitterionic polymerization mechanisms are favored under conventional experimental conditions. The polymerization by free radical initiation necessitates the introduction of suitable inhibitor into the system to avoid anionic or zwitterionic polymerization. Pepper's laboratory [26, 70, 71, 30, 31] has accomplished a series of studies to investigate the polymerization mechanisms of alkyl cyanoacrylates initiated by a variety of nucleophilic initiators. They have found that hydroxide ion provides optimal conditions for polymerization among all possible anions, leads to a fast initiation and near-ideal living polymerization kinetics [30, 31]. Upon reaction with anions, a reactive carbanion forms, which reacts with further monomers to finally form a polymer (Figure 1.7a). Covalent organic bases, such as phosphines and amines, are also sufficiently nucleophilic to initiate the alkyl cyanoacrylate polymerization, which produce zwitterions as the propagating species [26, 70]. This polymerization mechanisms is known as zwitterionic polymerization (Figure 1.7b). The reactivity of primary, secondary and tertiary amines exhibit significant difference in the initiation of cyanoacrylate polymerization [49]. Tertiary amines rapidly initiate alkyl cyanoacrylate polymerization through a strong exothermic reaction to produce high molecular weight polymers [43]. In contrast, the reaction of alkyl cyanoacrylate with primary or secondary amines occurs at a much slower rate resulting in low molecular weight oligomers or polymers. The different reaction pathway might due to the different chemical reactivity of amines towards alkyl cyanoacrylate. An intra-molecular proton transfer is favored for primary or secondary amines after the formation of the zwitterion, resulting in low molecular weight oligomers [49]. Costa *et al*. [17] and Donnelly *et al*. [26] also reported that the presence of acidic protons (H^+) leads to a chain-termination process. Therefore strong acid such as metaphosphoric

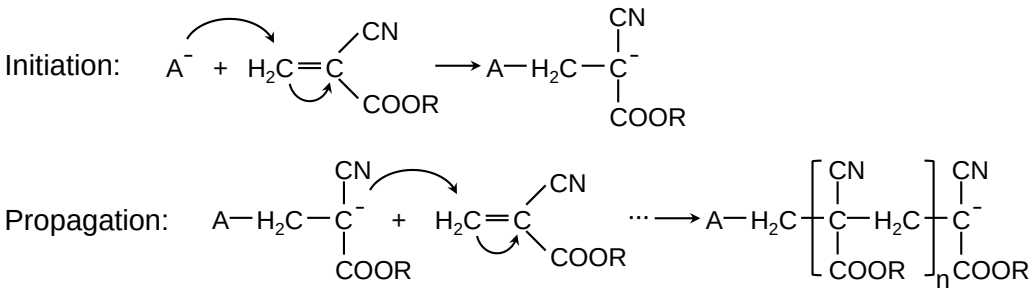

(a)

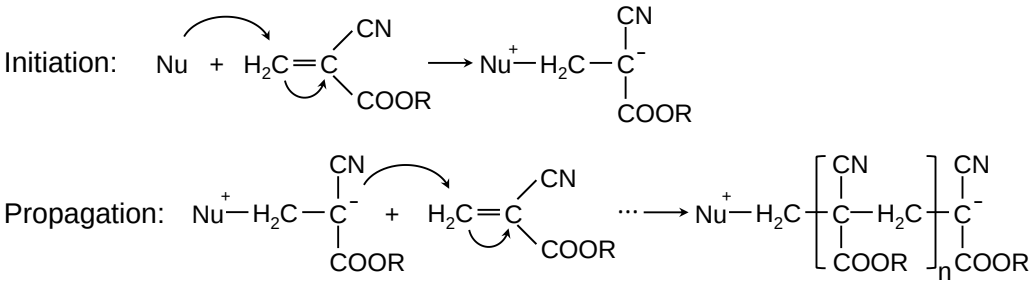

(b)

Fig. 1.7 Initiation and propagation steps in anionic and zwitterionic polymerization of alkyl (R) cyanoacrylate initiated by anions (A^-) and nucleophine (Nu), respectively.

acid, phosphorous pentoxide, and picric acid are used commercially as stabilizers to prevent premature polymerization of superglue [103]. The presence of weaker acids does not prevent polymerization but reduces the rate of chain growth and leads to lower molecular weights. This principle is employed in the formation of nanopaticles and nanocapsules of poly(alkyl cyanoacrylate) (PACA) used as drug delivery system. In most cases, nanoparticles are produced within the range of pH 2.5-3.5. Low molecular weight oligomers first form and then aggregate to make up the nanoparticles. When the pH is above 5, no nanoparticles form. Cyanoacrylate monomers rapidly polymerize, resulting in large molecular weight amorphous agglomerates [18, 28, 3, 101]. Behan *et al.* [3] have proposed a polymerization mechanisms of PACA particle formation, which is similar to the anionic polymerization scheme indicated in Figure 1.7a. A little difference is the existence of re-initiation and termination processes owing to the high concentration in hydrogen ion.

Many techniques are used to determine the rate and kinetic properties of polymerization reaction. To determine the rate of polymerization, it is necessary to measure the monomer concentration $[M]$ as a function of reaction time t and then determine the slope of a plot of $[M]$ versus t. The monomer concentration can be measured by many techniques: infrared (IR) [12, 94], Raman [29], and nuclear magnetic resonance (NMR) spectroscopy [44, 49, 92].

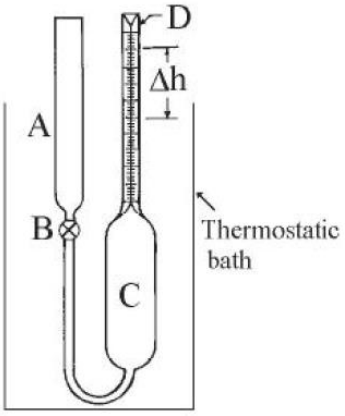

Fig. 1.8 Schematic of a simple dilatometer [14].

There is, however, a method which is significantly faster and also more convenient to determine polymerization rates. It consists of measuring some physical property changes that occur during the course of the polymerization reaction as a result of monomer conversion. Dilatometry (Figure 1.8) is a most commonly used laboratory equipment in practice [4, 81]. The polymerization rate is determined by measuring the decrease in the reaction solution volume as a result of the density increase during the polymerization, a process which is referred to as volume shrinkage or polymerization shringkage. Polymerization shrinkage of the monomers is due to the conversion of intermolecular van-der-Waals forces to the covalent single bonds during the polymerization. Based on this principle, the polymerization rate can be followed by observing the contraction (Δh) in a volume of fixed weight of monomer.

Firstly, a weight faction yield of polymerization y can be defined, y as

$$y = \frac{W_m^0 - W_m}{W_m^0}, \tag{1.1}$$

where W_m^0 and W_m are the weights of the monomer at time $t = 0$ and time t, respectively. Assuming that the entire monomer content is converted polymer after a sufficiently long time ($t = \infty$), W_m and W_m^0 can be related to the change in volume of the reaction system by

$$\frac{W_m}{W_m^0} = \frac{V - V_\infty}{V_0 - V_\infty}, \tag{1.2}$$

where V_0 is the initial volume of the reaction system, while V and V_∞ are the volumes at time t and time $t = \infty$, respectively. Combining Eq. 1.1 and Eq. 1.2, an expression of

polymerization rate can be given as

$$R_p = \frac{y[M]_0}{t} = \frac{V_0 - V}{V_0 - V_\infty}\frac{[M]_0}{t} = \frac{\Delta h(t)}{\Delta h(t=\infty)}\frac{[M]_0}{t}, \tag{1.3}$$

where Δh is the decrease in liquid height, $[M]_0$ is the initial concentration of the monomer. Since $\Delta h(t=\infty)$ can be calculated, R_p can be thus determined from the observed decrease in liquid height Δh at time t.

Fourier Transform Infrared Spectroscopy (FTIR) is another technique used to monitor the kinetics of polymerization reaction [12, 94]. FTIR takes advantage of the vibrational overtones and combination bands present in nearly all complex molecules. Light from an FTIR analyzer impinges on the sample, causing molecular vibrations at characteristic frequencies. The light is then collected by the analyzer and is displayed as spectra. Specific chemical groups, such as C−H bonds or C=C bonds, absorb infrared light at specific wavelengths that can be used for identification or quantification. In the case of cyanoacrylate glues, the C=C bond in the monomer is consumed during the polymerization, resulting in the decrease in magnitude at the wavelength 3128 cm^{-1}. Cambridge polymer group [12] have found that a commercially-available cyanoacrylate adhesive takes about 4-5 minutes to fully cure to the surface of a borosilicate glass slide. Tomlinson *et al.* [94] used FTIR to study the curing of ethyl cyanoacrylate adhesive on polished dental glass and microscope slide substrates. In the case of the dental glass substrate, 80% completion of polymerization of a 70-μm film takes 4 minutes and fully curing of the film needs 20 min. Similarly, in the case of microscope slide substrate, a 110 μm cyanoacrylate film converges to its maximum level of conversion after 20 min. Raman spectroscopic studies have been used to investigate the polymerisation of cyanoacrylate glues. Edwards & Day studied the polymerization of ethyl cyanoacrylate sealed with moisture in a glass tube (diameter 4 mm) [29] based on the consumption of the C=C bond. They have found that the polymerisation had proceeded to 85% completion after 92 days. The difference in results may be caused by the different types of cyanoacrylate used, humidity conditions of substrates and thicknesses of films in the experiments. The techniques mentioned above have been used to characterize polymerization kinetics of cyanoacrylate monomers and detailed kinetic descriptions have been produced. However pure cyanoacrylate glues are rarely used in vascular embolization and blood is a more complex substrate compared with the surface of glass slide. It is difficult to relate existing schemes to the more complicated situations, such as the polymerization kinetics of the glue-Lipiodol mixture with the blood.

1.2.3 Polymerization rates of glue mixtures

Rapid polymerization rates of cyanoacrylate glues lead to a few problems during embolization, such as incomplete embolization and adherent of catheter to the vessel wall. Lack of radiopacity of the embolic glue does not permit the accurate monitoring of the progress of embolization, resulting in possible failure to recognize the endpoint of the procedure and the attendant danger of reflux into the catheter [89]. Modification of glue mixtures and regulation of their polymerization rates are thus required to the control of the injection and subsequent occlusion process. A variety of agents are used to mix with cyanoacrylate glues not only to render the embolic glue radio-opaque but also to alter the polymerization rate. Besides the most widely used iodized oil Lipiodol, iophendylate [20], acetic acid [34], tungsten powder [91] and ethanol [45] have been reported to be mixed with cyanoacrylate glues. Numerous technique have been employed to determine the polymerization time of glue mixtures. The usual empirical technique consists of dropping a small quantity of mixture onto a plasma [51] or citrated blood substrate [20, 89]. The polymerization time is determined by visualizing the change in opacity (whitening) of the mixture through various observation methods, including naked-eye recognition of newsprint-sized letterings [11], naked-eye observation with a magnifying glass [89] and observation of the morphologic changes through videos [93]. This technique is qualitative: the change in opacity depends on the volume of deposited mixture and the ending criteria of polymerization are not precisely defined. Leonard [51] have observed that the spreadability of glue has an effect on the thickness of the resulting film from the deposited volume of glue (Figure 1.9). If the glue mixture has a good affinity to the substrate, a drop of mixture will spread on the substrate and result in a thin film. Consequently the dropping technique essentially provides information on the initial stage of polymerization inside a thin sheet of glue mixture. With this technique, numerous experimental studies have been performed to determine the polymerization time of various glue mixtures (Figure 1.10). The polymerization time for mixtures of nBCA and Lipiodol is in the range between 5 s and 40 s for the ratio of glue to Lipiodol from 1:1 to 1:4. At high glue proportion (glue:Lipdiodol $\geq$ 1:1), the glue mixture polymerizes fully within 10 s. Kawai *et al*. [45] conducted an *in vitro* to study the polymerization conformation of deposited mixtures of nBCA, Lipiodol and ethanol. The polymerization conformation was observed in two methods: dropping mixture into static saline and injecting mixture into flowing saline. They found that the polymerization conformation changed with increasing ratio of ethanol to nBCA and Lipiodol: it was modified from small sized droplets to medium-sized droplets, then a single large droplet and finally anoodle-shaped extrusion. The addition of ethanol shortens the polymerization time. The penetration distance increases

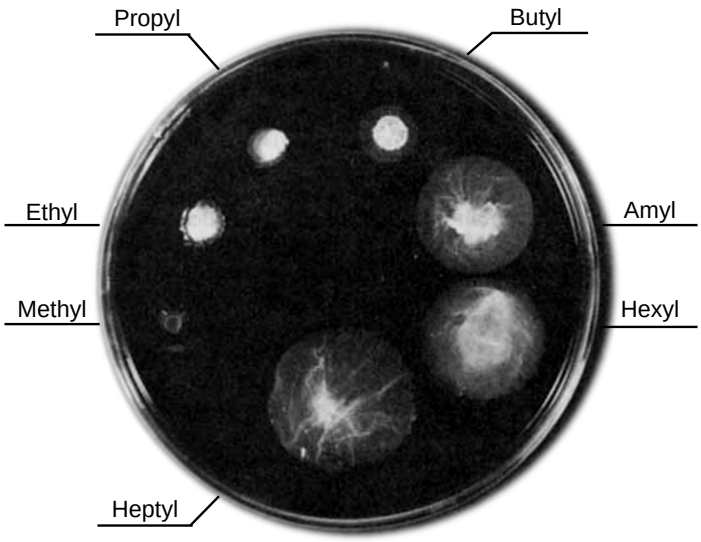

Fig. 1.9 Pictorial demonstration of polymerized cyanoacrylate glues on blood plasma [51].

with increasing ratio of ethanol. All these studies were conducted on Histoacryl or IBCA glue, and no studies ever investigated Glubran®2.

1.3 *In vivo* characterization of glue embolization

In vivo studies, such as animal experiments and clinical trials, are necessary to determine the efficacy and toxicity of an embolic agent. Various studies have been conducted to characterize the embolization with cyanoacrylate glues. It has been noted that *in vivo* cyanoacrylate polymerization occurs much more rapidly than *in vitro* [89, 104]. No significant difference in polymerization time is observed for mixtures at different concentrations. Proximal occlusions of the vessels have been observed for the mixture of high glue concentration (glue:contrast medium=3:1 or 4:1). A mixture at low glue concentrations (glue:contrast medium=1:3 or 1:4) leads to a more distal and later occlusion of the vessels. In the case of high-flow arteries, a mixture of high glue concentration is recommended. Gounis *et al*. [34] carried out an *in vivo* investigation to study the effect of glacial acetic acid (GAA) and ethiodized oil concentration on embolization with nBCA. An optimized model parameter, termed the time elapsed to flow arrest (TEFA), was used to characterize the polymerization time related to the embolization process. They have observed that TEFA showed a linear increase with the quantity of GAA in the mixture. In contrast, TEFA was independent of the variation of the ethiodized oil concentration in the mixture, which is consistent with previous studies [89, 87, 11, 104]. Kawai *et al*. [45] performed aneurysm occlusion with the mixture of nBCA, Lipiodol and ethanol (NLE). They concluded that three remarkable merits of NLE were revealed compared

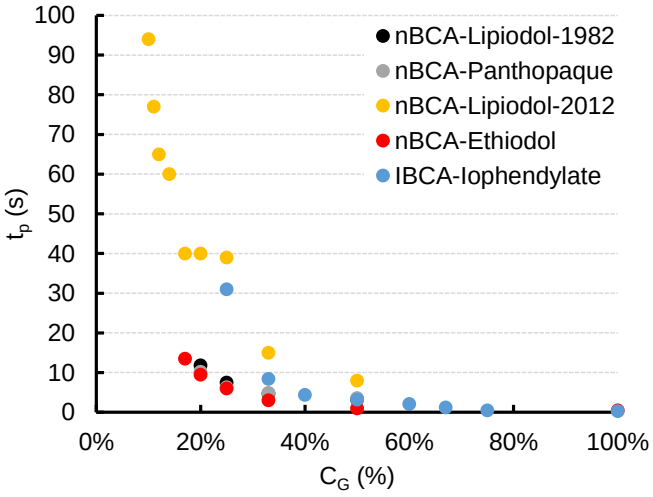

Fig. 1.10 Polymerization time t_p of glue mixtures at different glue concentration C_G. [20, 89, 11, 34]

with nBCA-Lipiodol mixture. The first is the low risk of adhesion to the microcatheter. Furthermore under balloon occlusion, NLE injection creates a solid-like embolic material with potent occlusion ability. Thirdly, it is feasible to use the same microcatheter for several injections. The addition of ethanol into the nBCA-Lipiodol mixture may be valuable for embolization of AVMs and for isolation of aneurysms. Stolesslein *et al.* [89] have made the histologic examination of polymerized mixture in an artery. They have found that embolic glue and oily contrast medium do not form a compound, which can be separately identified by selective histologic methods. The oily component usually lies in the center of artery section with a number of fat droplets, while adhesive component is situated in the periphery.

Other focuses of *in vivo* characterization of embolization with cyanoacrylate glues are the cytotoxicity and biocompatibility of embolic glues [96, 65, 54, 101, 69]. It is well known that cyanoacrylate-based embolic glue are toxic and leads to foreign-body/inflammatory response. The toxicity of cyanoacrylate glues results mainly from two processes: the first is related to the heat release of the exothermic reaction of polymerization; the second is linked to the degradation of cyanoacrylate polymers and the subsequent release of formaldehyde, resulting in tissue accumulation and inflammation [101, 69]. Short alkyl chain cyanacrylates, such as methyl and ethyl, degrade faster than those with long chains, and thus have a higher concentration of degradation products leading more prevalent cytotoxic and inflammatory effects. Increasing the number of carbons in the alkyl chains would slow degradation and therefore decrease the toxicity. This fact has led to the development of new cyanoacrylate glues, such as Glubran®2 (nBCA-MS) and Purefill® (nHCA). Pascual *et al.* [69] have reported that OCA exhibited mild formaldehyde release and was the most cytotoxic during

polymerization when compared to Glubran®2 and nHCA. However, it was the least cytotoxic once cured.

1.4 Summary

Previous studies have shown that two primary physical phenomena predominate in the vascular embolization with cyanoacrylate-based glues: one is the polymerization kinetics of the glue-Lipiodol mixture, the other is the dynamics of the injection process in complex blood flow. During the injection of glue mixture into flowing blood, the two processes are combined and coupled: they control and determine the result and efficacy of the embolization. An in-depth understanding of these two physical phenomena is thus important and necessary so that interventional radiologists achieve a safe and permanent obliteration of the vessels.

The polymerisation mechanisms of cyanoacrylate monomers have been extensively studied under different conditions, and detailed kinetic descriptions have been produced [30, 31, 26, 70, 71]. However all these investigations focused on the polymerization kinetics of cyanoacrylate monomers. It is difficult to relate such schemes to the more complicated situations, for instance the polymerization kinetics of the glue-Lipiodol mixture. Although various studies have been carried out to determine the polymerization rate of glue mixtures, the measurement technique that consists of dropping mixtures onto plasma or blood substrates is qualitative. This technique can only provide information on the initial stage of polymerization inside a thin sheet of glue mixture. The resulting polymerization time only corresponds to the time taken to polymerize the surface of an injected mixture drop. How the polymerization propagates inside the mixture drop and how long it takes to fully polymerize remain unknown. No study ever showed information on the volumetric polymerization within an injected drop of glue mixture.

The fluid dynamics of co-flow injection process of non-reaction fluids have been thoroughly investigated in the field of fluid mechanics through a large number of experimental, numerical and theoretical studies [99, 19, 35–37, 16]. Detailed state diagram of flow regimes and transitions have been reported. However the experimental and simulation conditions of these studies are different from the physiological conditions encountered during the procedure of vascular embolization. Existing results cannot be directly applied to explain the injection process during the vascular embolization. An study of the co-flow injection in a confined environment is required at conditions similar to the physiological case.

At present, the polymerization kinetics of glue mixture are unknown. No study ever investigated the injection and convection of glue mixtures in the blood flow to study the joint

influence of polymerization and hydrodynamics. The interventional radiologists thus face with multiple questions:

- Glue concentration

  The ratio of embolic glue to oily contrast medium affects the radio-opacity, viscosity and penetration ability of the resulting mixture.

- Polymerization time of mixture

  The polymerization time of glue mixture determines the time needed to the site of vessels to be occluded.

- Hydrodynamic environment and geometry of vessels

  Hydrodynamic environment and geometry of vessels determines the position of micro-catheter and the injection velocity of glue mixture.

- Injection velocity

  Injection velocity determines the size, shape and formation time of the injected mixture.

Determining the precise effect of each of these parameters will be key for a safe and permanent embolization of vessels. However, interventional radiologists have to base their understanding on training and experience, the knowledge still very much empirical. This has motivated us to conduct an *in vitro* characterization of cyanacrylate embolic glues used for vascular embolization, with the hope to help interventional radiologists understand, better control the glue and achieve a safe and permanent obliteration of the vessels.

1.5 Objectives of the PhD thesis

The objectives of the thesis are described as follows:

The first objective is to quantitatively investigate the physical properties of cyanoacrylate glues mixed with Lipiodol in different proportions, including the viscosity, density, interfacial tension and miscibility of nBCA glue with Lipiodol.

The main objective is to quantitatively and systematically characterize the polymerization kinetics of the glue-Lipiodol mixture. We have designed a new experimental setup to characterize the polymerization process of a glue-Lipiodol mixture upon contact with an ionic or proteinaceous solution. The influences of ion contents and plasma proteins of blood on the polymerization process are studied. The effects of ionic concentration in the ionic solution and mixing methods of mixtures are taken into account.

Another objective is to analyze the injection dynamics during the embolization process. Firstly, an *in vitro* liquid-in-liquid injection system is used to investigate the injection dynamics of two non-reacting immiscible flows. The fluid parameters which characterize the drop formation process are determined. Finally, the injection of a glue mixture into a flowing substitute solution of blood is performed to show the joint influence of polymerization and hydrodynamics.

1.6 Outline

In Chapter 2, we first present the preparation methods of glue mixtures and ionic solutions. The techniques for the measurements of physical properties are detailed. Afterwards we describe the experimental technique used to enquire on the miscibility of glue and Lipiodol. The experimental setups are then described to characterize the polymerization process of glue mixtures upon contact with ionic or proteinaceous solutions. At the end of the material and method section, the experimental setup designed to characterize the injection process of glue mixtures is detailed.

In Chapter 3, we first show the results for the miscibility of nBCA glue with Lipiodol. Then the results for the polymerization of glue mixture on contact with ionic solution are summarized, including the volumetric polymerization and interfacial polymerization. The factors that influence the polymerization of the glue-Lipiodol mixture are investigated. The results shown in this chapter have been published in Li *et al.* [55].

In Chapter 4, we show the results for the polymerization of glue mixture after contact with proteinaceous substrates and discuss the influence of the protein on the polymerization of glue mixtures. The results in this chapter have been submitted to the *Journal of the Mechanical Behavior of Biomedical Materials* in 2017 [56].

In Chapter 5, results of drop formation in confined co-flow are first summarized before providing results of glue mixtures injected into a flowing ionic solution.

In Chapter 6, we provide the conclusions of the study and discuss the perspectives of the thesis.

Chapter 2

Materials and methods

2.1 Preparation of glue mixtures and ionic solutions

Glue mixtures

Two cyanoarylate-based glues are used in the experiments: Glubran 2 (nBCA-MS glue) (GEM, Viareggio, Italy) and Histoacryl (pure nBCA glue) (B. Braun, Melsungen, Germany). All the glues are packaged in the hermetically sealed vials and stored at a constant temperature of 4 °C protected from direct sunlight and humidity. Before use, glues are left at room temperature for a few minutes after their transparency and fluidity have been checked.

Glues are mixed with Lipiodol (Laboratoire Guerbet, Aulnay-sous-Bois, France). Lipiodol is packaged in a 10-mL glass ampoule and stored at room temperature. If not particularly indicated, Glubran 2-Lipiodol (G-L) and Histoacryl-Lipiodol (H-L) mixtures are prepared by means of a female luer connector attached to two 1-ml syringes, one loaded with glue and the other with Lipiodol (Figure 2.1c). A 0.2 ml total volume of glue and Lipiodol is mixed with volume ratios 1:0, 3:1, 1:1 and 1:3, corresponding to glue concentrations $C_G = 100\%$, 75%, 50% and 25%, respectively. The mixing process consists of manually passing the liquids from one syringe to the other several times at a high frequency (about 150 times in 90 seconds). The resulting mixtures are left to stand at least 5 minutes to eliminate air bubbles. All the experiments are conducted at 21 °C.

Mixing methods

For investigating the influence of mixing methods on the polymerization of the glue mixtures, we have performed two other mixing processes (Figure 2.1) at the same glue concentration C_G =50% . The first one is performed by putting equal volumes of Glubran 2 and Lipiodol

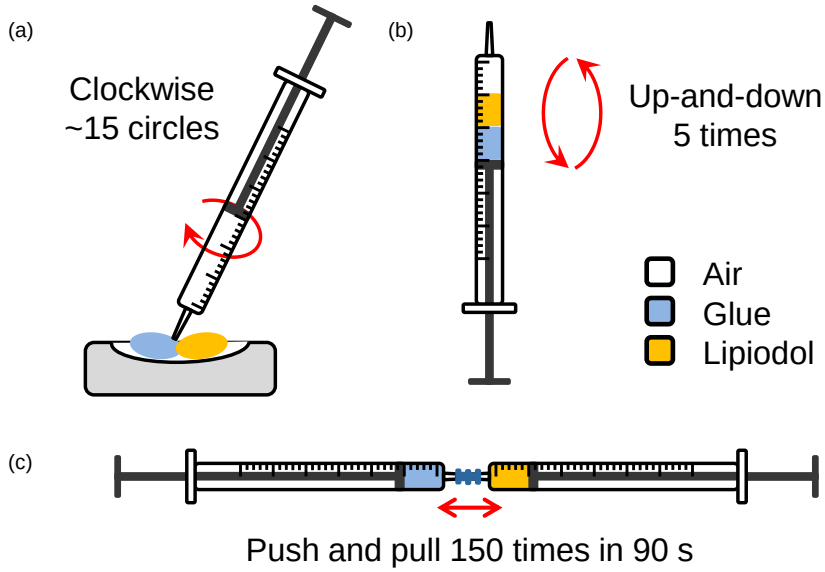

Fig. 2.1 Three mixing methods for the preparation of glue mixtures. (a) Cup-Syringe method, (b) Air-Syringe method, (c) Luer-Syringe method.

(0.2 ml for each solution) in a small cup and stirring the two solutions clockwise $\sim$ 15 circles with a 1-ml syringe (Figure 2.1a). The other mixing consists of aspirating sequentially 0.2 ml Glubran 2, 0.2 ml Lipiodol and 0.2 ml air into a 1-ml syringe and flipping it up-and-down 5 times (Figure 2.1b). The former is called as 'Cup-Syringe' method and the latter is referred as 'Air-Syringe' method. Results of both mixing methods are compared with the one mixed with two syringes and a luer connector, which is called as 'Luer-Syringe' method.

Ionic solutions

Blood naturally consists of a suspension of cells in plasma, which is made of proteins (8%), metallic ions (1%) and water (91%). All these components can initiate the polymerization of cyanoacrylate glues. In order to study the different components of blood plasma on the polymerization of glue mixtures, ionic solutions with different compositions are reproduced part of the constituents of blood.

To determine the influence of blood anions on the glue polymerization, we have reproduced an ionic solution with glycerol (ISG) and use it to initiate the polymerization reaction. The composition of the ISG solution is indicated in Table 2.1. It is prepared by weighting each of the components and dissolving them into the desired volume of deionized water. Mixing is performed with a magnetic stirrer (Microstirrer, VELP scientifica) for at least 30 min at room temperature. ISG has the same ionic composition and pH = 7.3 ± 0.1 as blood. To match the solution viscosity to that of blood, some glycerol is incorporated into it. The

Solute	Quantity
NaCl	7.19 g
KCl	0.2 g
KH_2PO_4	0.2 g
$Na_2HPO_4{\cdot}12H_2O$	2.864 g
Glucose	0.8 g
Glycerol	320 ml
Deionized water	680 ml

Table 2.1 Composition of 1 L of ionic solution with glycerol (ISG).

Solute	Quantity
NaCl	7.19 g
KCl	0.2 g
KH_2PO_4	0.2 g
$Na_2HPO_4{\cdot}12H_2O$	2.864 g
Glucose	0.8 g
Deionized water	1 L

Table 2.2 Composition of 1 L of ionic solution without glycerol (IS).

ionic solution has a density of 1094.5 kg/m^3 and dynamic viscosity of 3.8×10^{-3} Pa·s at 21 °C. The interfacial tension is slightly higher than that of blood (69×10^{-3} N/m vs 50×10^{-3} N/m for blood), but this should not affect the present results [83].

For investigating the influence of anion concentrations on the glue polymerization, we have reproduced an ionic solution (IS) (Table 2.2) with the same anion compositions as ISG. Glycerol is removed from the ISG to neglect the effect of viscosity. IS is diluted with one volume or three volumes of deionized water to get one-half or one-fourth the anion concentration of IS. The resulting solutions are referred to as IS1/2 and IS1/4 respectively. IS1/2 and IS1/4 solutions are stirred with a magnetic stirrer for at least 30 min to make them homogeneous. All the experiments are conducted at 21 °C.

The plasma proteins consist of albumins (55%), globulins (38%), fibrinogen (7%) and regulatory proteins ($< 1\%$). To determine the influence of one of the main proteins (albumins) on the polymerization of glue mixtures, we have reproduced a proteinaceous solution to initiate the polymerization reaction. The solution is composed of an ionic solution (IS) with the same ion contents as blood and add to it a given quantity of bovine serum albumin (BSA) (Sigma-Aldrich, France), which is usually used as a protein concentration standard in laboratory experiments. IS is prepared with the same composition indicated in Table 2.2.

Solute	Quantity
NaCl	7.19 g
KCl	0.2 g
KH_2PO_4	0.2 g
$Na_2HPO_4 \cdot 12H_2O$	2.864 g
Glucose	0.8 g
Deionized water	1 L
BSA	40 g or 80 g

Table 2.3 Composition of 1 L of ionic solution with BSA.

BSA powder is then incorporated into IS and stirred with a magnetic stirrer for at least 30 min. The proteinaceous solutions are prepared at two different BSA concentrations: 80 g/L (8%) which can be considered as a model of blood plasma where all the proteins are represented by BSA; 40 g/L (4%) allows us to investigate the influence of the BSA concentration on glue polymerization. The two proteinaceous solutions are respectively referred to as IS-BSA8 and IS-BSA4 in the following text.

2.2 Characterization of physical properties of glue mixtures and ionic solutions

The physical properties of G-L mixtures had to be characterized first, as no information is available in the literature. The viscosity was measured with a rheometer (RheoStress1, Thermo Haake, Germany) in cone-plane configuration (diameter 60 mm, angle 0.5°). The density of the solutions was determined with a digital density-meter (DMA 45, Anton Paar, Austria) with an accuracy of $\pm\ 10^{-4}$ g/cm^3 (manufacturer values). For pure Glubran 2, the density was determined by weighting a sample of known volume with a high precision scale (Precisa 92SM-202A, Elsichrom, Sweden) having an accuracy of $\pm\ 10^{-4}$ g. The risk was indeed too high to clog the internal tube of the density-meter with Glubran 2. The viscosity μ and density ρ are given at 21 °C in Figure 2.2 as a function of glue concentration. The results indicated for Histoacryl in Figure 2.2 have been obtained by interpolating the values of Bracard *et al.* [6] for the temperature of 21 °C. It appears that the two glue mixtures have almost the same viscosity and density.

The interfacial tension γ between the glue mixtures and purified water (Milli-Q, Merck Millipore, USA) was measured at 21 °C with the pendant drop technique (Drop Shape Analyzer DSA10, Kruss, Germany). The results are shown in Figure 2.3. It was, however, not

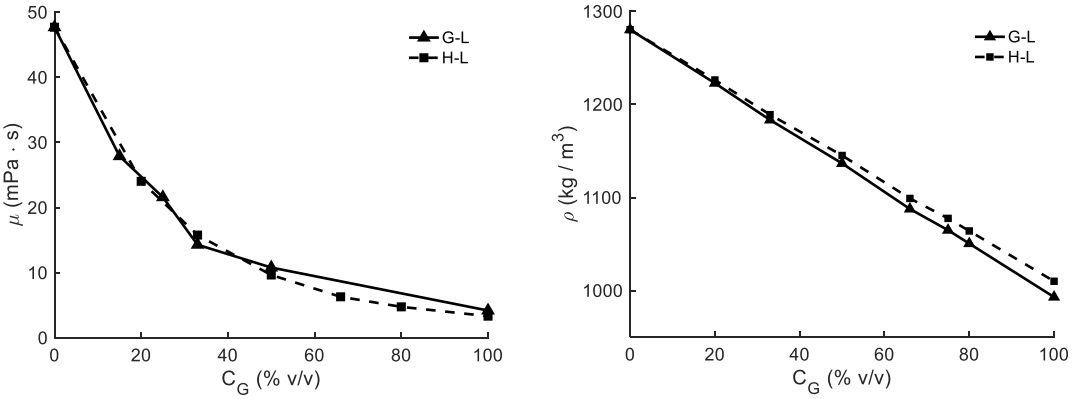

(a) (b)

Fig. 2.2 Viscosity μ (a) and density ρ (b) of G-L and H-L mixtures at 21 °C [82]. The viscosity of H-L mixtures is inferred from Bracard *et al.* [6].

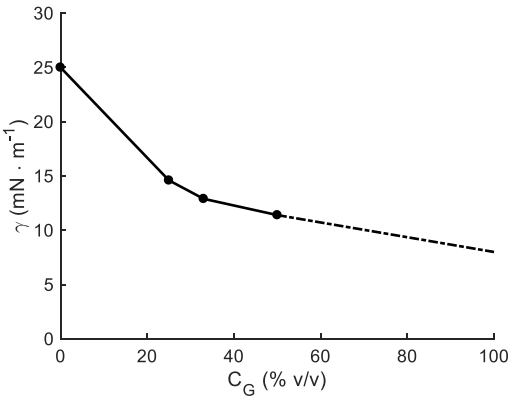

Fig. 2.3 Interfacial tension γ between purified water and G-L mixtures at 21 °C [82]. The dashed line is an extrapolation.

possible to use this technique for glue concentrations larger than 50%, because polymerization occurred immediately after contact with water. Since the γ vs C_G curve seems to level off, we have extrapolated linearly the curve for $C_G > 50\%$.

The pH of various ionic solutions and waters are measured with a pH meter (FE20-Kit, Mettler Toledo, Switzerland) with an accuracy of ± 0.01. Before use, the pH meter undergoes a 2-point calibration with two pH buffer solutions at pH = 4.01 and pH = 7.0. All the measurements have been repeated at least 3 times for each solution. The pH measurement results are shown in Table 2.4.

Solutions	pH
IS	6.37 ± 0.02
IS1/2	6.49 ± 0.02
IS1/4	6.59 ± 0.00
ISG	7.16 ± 0.01
MilliQ water	6.28 ± 0.03
Deionized water	6.20 ± 0.01
IS-BSA4	6.16 ± 0.02
IS-BSA8	6.21 ± 0.02

Table 2.4 pH measurements of different solutions.

2.3 Miscibility of nBCA glue and Lipiodol

The miscibility of nBCA glues with Lipiodol is assessed in a diffusion device, consisting of a parallelepipedic transparent cup (UV cuvette, Brand, Germany), as shown in Figure 2.4a. The bottom of the cup is first filled with $\sim$135 μL of Lipiodol (translucent, pale yellow). Then $\sim$150 μL of Histoacryl (translucent, blue) is carefully poured onto the Lipiodol, taking care that minimum mixing takes place during the procedure. The cup is then closed hermetically to limit evaporation, and placed vertically in front of a high-speed camera (SA3, Photron, USA). An optical fibre panel (Schott-Fostec, LLC, USA) is used as back illumination source (Figure 2.4a). The diffusion process between the two liquids is captured by the camera at the rate of one frame every 30 seconds over 2 days. The recorded images are encoded in 16 bits which are converted to 8 bits in the measurement process, providing 256 possible shades of grey: 0 corresponding to black and 255 to white. The concentration distribution is then assessed from the image grey level distribution G_m. The z-axis is aligned with the tube centerline, the origin $z = 0$ corresponding to the initial position of the glue-Lipiodol interface. Initially, the glue is thus in the $z > 0$ region and Lipiodol in the $z < 0$ region (Figure 2.4b). The grey levels are measured at 24 test points, equally distributed along the z-axis with a 0.38 mm interval. The value $G_m(z)$ corresponds to the average of G_m within a box of width 1.36 mm and height 0.28 mm centered on each test point. Note that the grey level values are relative and may vary between two experiments, depending on light settings for example. However, the grey level basis is constant during one experiment.

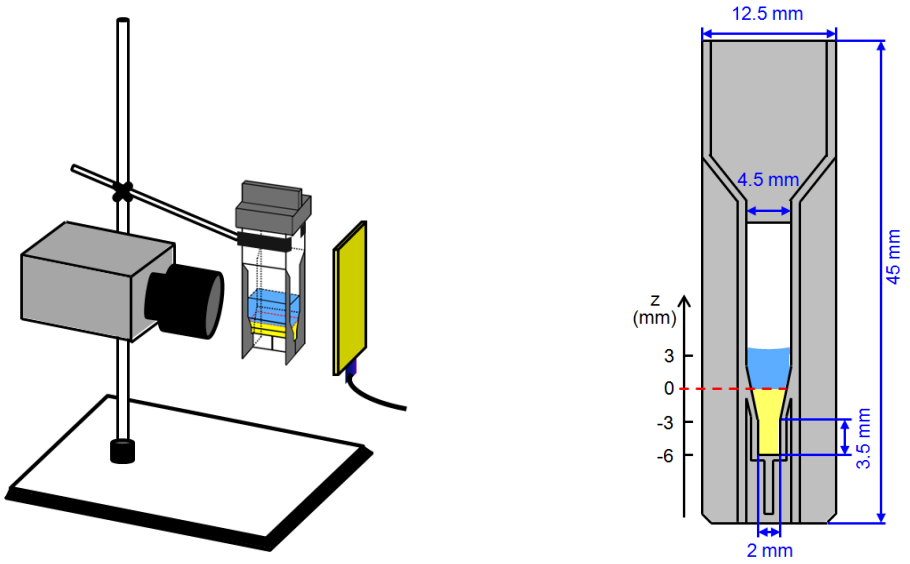

(a) (b)

Fig. 2.4 Experimental setup to study the miscibility of glue and Lipiodol (at the top and bottom of the cup, respectively). (a) The two fluids are put in contact in a cup and the change in opacity of the system is monitored by a camera with a back-light device. (b) Detail of the cup cross-section.

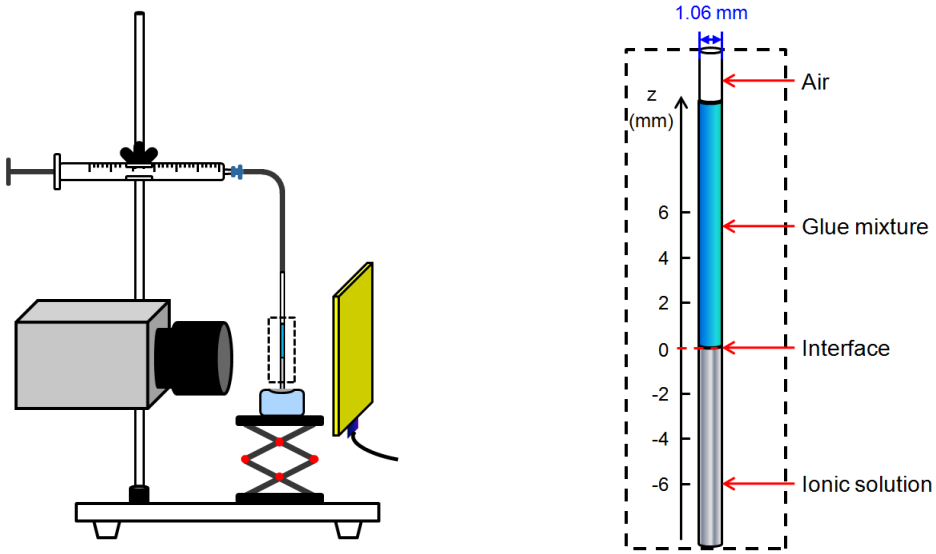

(a) (b)

Fig. 2.5 Experimental setup to study the polymerisation of glue-Lipiodol mixtures in contact with the ionic solution. (a) The two fluids are put in contact in a micro-tube and the change in opacity of the system is monitored by a camera with a back-light device. (b) Detail of the tube.

2.4 Characterization of the polymerization of glue mixtures with ionic solutions

An experimental setup has been designed to visualize the polymerization of the glue-Lipiodol mixture when it is put in contact with the ionic solution. The principle consists of creating a small well-defined interface between the two fluids and following the propagation of the reaction through the change in opacity of the glue volume.

Specifically, the polymerization reaction is studied under static conditions in a vertical glass micro-tube (internal diameter $D_t = 1.06 \pm 0.01$ mm). First a volume of glue mixture is aspirated into the tube from a small cup placed underneath, by means of a syringe connected to the tube upper end (Figure 2.5a). The glue cup is replaced by one containing the ionic solution: the glue mixture and ionic solution then come into contact and are aspirated quickly together from the lower tube tip to a static position (Figure 2.5b). The contact surface between the glue mixture and the ionic solution corresponds to the tube cross section. The polymerization can only propagate from this surface into the glue volume inside the tube. With this device, we have essentially reduced the volume polymerization to a one-dimensional front propagation along the tube axis. A z-axis is defined along the axis of the tube with the origin $z = 0$ corresponding to the position of the interface at the end of the aspiration process, which lasts between 5 and 10 s (Figure 2.5b). The glue mixture is initially in the $z > 0$ region and the ionic solution in the $z < 0$ region. The progression of the polymerization reaction is then evaluated from the change in opacity of the glue mixture for different values of z. The image grey level $G_p(z)$ of the fluids is monitored with the imaging system consisting of the high-speed Photron camera coupled to the back illumination source.

The beginning of the polymerization process is continuously recorded at a rate of 50 fps with image resolution 128×1024 pixels^2 during a maximum recording time of 217.8 s. A time-lapse recording mode is then used to monitor the long time polymerization process with a frame rate of 0.5 fps and image resolution 128×1024 pixels^2. The total recording time ranges from 90 min to 120 min in the different experiments. In both modes, the shutter time is 0.5 ms. All the experiments are conducted at a controlled room temperature of 21 °C. All the experiments have been repeated between 5 and 10 times for each concentration of Glubran 2 and Histoacryl.

The distance between two contiguous measuring points is $0.5\,D_e$, where D_e is the diameter of the liquid region as measured on the image (D_e is slightly smaller than D_t because of optical effects). Grey levels are averaged within boxes of width $0.7\,D_e$ and height $0.4\,D_e$ centered on each test point.

Factors	Glue mixture	Mixing methods	Ionic solution	C_G = 50%	C_G = 75%	C_G = 100%
Glue	G-L	Luer-Syringe	ISG	√	√	√
	H-L			√	√	√
Ionic concentration	G-L	Luer-Syringe	IS	√	×	×
			IS1/2	√	×	×
			IS1/4	√	×	×
Mixing methods	G-L	Luer-Syringe	ISG	√	×	×
		Cup-Syringe		√	×	×
		Air-Syringe		√	×	×

Fig. 2.6 Experimental conditions for the polymerization of glue mixture with ionic solutions.

All the experimental conditions for the polymerization of glue mixtures with ionic solutions are indicated in Figure 2.6. The influences of ionic concentrations and mixing methods on the polymerization process are studied at the glue concentration of $C_G = 50\%$.

2.5 Characterization of the polymerization of glue mixtures with proteinaceous solutions

In order to visualize the polymerization of a glue mixture with a proteinaceous solution, the experimental setup (Figure 2.7) has been slightly modified. In the section 2.4, the glue mixture and the ionic solution are successively aspirated in a glass capillary tube to create a sharp well-defined interface. When a proteinaceous solution is used, however, the polymerization is so fast that we do not have time to perform the aspiration. The polymerization reaction is created by contacting the glue mixture with the proteinaceous substrate and monitored with a high speed camera to detect the change in opacity of the mixture volume.

As shown in figure 2.7, the polymerization reaction is studied in a vertical glass micro-tube. First a volume of glue mixture is aspirated into the vertical tube from a small cup placed underneath, by means of a syringe connected to the tube upper end (Figure 2.7a). The glue cup is removed and the lower glue meniscus is positioned at the bottom of the tube. Another cup containing the proteinaceous solution is then raised up to touch the lower tube tip and start up the polymerization reaction (Figure 2.7b).

The polymerization reaction process is monitored with two recording phases: a continuous recording to monitor the beginning of the polymerization process at a frame rate of 50 fps; a time-lapse recording to monitor the long-term polymerization process at a frame rate of 0.5 fps. The continuous recording time is maximum 217.8 s or 435.7 s corresponding to the image resolution 128×1024 pixels^2 or 128×512 pixels^2. The duration of the time-lapse

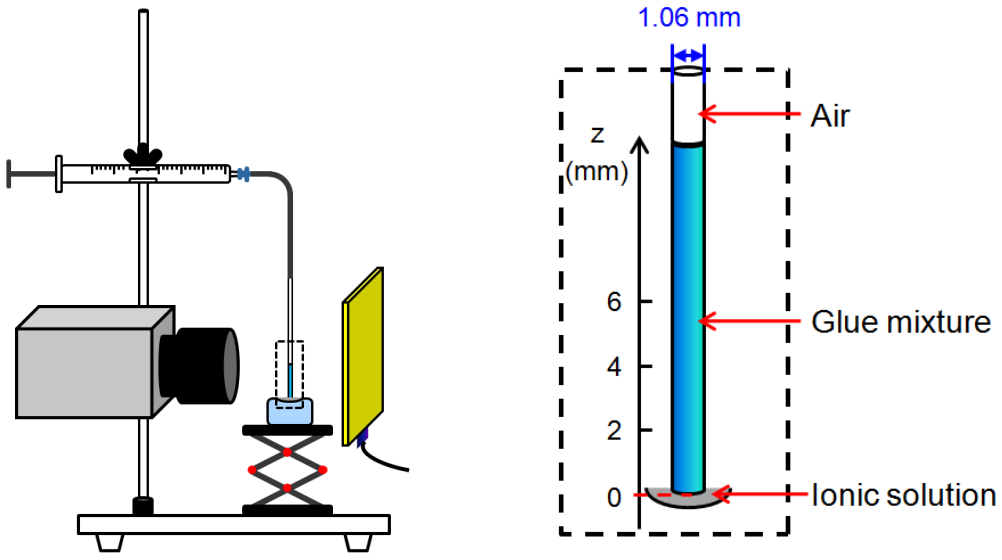

(a) (b)

Fig. 2.7 Experimental setup to study the polymerisation of glue-Lipiodol mixtures in contact with the proteinaceous substrates. (a) The two fluids are put in contact in a micro-tube and the change in opacity of the system is monitored by a camera with a back-light device. (b) Detail of the tube.

Factors	Glue mixture	Mixing methods	Proteinaceous solution	C_G = 25%	C_G = 50%	C_G = 100%
BSA concentration	G-L	Luer-Syringe	IS-BSA4	×	√	×
			IS-BSA8	×	√	×
Glue concentration	G-L	Luer-Syringe	IS-BSA8	√	√	√

Fig. 2.8 Experimental conditions for the polymerization of glue mixture with proteinaceous solutions.

recording ranges from 60 min to 120 min in the different experiments. In both modes, the shutter time is 0.5 ms.

In the analytical procedure, an upwards vertical z-axis is defined along the axis of the tube with the origin $z = 0$ corresponding to the tip of the micro-tube. (Figure 2.7b). The glue mixture is thus in the $z > 0$ region. The progression of the polymerization reaction is then evaluated from the change in image grey level $G_p(t,z)$ of the glue mixture for different values of z and different instants t. Time $t = 0$ corresponds to the time when the proteinaceous solution is put in contact with the tube bottom. The distance between two contiguous measuring points and the size of the average box are same as described in Section 2.4.

The experimental conditions for the polymerization of glue mixtures with proteinaceous solutions are indicated in Figure 2.8. Experiments are carried out with IS-BSA8 and IS-BSA4 to investigate the influence of the BSA concentration on the polymerization of the G-L

mixture $C_G = 50\%$. G-L mixtures at three glue concentrations ($C_G = 25\%$, 50% and 100%) allow to study the influence of the glue concentration on the polymerization process.

2.6 Characterization of drop formation of two immiscible fluids

2.6.1 Experimental setup and procedure

For simulating the injection of the embolization process, we first neglect the polymerization reaction and study the fluid dynamics of the injection into a co-flowing immiscible liquid through a capillary tube.

An experimental setup (Figure 2.9) has been designed to create and visualize the confined co-flow injection of two immiscible fluids. The inner fluid (disperse phase) is injected through a brass capillary tube (internal diameter $d_i = 0.45$ mm and external diameter d_t = 0.90 mm). It is placed concentrically in a straight cylindrical glass tube of inner diameter $d_o = 7$ mm (Figure 2.10). The tip of the capillary tube is placed far from the glass tube entrance to ensure that the outer flow is fully developed at the location of injection. The glass tube is placed in a transparent tank filled with water to eliminate the visual distortions caused by the tube curvature.

A continuous-flow gear pump (Ismatec MCP-Z with head Z-130) generates the outer fluid flow with flow rate Q_o (Figures 2.9 and 2.10). The inner fluid flow is generated at flow rate Q_i by a syringe pump (KDS 200P, kdScientific). Both fluids flow in the anti-gravitational direction. The gear pump is started at the minimum flow rate (65 ml/min), which is increased by 50 ml/min every 2 minutes until the desired flow rate is reached. This procedure avoids the generation of air bubbles into the circuit of the outer fluid. After about ten minutes, all the air bubbles in the outer fluid have disappeared.

The drop formation process is monitored with a high-speed imaging system coupled with an optical fibre panel used as back illumination source. All the recordings are performed at least 10 min after the onset of the outer flow, to ascertain that it is fully established and stationary. The syringe pump is then started and a continuous recording begins. The recording time varies from 1 min to 2 min depending on the injection velocity and the image acquisition frequency. All the experiments are carried out at the ambient temperature of 21 °C.

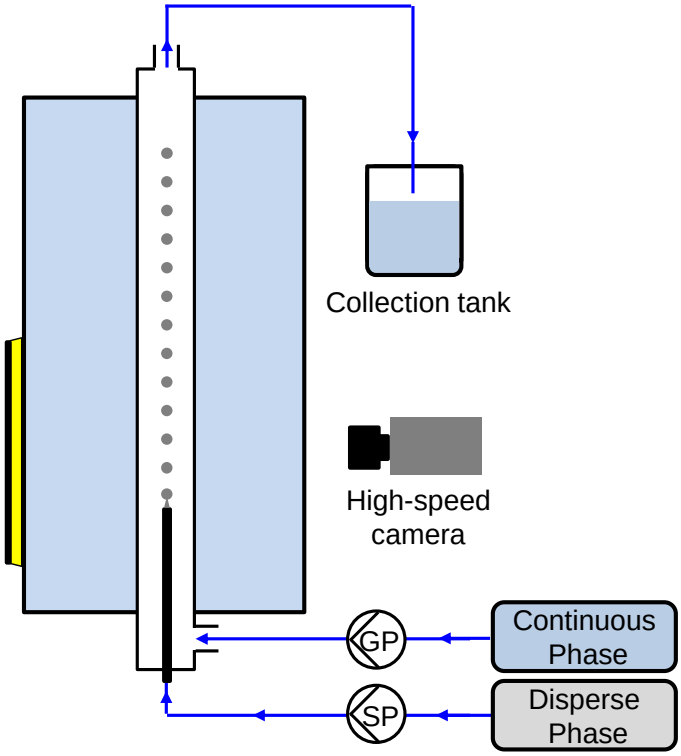

Fig. 2.9 Experimental setup to study the drop formation by co-flow injection.

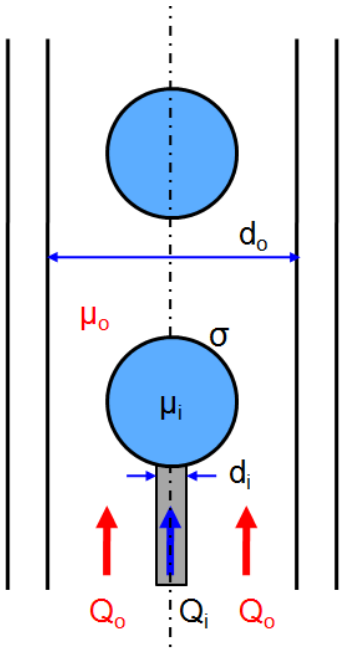

Fig. 2.10 Physical and geometrical quantities controlling the liquid-in-liquid co-flow injection.

	μ_k ($\times 10^{-3}$ Pa·s)	ρ_k (kg/m^3)	γ ($\times 10^{-3}$ N/m)
Silicon oil ($k = i$)	10	993	32
Deionized water ($k = o$)	1.003	998	

Table 2.5 Physical properties of the modeling fluids used in vitro.

2.6.2 Modeling fluids and dimensionless numbers

Deionized water is used as the outer liquid and a silicon oil (DC200, Sigma-Aldrich 85411) is used as the inner liquid. Physical properties of the two liquids have been measured at room temperature. The measured values of viscosity μ_k are indicated in Table 2.5, along with the values of the density ρ_k and the interfacial tension γ.

For each liquid, ρ_k, μ_k, Q_k and d_k are density, viscosity, flow rate and diameter of the tube respectively, the index k referring either to the inner fluid ($k = i$) or outer fluid ($k = o$). Based on the physical and geometrical quantities defined in Figure 2.10 and Table 2.5, the following the dimensionless numbers are defined to characterize the fluid dynamics of the liquid-to-liquid system.

* The Reynolds numbers of the inner ($k = i$) and outer ($k = o$) fluids:

$$Re_k = \frac{4\rho_k Q_k}{\pi d_k \mu_k} \tag{2.1}$$

* The Weber number of the inner fluid:

$$We_i = \frac{16\rho_i Q_i^2}{\pi^2 d_i^3 \gamma} \tag{2.2}$$

* The capillary number of the outer fluid:

$$Ca_o = \frac{4\mu_o Q_o}{\pi d_o^2 \gamma} \tag{2.3}$$

* The Bond number:

$$Bo = \frac{(\rho_i - \rho_o) d_i^2 g}{\gamma} \tag{2.4}$$

* The viscosity ratio:

$$\eta = \frac{\mu_o}{\mu_i} \tag{2.5}$$

	In vitro	*In vivo*
$\delta = d_o/d_i$	15.6	4.4–20
$\eta = \mu_i/\mu_o$	10	1–8
Re_i	11–39	$\leq$15
Re_o	177–530	200–600
We_i	0.9–11	$\leq$2
Ca_o	0.9×10^{-3}–2.7×10^{-3}	28×10^{-3}–50×10^{-3}
Bo	3.8×10^{-3}	$\leq 6 \times 10^{-2}$

Table 2.6 *In vitro* values of the dimensionless numbers used for the drop formation.

* The diameter ratio:

$$\delta = \frac{d_o}{d_i} \tag{2.6}$$

where g is the gravity. The Reynolds number Re is the ratio of inertial forces to viscous forces. The capillary number Ca_o compares the viscous forces from the external fluid to the surface tension forces. The Weber number We_i corresponds to ratio of the inertial forces for the inner fluid to the surface tension forces. The Bond number Bo measures the ratio of gravitational forces to surface tension forces.

We have varied the flow rates of both the inner and outer fluid flows to study the drop formation process. All the values of the non-dimensional parameters are chosen to ascertain that the in vitro experiments are similar to the physiological case of the portal vein embolization (PVE). The values of the dimensionless numbers tested are listed in Table 2.6.

2.6.3 Analytical procedure

The drop size and drop formation time are measured by means of an image processing system, programmed with MATLAB R2013b. Figure 2.11 shows the chart flow diagram for the measurement of drop size. The different stages of image processing consist of image preprocessing, edge detection, circle detection and size measurement.

Image preprocessing begins with the definition of an observation window, which is at least 15 mm away from the capillary tip, to ensure that drops have stable shapes. The grayscale image within the window is filtered to remove noise with the function ***wiener2*** based on statistics estimated from a local neighborhood of each pixel. This function applies a Wiener filter (a linear filter) to an image adaptively, tailoring itself to the local image variance. When the variance is large, ***wiener2*** performs a little smoothing. When the variance is small, ***wiener2*** performs much smoothing.

Group	Test	We_i	Re_i	Ca_o $(\times 10^{-3})$	Re_o
Group 1	Test1-1	0.9	11.1	0.91	176.7
	Test1-2	2.1	16.7		
	Test1-3	3.7	22.2		
	Test1-4	5.7	27.8		
	Test1-5	8.2	33.3		
	Test1-6	11.2	38.9		
Group 2	Test2-1	0.9	11.1	1.81	353.3
	Test2-2	2.1	16.7		
	Test2-3	3.7	22.2		
	Test2-4	5.7	27.8		
	Test2-5	8.2	33.3		
	Test2-6	11.2	38.9		
Group 3	Test3-1	0.9	11.1	2.72	530.0
	Test3-2	2.1	16.7		
	Test3-3	3.7	22.2		
	Test3-4	5.7	27.8		
	Test3-5	8.2	33.3		
	Test3-6	11.2	38.9		

Table 2.7 Values of the dimensionless numbers in three groups of experiments.

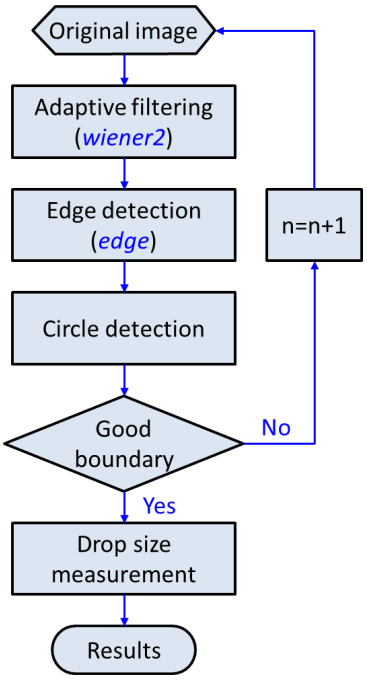

Fig. 2.11 Flow diagram of the image processing for drop size measurements.

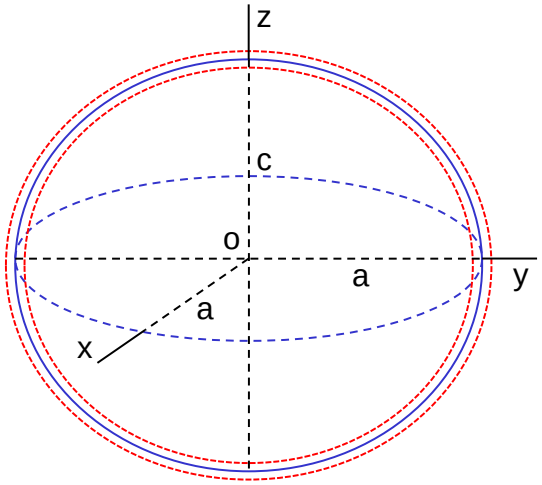

Fig. 2.12 Schematic of a oblate spheroid drop.

After the preprocessing, edge detection is performed to find the boundaries of drops within the image with the function ***edge***. It consists of detecting discontinuities in brightness. The Canny edge detector is used in the edge detection which is the most powerful method that ***edge*** provides. It finds edges by looking for local maximum of the gradient, which is calculated using the derivative of a Gaussian filter. The Canny method differs from the other edge-detection methods (Sobel, Prewitt, Roberts...) in that it uses two different thresholds to detect strong and weak edges. The weak edges are included in the output only if they are connected to strong edges. This method is therefore less likely than the others to be fooled by noise, and more likely to detect true weak edges. After edge detection, the resulting binary image is post-processed to eliminate undesired edges. The function ***BW2 = bwareaopen (BW, P)*** is used to remove all connected components (objects) that have fewer than ***P*** pixels, producing another binary image ***BW2***.

Based on the quasi-circular shapes of drops, a circle detection is performed to find edges of drops. The principle is according to the relation between perimeter and area of a circle: the square of the perimeter is equal to 4π times the area. We thus define a parameter as $4\pi area/perimeter^2$. If it is larger than a threshold (0.9 in the program), the object can be recognized as a circle. In special cases, small holes may exist on the edge of a circle, this method would not work at all. Hough transform is thus used for the circle detection. If a drop boundary is well detected, two circles are obtained to indicate the position of drop boundary (see red circles in Figure 2.12).

When the edges of drops are well detected and repaired, drop sizes are measured. The great majority of drops are oblate spheroids (Figure 2.12), the lengths of the major axis

($L_h = 2a$) and the minor axis ($L_v = 2a$) are measured as the maximum lengths in the horizontal and vertical directions, respectively. The reference length used for calibration is the external diameter (10 mm) of the glass tube. The equivalent diameter d_d of the drop is the diameter of the sphere having the same volume as the oblate spheroid. The diameter d_d is thus expressed as:

$$d_d = \sqrt[3]{L_h^2 L_v} \tag{2.7}$$

For each set of experimental conditions, the average drop size $\overline{d_d}$ is calculated by averaging numerous drops. The total number of drops with good boundaries varies in different set of experiments, which ranges from 100 to 800.

In the cases of high flow rates, the above image processing cannot obtain good boundary detection because of satellite drops, short interval distance between successive drops and small drop size. In these cases, the measurement of drop size is conducted with ImageJ by manually measuring the lengths of the major axis L_h and the minor axis L_v. If a parent drop is followed by a satellite drop, only the size of the parent drop is measured.

2.7 Characterization of the polymerization of a glue mixture in a flowing ionic solution

2.7.1 Experimental setup and procedure

In order to study the embolization process *in vitro*, the experimental setup for the co-flow injection of two immiscible liquids (Figure 2.9) has been improved to create and visualize the injection of glue mixtures into the flowing ionic solution (Figure 2.13). The experiment consists of injecting the G-L mixture into an *in vitro* ionic solution that is used to model the blood. The inner fluid is injected through a brass capillary tube (MBT3M, Albion Alloys) of internal diameter d_i = 0.45 mm. It is placed concentrically in a straight cylindrical glass tube of inner diameter d_o = 10 mm. The end of the capillary tube is connected to the mixture syringe with a three-way stopcock (CAD6011, Sigma-Aldrich). A syringe with a 5% glucose solution is attached to the other inlet of the stopcock. The outlet of the glass tube is connected to a silicon tube immersed in a beaker at its lower end. The beaker is used for collecting the polymerized drops. A magnetic stirrer (Microstirrer, VELP scientifica) is put beneath the beaker to avoid drops sticking together. A filter mesh is used to prevent drops flowing into the circuit of the outer fluid.

Before assembling and installing the experimental setup, the capillary tube and stopcock are flushed with the silicon oil and 5% glucose solution to avoid premature polymerization.

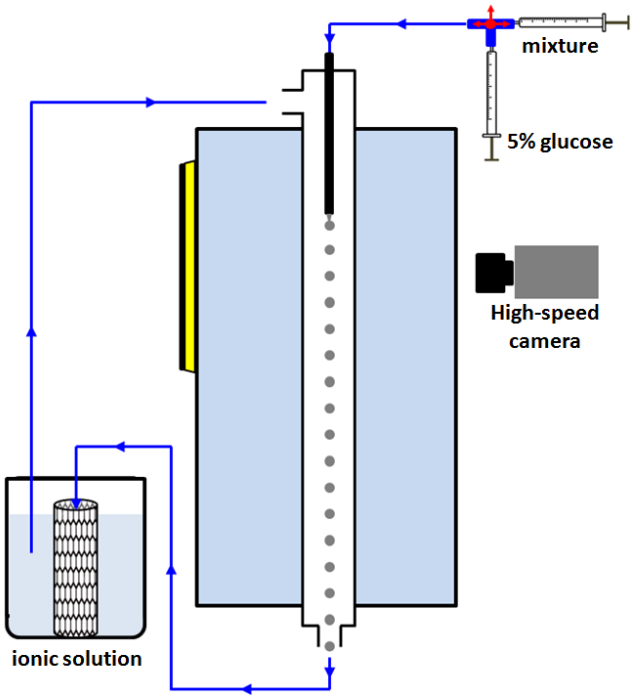

Fig. 2.13 Experimental setup to study the polymerisation of glue mixtures in flowing ionic solution.

The continuous-flow gear pump is first started. Its flow rate increases step-by-step from the minimum flow rate (65 ml/min) to the desired flow rate to avoid the generation of air bubbles into the circuit of the outer fluid. After about ten minutes, when the outer flow is fully developed, the syringe pump is started to inject the glue mixture. Both glue mixture and ionic solution are injected in the gravitational direction because of the larger density of the mixture compared to the ionic solution. After each injection of glue mixture, the capillary tube and stopcock are flushed again with 5% glucose solution (about 10 ml) to remove the residual glue mixture and avoid the blockage. After experiments, the injection tube is removed from the tank and cleaned thoroughly with acetone, which is a good solvent of cyanoacrylate glues. The cleaned injection tube can be reused again for a new injection to be made.

The injection process is recorded with a high-speed imaging system coupled with a back illumination source. All the recordings are performed immediately after the start-up of the injection. The recording time varies from 1.5 min to 2 min at the image frame rate 50 fps. All experiments are carried out at ambient temperature of 21 °C.

	μ_k ($\times 10^{-3}$ Pa·s)	ρ_k (kg/m^3)	γ ($\times 10^{-3}$ N/m)
G-L mixture 25% ($k = i$)	21.6	1208.5	∼14.6
Ionic solution ($k = o$)	3.8	1094.5	

Table 2.8 Physical properties of the modeling fluids used for the glue injection *in vitro*.

	In vitro	*In vivo*
$\delta = d_o/d_i$	22.2	4.4–20
$\eta = \mu_i/\mu_o$	5.7	1–8
Re_i	4.1	≤15
Re_o	395.9	200–600
We_i	1	≤2
Ca_o	3.9×10^{-2}	28×10^{-3}–50×10^{-3}
Bo	1.6×10^{-2}	$\leq 6 \times 10^{-2}$

Table 2.9 *In vitro* values of the dimensionless numbers used for the glue injection compared with *in vivo* values during portal vein embolization [83].

2.7.2 Modeling fluids and dimensionless numbers

The experiment is conducted with the same glue mixture used for the embolization procedure. We recreate the similar conditions as those of the physiological case (Table 2.9). A capillary number of 3.9×10^{-2} is chosen which is the mean value of the physiological range of Ca_o. A Weber number of 1 is simulated, which corresponds to the dripping regime. Ionic solution with glycerol is used as the outer liquid and the G-L mixture (C_G = 25%) as the inner liquid. The ionic solution is prepared with the composition in Table 2.1. The G-L mixture (C_G = 25%) is mixed with the Luer-Syringe method. The physical properties of the two liquids have been measured and shown in Table 2.8. The values of dimensionless numbers tested are shown in Table 2.9.

Chapter 3

Polymerization kinetics of glue mixtures with ionic solutions

In the embolization procedure, the embolic glue polymerizes quickly when it is exposed to the blood. The polymerization kinetics thus play an essential role in the control of the injection and subsequent flow occlusion processes. In this chapter, we first assess the miscibility of nBCA glues with Lipiodol and then study the influence of the blood anions on the glue polymerization. A new experimental setup has been designed to systemically characterize the polymerization of the glue mixture on contact with an ionic solution, which reproduces the similar ionic composition as the human blood. The results shown in this chapter have been published in Li *et al*. [55].

3.1 Miscibility of pure nBCA glue with Lipiodol

Images of a Histoacryl-Lipiodol system at different time intervals are shown in Figure 3.1. At the beginning of the experiment ($t = 0$ h), the interface ($z = 0$) between the glue (dark) and Lipiodol (clear) is sharp. An interdiffusion process then takes place until a homogeneous mixture is formed at $t = 46$ h. This indicates that nBCA glue and Lipiodol are miscible. Grey level profiles $G_m(z,t)$ along the z-axis at different times are shown in Figure 3.2. At the beginning of the experiment ($t = 0$ h), $G_m(z,0)$ is a step function: $G_m(z,0) = 91$ for $z < 0$ (clear Lipiodol) and $G_m(z,0) = 27$ for $z > 0$ (dark Histoacryl glue). As nBCA molecules diffuse into Lipiodol, the diffusion front, which corresponds to the position along the z-axis where the grey level begins to decrease, moves downwards. Owing to this process, the grey level profile changes from a step function to a sigmoidal shape. The distance, over which the diffusion front propagates is defined as the diffusion length. It increases with time until

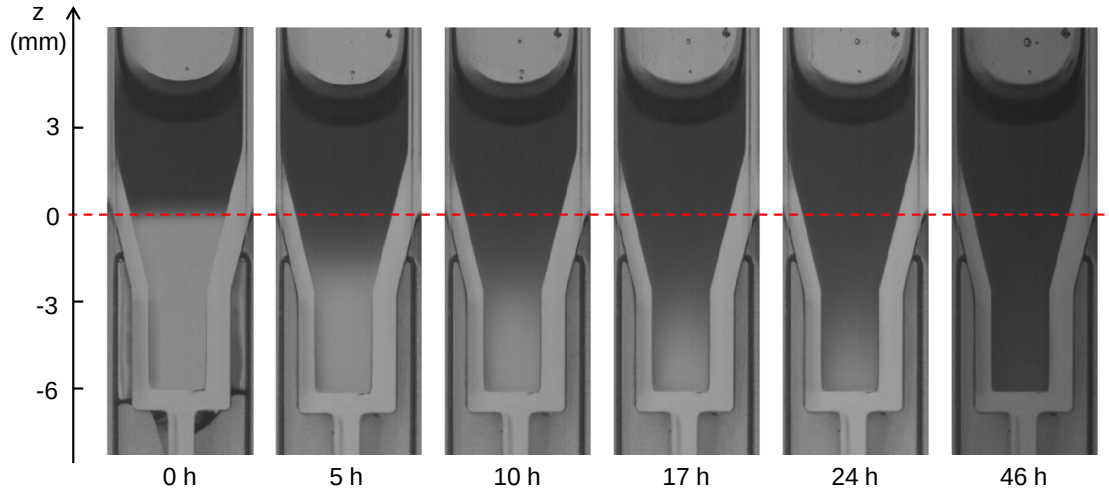

Fig. 3.1 Time evolution of nBCA glue put in contact with Lipiodol: the darkening of the system over time shows that the two liquids are miscible. The dashed line shows the initial position of the interface.

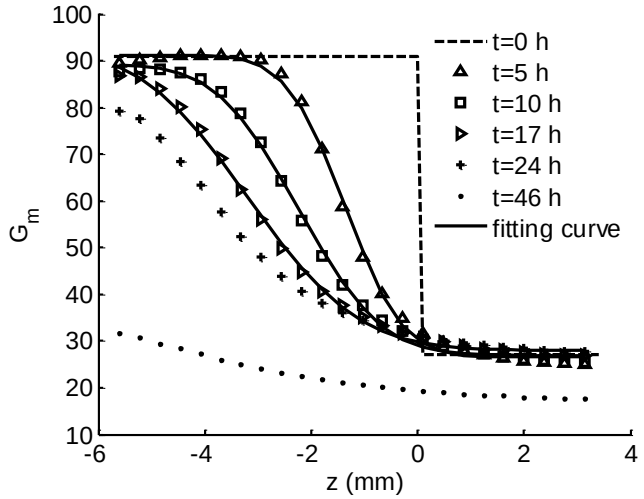

Fig. 3.2 Grey level distribution along the cup axis for different times. The dashed line shows the initial position of the interface. Here, the bottom of the cup is at $z = -6$ mm.

the diffusion front reaches the bottom of the cup at $t \sim 17$ h, which corresponds to $z = -6$ mm (Figure 3.2). Afterwards, the diffusion process continues leading to a further decrease in the grey levels in the Lipiodol region ($z < 0$) until a quasi-uniform distribution $G_m(z,\infty)$ is reached.

Since the grey level is proportional to the local concentration at each point in the domain, one can evaluate the diffusion coefficient of nBCA glue in Lipiodol by means of Fick's second law. We consider the one-dimensional case of diffusion, in which two miscible liquids of different concentrations ϕ_1 and ϕ_2 ($\phi_1 > \phi_2$) are initially put in contact at position $z = 0$. We only study the early stages of diffusion, for which the boundary conditions are $\phi(z) \to \phi_1$ for $z \to -\infty$ and $\phi(z) \to \phi_2$ for $z \to +\infty$. Fick's second law thus leads to the concentration distribution:

$$\phi(z,t) = \frac{\phi_1 + \phi_2}{2} - \frac{\phi_1 - \phi_2}{2} \mathrm{erf}\left(\frac{z}{2\sqrt{Dt}}\right), \tag{3.1}$$

where $\phi(z,t)$ is the molecular concentration, erf is the error function and D is the diffusion coefficient. As illustrated in Figure 3.2 for three instants of time, we fit the data with Eq. (3.1), in which we replace ϕ by G_m, and deduce the value of the diffusion length $2\sqrt{Dt}$ at time t. The diffusion lengths are thus measured by fitting the grey level profiles between 0 and 17 hours. As shown in Figure 3.3, the square of the diffusion length $4Dt$ is directly proportional to time t. We deduce the value of the diffusion coefficient D and find $D = 2.1 \times 10^{-11}$ m^2/s, which is lower than in the case of an aqueous solution ($D \sim 10^{-10} - 10^{-9}$ m^2/s). Diffusion of nBCA glues in the Lipiodol oil is thus slower than diffusion in water solutions. A similar diffusion process is obtained for Glubran 2, proving that cyanoacrylate glues are miscible in Lipiodol. We have also checked that a mixture of Glubran and Lipiodol is stable over days: no tendency towards phase separation is observed.

The last point that remains is to estimate how homogeneous the mixture is upon the mixing process. In the present study, the two liquids are mixed by forcing a volume of 0.2 mL through a luer connector of diameter $d_L = 2$ mm every 0.6 s, which corresponds to a shear rate $\dot{\gamma} \sim 200$ s^{-1}. The ratio between the convection and diffusion times is thus $Dd_L^2/\dot{\gamma} \sim 10^{-19}$. It follows that the convective mixing procedure is efficient.

3.2 Characterization of the volumetric polymerization

3.2.1 Time-evolution of the glue-mixture opacity

We first analyze the volume polymerization and the propagation of a polymerization front within the glue mixture. Tens of minutes after the end of the aspiration, a polymerization front begins to propagate upwards from the interface within the glue mixture (Figure 3.4a).

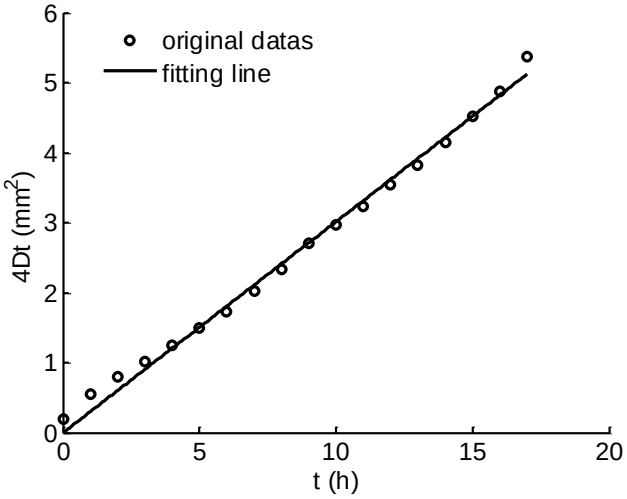

Fig. 3.3 Correlation between the diffusion length and time.

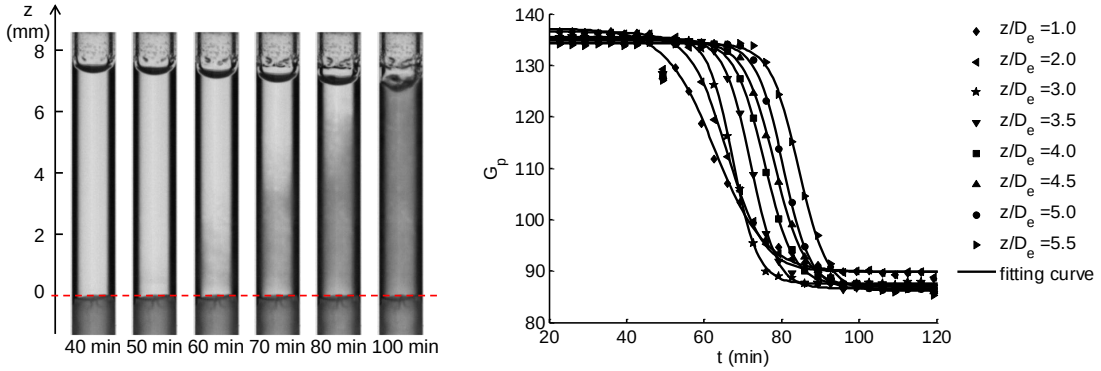

(a) (b)

Fig. 3.4 Time evolution of G-L mixture ($C_G = 50\%$) in contact with the ionic solution. (a) The darkening in the glue mixture over time shows the propagation of a polymerization front upwards from the interface. (b) Time evolution of the grey level at different positions in the glue mixture: the symbols correspond to experimental points and the continuous lines to the correlations given by Eq. (3.2).

Since the interface between the mixture and the ionic solution is dark, the grey level change cannot be measured in its vicinity. Measurements are only meaningful for $z \geq D_e/2$. We show in Figure 3.4b the time evolution of the grey level at different locations along the tube axis for $z/D_e \geq 0.5$. The grey levels decrease from the initial value $G_{p0} \sim 135$ to the asymptotic value $G_{p\infty} \sim 90$. Since the polymerization front propagates from the interface, the further the point location is from the interface, the later the decrease in G_p starts occurring. The fact that the curves get closer to one another as z increases indicates that the propagation velocity increases with z. One can also note that the front becomes steeper.

For every value of z, the curve $G_p(z,t)$ can be fitted with a sigmoid:

$$G_p(z,t) = G_{p0} - \frac{G_{p0} - G_{p\infty}}{1 + \exp\left(-\dfrac{t - t_{1/2}(z)}{\tau_v}\right)}, \tag{3.2}$$

where τ_v is the characteristic time and $t_{1/2}(z)$ is the half time, such that $G_p(t_{1/2}) = (G_{p0} + G_{p\infty})/2$. The sigmoidal fitting of the grey level time-evolution works as well as in the example shown in Figure 3.4 for all the tested concentrations in Glubran 2 and Histoacryl. The time τ_v corresponds to an empirical measure of the time that it takes the polymerization to be completed at position z (based on the grey level in the fluid). Indeed, it takes about $5.9\tau_v$ for the grey level at z to drop from $G_{p0} - 0.05(G_{p0} - G_{p\infty})$ to $G_{p0} - 0.95(G_{p0} - G_{p\infty})$. Figure 3.5a shows values of τ_v for Histoacryl and Glubran 2. Results are only provided for $C_G = 50\%$ and 75%, as no value could be obtained with sufficient precision for $C_G = 100\%$, the propagation being too fast. In all the cases, τ_v decreases with z, the distance away from the interface. It indicates that the polymerization reaction is slow near the interface during the initiation of the process, and that the reaction accelerates as it propagates away from the interface. A constant value for τ_v is always reached for $z/D_e \geq 2.5$. Figure 3.5a also shows that the polymerization time decreases significantly when the glue concentration increases. All these results hold both for Glubran 2 and Histoacryl.

Figure 3.5b shows the half time $t_{1/2}$ for all the glue concentrations, which is a measure of the polymerization front progression. The half time increases slightly with z. It also strongly increases with the Lipiodol concentration, as indicated by the logarithmic scale used to plot the results (Figure 3.5b). This means that low glue concentration leads to a delay in the propagation of the volumetric polymerization, while this process is very fast for pure glue, as can be surmised from the corresponding small value of $t_{1/2}(z)$. It is also possible to infer the propagation speed of the polymerization front $v_p = z/t_{1/2}(z)$. Since $t_{1/2}(z)$ levels out when z increases, the propagation speed increases almost linearly with z, as shown in Figures 3.6a-b. The value of v_p increases with C_G and z, which may be due to the fact that

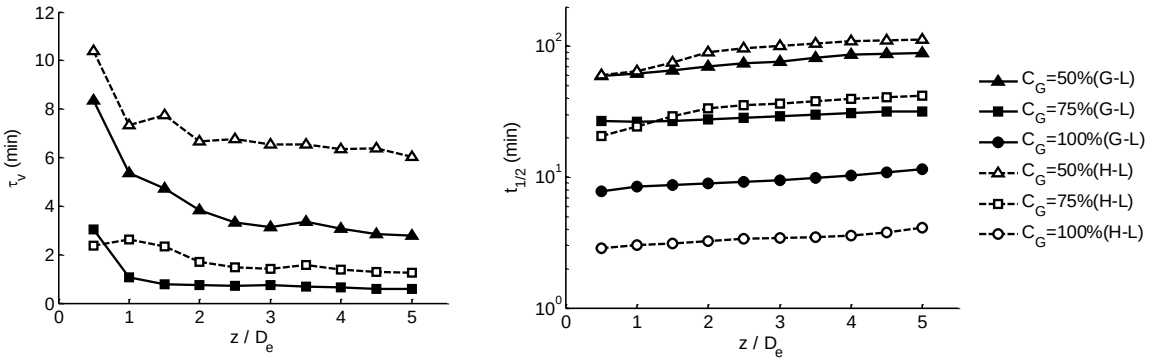

(a) (b)

Fig. 3.5 Average characteristic time τ_v (a) and half time $t_{1/2}$ (b) of volume polymerization for different glue concentrations.

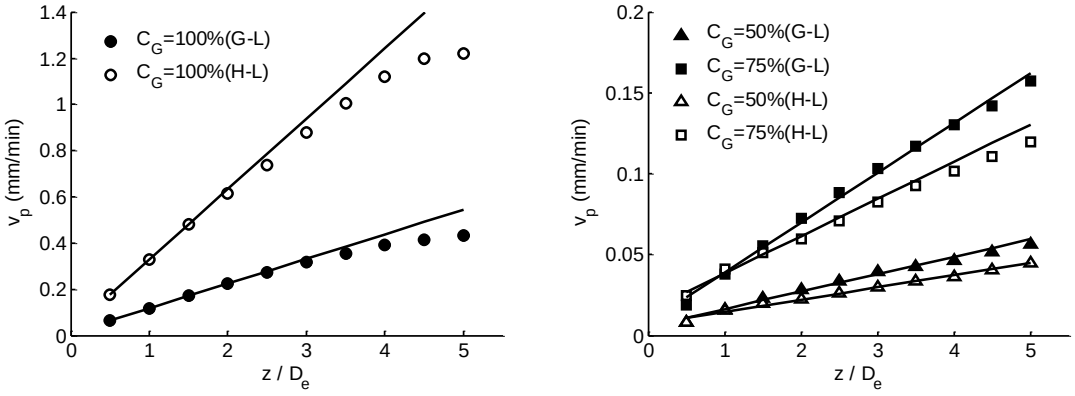

(a) (b)

Fig. 3.6 Average propagation velocity v_p for G-L and H-L mixtures at different glue concentrations.

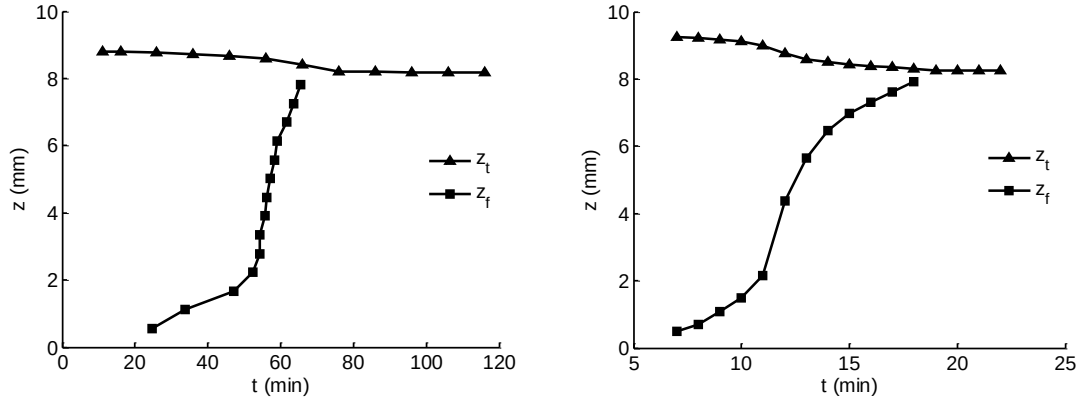

Fig. 3.7 Total length H and position of the beginning of the polymerization front z_f as a function of time for G-L mixtures. (a) $C_G = 50\%$, (b) $C_G = 100\%$.

the polymerization reaction is exothermic and that the temperature increases along z. The increase of the front velocity with temperature and monomer concentration has been indeed predicted by propagation models [86, 38].

3.2.2 Time-evolution of the glue mixture height

As is apparent in Figure 3.4a, a change in volume occurs in the glue mixture during volumetric polymerization. To assess the change in volume and see whether it is linked with the chemical reaction, we plot the time-evolution of the coordinate $z_t(t)$ of the top of the glue mixture column in Figure 3.7, along with the coordinate $z_f(t)$ of the polymerization front. The front position in the glue mixture ($z_f > 0$) is calculated assuming that polymerization begins at the location, where the grey level has decreased by 5% from its initial value, which occurs at time $t_{1/2}(z_f) - 3\tau_v(z_f)$. The results are plotted for two concentrations in Glubran 2 for illustration, similar results having been obtained for Histoacryl. Figure 3.7 shows that the decrease in glue mixture height can be correlated with the progression of the polymerization inside the glue: as the polymerization front advances, the coordinate $z_t(t)$ moves down with time. Since the height decrease stops when $z_f \sim z_t$, i.e. when the polymerization front has reached the top of the glue column, it is clear that the two processes, glue polymerization and height reduction, are coupled. Note that the time evolution of $z_f(t)$ again shows the significant acceleration of the polymerization, as it progresses inside the glue.

The decrease in volume means that the density of the glue increases as it polymerizes. It is thus possible to assess the relative increase in density of the polymerized glue from the

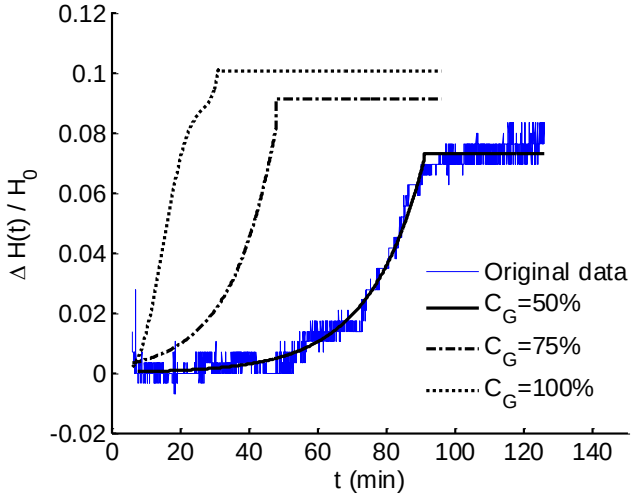

Fig. 3.8 Height reduction at different glue concentrations for G-L mixtures.

$\Delta\rho/\rho_\infty(\%)$	$C_G = 50\%$	$C_G = 75\%$	$C_G = 100\%$
G-L	7.6 ± 2.2	9.1 ± 1.4	11.1 ± 1.1
H-L	9.8 ± 0.9	10.3 ± 0.8	11.5 ± 0.7

Table 3.1 Average relative density increase for different glue concentrations.

relative reduction in height:

$$\frac{\rho(t)-\rho_0}{\rho(t)} = \frac{z_t(0)-z_t(t)}{z_t(0)}. \tag{3.3}$$

The relative height decrease is shown in Figure 3.8 as a function of time in the case of G-L mixtures. Note that instead of writing $(z_t(0)-z_t(t))/z_t(0)$, we have chosen to denote the relative height reduction as $\Delta H(t)/H_0$ in the figure. It appears that the volume reduction increases with the glue concentration. We also recover the fact that the polymerization speed increases with C_G. The relative density increase is shown in Table 3.1, where $\Delta\rho$ is the density increase after full polymerization. For G-L mixtures, the higher the glue concentration, the greater the density increase due to polymerization. For H-L mixtures, the density increase is almost independent of concentration, and somewhat larger than for G-L mixtures.

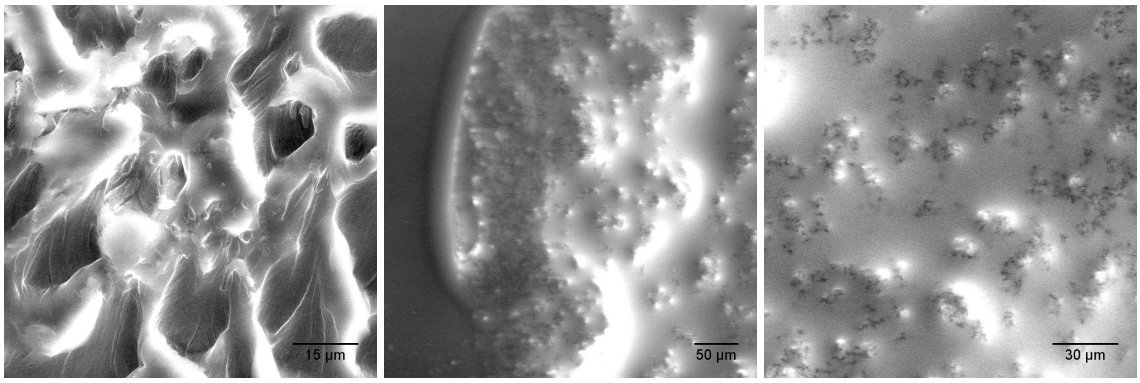

(a) (b) (c)

Fig. 3.9 Scanning electron micrograph of the polymerized glue mixture. (a) Pure Glubran $C_G = 100\%$, (b) and (c) Glubran-Lipiodol mixture $C_G = 50\%$: the polymerized glue structure is immersed in oil.

3.2.3 Microscopic observation of the polymerized glue-mixture

The cross section of the polymerized cylinder of the glue mixture has been observed with a scanning electron microscope (QUANTA FEG 250, FEI, US). Pure Glubran glue (C_G = 100%) exhibits a complex polymerized network (Figure 3.9a). In the case of a glue-oil mixture, the oil invades all the void space between the polymerized glue, as shown in Figures 3.9b-c for $C_G = 50\%$. The oil appears as a smooth film from which emerge some glue islets.Since the oil surface is smooth, it is very difficult to get a good SEM definition. The spectroscopy analysis does indeed show the presence of iodine, and thus proves that oil is indeed present (recall that Lipiodol is an iodized oil).

3.3 Characterization of the initiation of the polymerization: interfacial polymerization

3.3.1 Time-evolution of the glue-mixture opacity

Interestingly enough, the tube device can also be used to study the initiation of the polymerization process and its propagation in a thin film of glue. Indeed, as soon as the aspiration is stopped ($t = 0$), the ionic solution begins to darken (Figure 3.10a), indicating that a polymerization process is occurring. This phenomenon corresponds to the polymerization of a thin film of glue, which is left behind in the $z < 0$ region, during the quick ascension of the glue mixture, when the ionic solution is aspirated. Figure 3.10b shows the time evolution of the grey level at 3 locations in the ionic solution ($z < 0$) for the measurements of Figure 3.10a.

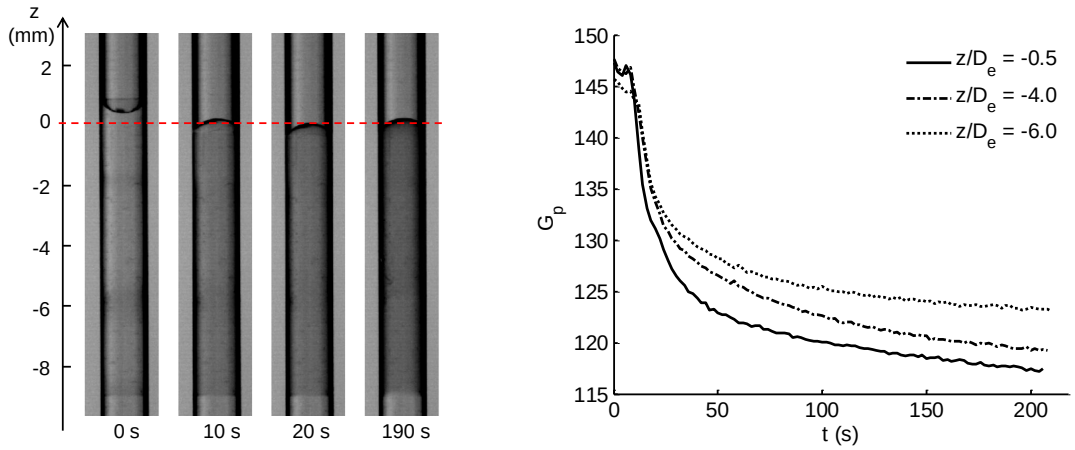

(a) (b)

Fig. 3.10 Change in opacity observed in the ionic solution in the case of a G-L mixture ($C_G = 50\%$). (a) Darkening in the ionic solution revealing a polymerization of the G-L film left behind on the tube wall. (b) Grey level time evolution at different positions within the ionic solution.

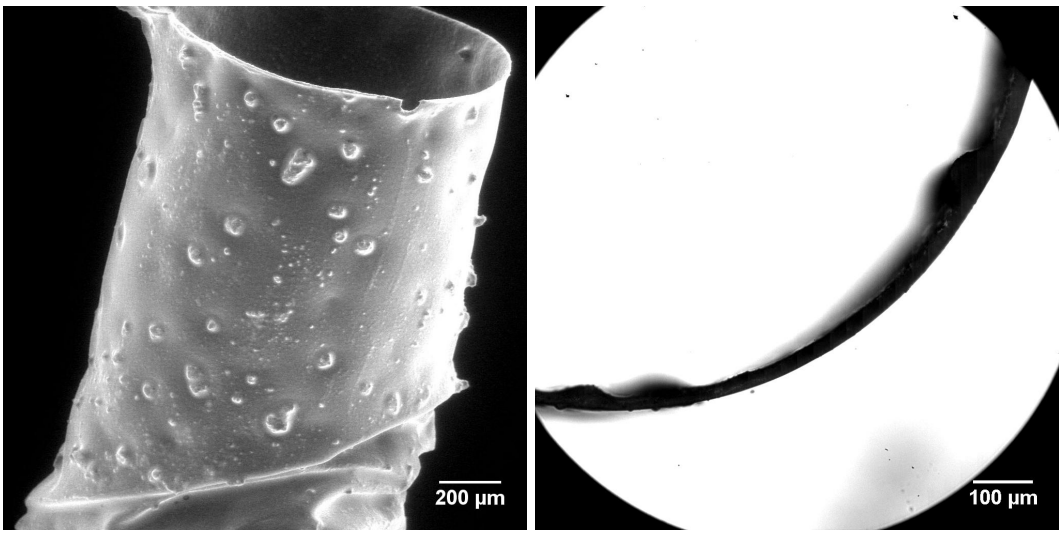

(a) (b)

Fig. 3.11 G-L mixture ($C_G = 50\%$): (a) Scanning electron micrograph of a G-L film removed from the tube, (b) optical micrograph of a film section.

$\tau_f \pm \sigma$ (s)	C_G = 50%	C_G = 75%	C_G = 100%
G-L	116 ± 8	79 ± 11	54 ± 9
H-L	86 ± 9	66 ± 13	41 ± 3

Table 3.2 Average characteristic times τ_f for which 90% of film polymerization has occurred. Results are for Glubran-Lipiodol and Histoacryl-Lipiodol mixtures, with different glue concentrations.

The initial value of the grey level $G_p(z,0) \sim 147$ corresponds to that in the ionic solution prior to any polymerization reaction. It then decreases with time, first sharply ($t \leq 50$ s), then slowly for 50 s $< t <$ 200 s and finally very slowly ($\sim$ 5 grey level unit change ov er for 90 min or more). Similar trends are obtained for all the glue concentrations, both in the case of Glubran 2 and Histoacryl. At the end of the experiments, when the polymerization is well completed, the thin film can be removed from the tube (Figure 3.11a), cut in sections and measured under a microscope (Figure 3.11b). The thickness of the film has nearly the same value $e = 24 \pm 2$ μm for all glue concentrations. The theoretical value of e can be estimated using Bretherton's theory [8]:

$$e = \alpha \frac{D_t}{2} (\mu V/\gamma)^{2/3}, \tag{3.4}$$

where D_t is the internal tube diameter and V is the ascending velocity during the aspiration phase. The factor α takes values between 1.34 (in the case of a clean interface) and 3.37 (in the case where Marangoni effects have the most important effect due to the presence of surfactants) [88]. Using the results of section 2.2 and $V \sim 3$ mm/s, we find $e \sim$ 14 - 35 μm for all the glue concentrations. The experimental value that we have measured falls within those limits, which is satisfying knowing that the film is presently generated under the combined effects of flow and polymerization.

The time evolution of the grey levels measured in the film (e.g. Figure 3.10b) can be used to assess the early stages of polymerization in a thin film. As it is not possible to fit the time-evolution curves with a simple exponential curve, we define the time τ_f as the time for which the grey level has decreased by 90% in the first 200 s:

$$G_p(z,\tau_f) = G_p(z,0) - 0.9[G_p(z,0) - G_p(z,200)]. \tag{3.5}$$

For all the glue concentrations, we find that τ_f decreases slightly when z decreases, a result which can be inferred from Figure 3.10b: this effect is due to gravity-induced film thinning. To exclude a possible influence of gravity, we thus consider the values of τ_f obtained for $z/D_e \in [-1,-3]$, a location where the film thickness has roughly the value given

by Eq. (3.4). The average values of the characteristic time τ_f are shown in Table 3.2 for the different glue mixtures. In all the cases, τ_f is of the order of 1 to 2 min, which is much shorter than the propagation times which were measured for volumetric polymerization in section 3.2.1. This can be explained by the fact that the film interface between the glue mixture and the ionic solution has a small thickness along which the reaction can propagate, and a comparatively large area. The time τ_f then essentially measures the initiation of the polymerization upon contact with anions. This explains why, for a given glue, increasing the Lipiodol concentration increases τ_f: the initiation of polymerization takes more time because there are less monomer molecules available. For any concentration, the polymerization time is shorter for pure nBCA glue than for Glubran 2 (Table 3.2), thus indicating that the functional monomer MS leads to an increase in the polymerization time of the glue.

3.3.2 Microscopic observation of the polymerized film

SEM micrographs of the film surface are shown in Figure 3.12. For pure Glubran 2, the film structure (Figure 3.12a) is analogous to the one observed for the volume polymerization in the bulk (Figure 3.9a). However, in the case of glue-oil mixtures, the process is different: the mixture undergoes phase separation upon contact with the aqueous ionic solution. The tensioactive glue molecules are now located on the surface of the oil droplets. When the glue polymerizes, it encapsulates the oil droplets in a manner which is analogous to the procedure used to produce cyanoacrylate nanocapsules for drug transport [32]. The spectroscopic analysis of the white spherical particles in Figure 3.12b indicates the presence of iodine, and thus of Lipiodol. The defects that are observed on the surface of the film (Figure 3.11a) are probably due to the damage of encapsulated oil droplets during the removal of the film from the tube. Note that this phase separation/encapsulation process does not occur in the glue mixture volume, because there is no direct contact between the oil and the aqueous solution except at the tube wall.

3.4 Influencing factors of the polymerization process

The polymerization of glue mixture can be affected by many factors such as the preparation methods of glue mixtures and the compositions of ionic solutions. In this section, the influences of three factors on the polymerization of the G-L mixture at $C_G = 50\%$ are studied. The factors include the mixing methods of glue mixtures, ionic concentrations and glycerol in ionic solutions.

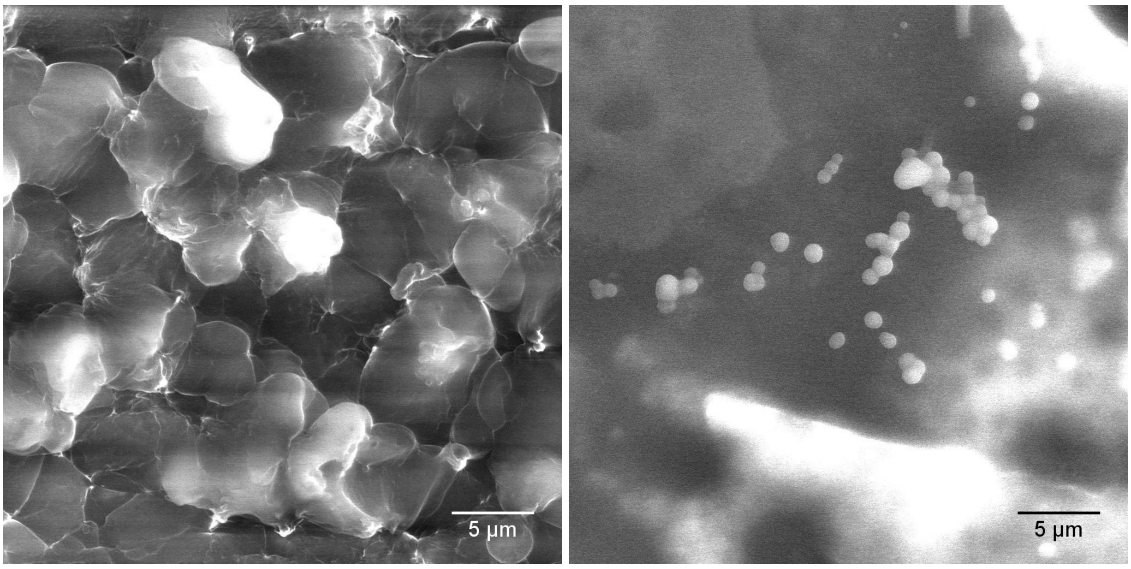

(a) (b)

Fig. 3.12 Scanning electron micrograph of the film surface: (a) pure Glubran, (b) G-L mixture ($C_G = 50\%$) where encapsulated oil droplets appear on the surface.

τ_f (s)	Luer-Syringe	Cup-Syringe	Air-Syringe
G-L ($C_G = 50\%$)	116 ± 8	132 ± 10	113 ± 6

Table 3.3 Average characteristic times τ_f for which 90% of film polymerization has occurred. Results are for G-L mixture ($C_G = 50\%$), with different mixing methods.

3.4.1 Effect of the mixing method

The three mixing methods presented in section 2.1 are used to prepare the G-L mixture ($C_G = 50\%$). Both the interfacial and volumetric polymerization of the mixture are observed in all the cases. In the interfacial polymerization, the average values of the characteristic time τ_f are shown in Table 3.3. τ_f is in the order of 2 min, which is almost independent of mixing methods considering the standard deviations. Figure 3.13 shows the average characteristic time τ_v and half time $t_{1/2}$ of volumetric polymerization for different mixing methods. In all cases, τ_v decreases with z and reaches a constant value for $z \geq 2.5$ mm (Figure 3.13a). Half time $t_{1/2}$ for the Air-Syringe method is larger than that for the other two methods, indicating that mixtures prepared by Air-Syringe method polymerize more slowly (3.13b). This phenomenon may result from the insufficient and inhomogeneous mixing of the Air-Syringe method, which can be inferred from the large standard deviation.

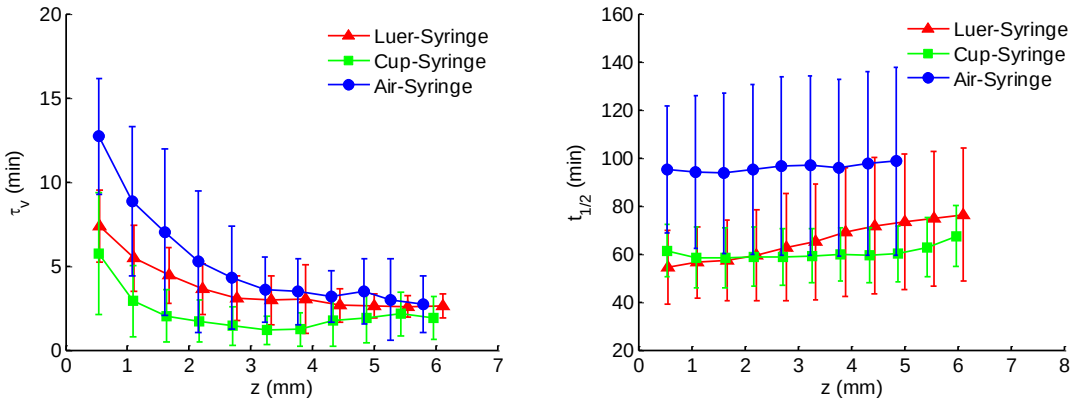

(a) (b)

Fig. 3.13 Average characteristic time τ_v (a) and half time $t_{1/2}$ (b) of volume polymerization for different mixing methods.

τ_f (s)	IS	IS1/2	IS1/4
G-L ($C_G = 50\%$)	41 ± 3	51 ± 6	60 ± 12

Table 3.4 Average characteristic times τ_f for which 90% of film polymerization has occurred. Results are for G-L mixture ($C_G = 50\%$), with different diluted ionic solutions.

3.4.2 Effect of the ionic concentration

Ionic solutions with different dilution levels are used to initiate the polymerization of the G-L mixture ($C_G = 50\%$). In all the cases both the interfacial and volumetric polymerization are observed. The characteristic time τ_f slightly increases with the dilution level (Table 3.4).

3.5 Discussion and conclusion

We have conducted an *in vitro* study to quantitatively investigate the physical properties and the polymerization process of cyanoacrylate glues mixed with Lipiodol at various concentrations, Lipiodol being added to make them radio-opaque. Two glues have been investigated: Histoacryl, which is a pure nBCA glue, and Glubran 2, which is composed of nBCA and metacryloxysulpholane. We have confirmed that glue and Lipiodol are miscible. The addition of Lipiodol has the effect of modifying the physical properties of the glue: the viscosity, density and interfacial tension of the mixture with water all increase with the relative concentration in Lipiodol.

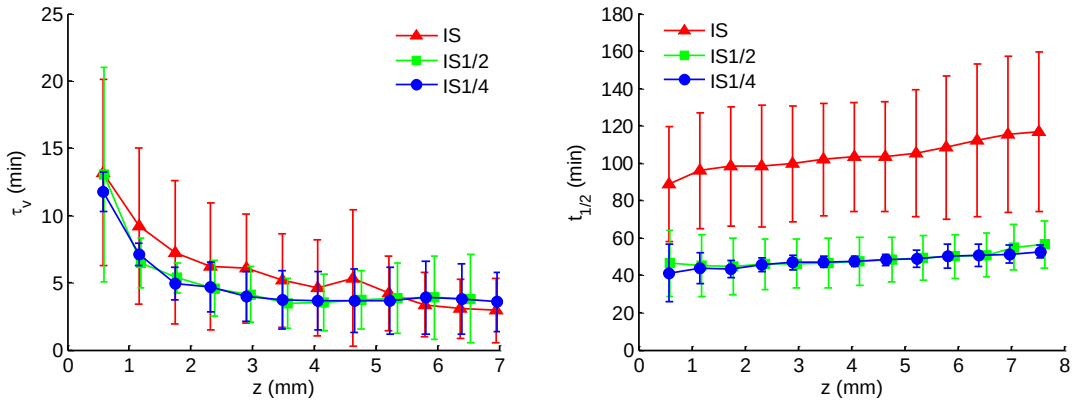

(a) (b)

Fig. 3.14 Average characteristic time τ_v (a) and half time $t_{1/2}$ (b) of volume polymerization for diluted ionic solutions.

The experimental setup allows to rigorously investigate the glue polymerization when it is brought in contact with an anionic solution, analogous to blood. The principle of the technique relies on the formation of a well-defined interface between the two liquids and on an objective measurement of the progression of the polymerization reaction by means of a high-speed imaging system, which measures the grey level change in the system. The results are very reproducible.

Various studies have reported on the polymerization mechanisms of nBCA under different experimental conditions [26, 57, 67]. They indicate that there are three distinct mechanisms whereby polymerization of pure nBCA may be initiated: anionic polymerization initiated by simple anions (acetate, hydroxide, cyanide, ...), zwitterionic polymerization initiated by covalent organic bases (either weak ones such as alcohol and amine, or strong ones such as triethylamine or pyridine), radical polymerization initiated by radicals. But in practice, the two favored modes are anionic and zwitterionic under classical experimental conditions. Hydroxide ions have been shown to provide optimal conditions for polymerization among all possible anions [30, 31]. As for Glubran 2, Levrier *et al.* [54] briefly mentioned in the introduction that the Glubran 2 polymerization pathway is radical contrary to pure nBCA, but none of the studies provided as references were conducted on the nBCA-MS monomers. It is, thus, difficult to know from the literature the exact mechanism responsible for the polymerization of Glubran 2.

We find that there is an initial polymerization phase, which is first very fast, since a 24-μm film is almost completely polymerized (and solidified) in 1 to 2 min depending on glue concentration. The polymerization of the mixture starts seconds after contact with the ionic solution and occurs at the interface between the two liquids. We confirm that the initial

polymerization time increases with the proportion of Lipiodol, as was also found in previous studies with other methods [11, 93, 20]. This increase might be caused by the screening effect of oil molecules, which lowers the contact probability between the glue and anions. However, for nBCA-oil mixtures with $C_G = 50\%$, these previous studies report polymerization times between 3 s and 9 s, which are significantly smaller than the ones we measure ($\tau_f \sim 86$ s). The discrepancy may be due to the rather imprecise way the polymerization was assessed (change of opacity) in those studies and to the ionic fluid used (foetal veal serum, usually). Indeed, Figure 3.10 shows clearly that there is a fast drop in opacity during the first 10 s of contact, which is followed by a slower process as the reaction progresses inside the film. The differences in grey levels of the images in Fig. 3.10a for $t \geq 10$ s are not measurable with the naked eye and it takes a good imaging system to detect them.

Once the reaction is initiated, the glue mixture gradually polymerizes in volume, leading to the propagation of a polymerization front along the tube axis. This propagation process is slow and can take between 10 to 60 min for a 0.5 mm progression, the shortest time occurring for pure Glubran 2. Note that, for pure Histoacryl, the propagation over 0.5 mm takes only 3 min, which is extremely fast. During volume propagation, the initiated polymer chain increases by successively adding monomer molecules. Owing to this process, the intermolecular van-der-Waals forces convert to covalent bonds [1]. This results in a volume reduction and a density increase. Monitoring the volume shrinkage, or equivalently the change in length of the glue mixture, can thus be a simple alternative to the grey level analysis. As expected, the shrinkage increases with glue concentration (Figure 3.8). Indeed, the addition of Lipiodol increases the dilution of monomer molecules and increases both the polymerization half time and the shrinkage of the volumetric polymerization. Note that Glubran 2 results from the addition of a MS group to nBCA molecules, in order to slow down the polymerization process. Our results confirm that this objective is reached for pure glue (100%), but that the effect is inverted or not very important when the glue is mixed with Lipiodol (Figure 3.5).

We have also tested very dilute mixtures ($C_G = 25\%$), which are sometimes used by some surgeons for embolization. The results of the experiments showed that no measurable grey level change could be obtained within the G-L volume, and that the glue mixture was still liquid days after the experiment was stopped. This proves the difficulty of the reaction to propagate within the glue volume for low concentrations such as $C_G = 25\%$. A polymerization reaction, however, occurred at the interface between the glue mixture and the ionic solution and led to the formation of a sheet of solidified glue: its existence was verified by introducing a wire into the tube. Measurement of the time constant of the interfacial polymerization was obtained within the thin film of glue mixture left on the tube wall below

the interface. A value of $\tau_f = 123$ s was measured, which is consistent with the other results indicated in Table 3.2. We conclude that, for $C_G = 25\%$, the polymerization only occurs over small distances at a slow reaction rate.

For the sake of completeness, we have also tested very dilute mixtures of Glubran or Histoacryl with Lipiodol, $C_G = 25\%$, a concentration that is sometimes used by surgeons for embolization. The vertical setup of Figure 2.5 could not be used as such in this case, since the glue mixture is denser than the ionic solution (see Figure 2.2): the configuration would have been prone to a Rayleigh-Taylor instability. The experiment was thus conducted in a horizontal tube. No measurable grey level change could be obtained within the glue mixture, which remained liquid for days after the experiment was stopped. This proves that it is very difficult for the polymerization to propagate within the glue volume when the concentration is as low as $C_G = 25\%$ in the case of an anionic initiation of the reaction. A polymerization reaction, however, occurred at the interface between the glue mixture and the ionic solution in the tube cross-section and led to the formation of a film of solidified glue: its existence was verified by introducing a wire into the tube. A thin film of glue was also left along the tube wall, which led to a grey level change in the ionic solution, as discussed previously (see section 3.3). The corresponding time constant of the film polymerization was found to be $\tau_f = 123$ s, which is consistent with the results of Table 3.2. We conclude that, for $C_G = 25\%$, the polymerization only occurs over micron scale distances and is slow.

All the present findings provide interesting results to interventional radiologists, who use Glubran 2 and Histoacryl as liquid embolic adhesives for vascular embolization. The glues are rarely used pure, because of the necessity to visualize their propagation in the vascular network and because of their very fast rate of polymerization on contact with anions. They are mixed with the radio-opaque Lipiodol oil, which, we have shown, modifies the time constants of polymerization: it results in a lengthening of the polymerization time and thus in a safer use of the mixture for embolization. To prevent premature polymerization in the micro-catheter or its blockage in the vessel during glue injection, clinicians tend to use glue concentrations $C_G \leq 50\%$. Our study shows that there is then a trade-off between delayed interfacial polymerization and full volume solidification.The hydrodynamic stresses exerted by blood circulation could well break up the droplets of injected glue at the early stages of their formation and prevent them from reaching the targeted site [2]. It is thus of paramount importance to study the interaction between injection hydrodynamics and glue polymerization, and extend the two-fluid injection study previously conducted on non-reacting liquids [83].

Chapter 4

Polymerization kinetics of glue mixtures with proteinaceous solutions

The plasma proteins consist of albumins (55%), globulins (38%), fibrinogen (7%) and regulatory proteins ($< 1\%$). In order to determine the polymerization kinetics of Glubran-Lipiodol mixtures upon contact with proteins, we have reproduced a proteinaceous solution to initiate the polymerization reaction. The solution is composed of an ionic solution (IS) with the same ion contents as blood and a quantity of BSA, which is used to represent the main protein in blood. The results shown in this chapter have been submitted to the *Journal of the Mechanical Behavior of Biomedical Materials* in 2017 [56].

In the following, we first present the results obtained with the 8% BSA ionic solution, which are considered as reference, and then consider the effect of the protein concentration of the ionic solution and of the concentration in glue of the glue-Lipiodol mixture. Interestingly, we find a similar polymerization kinetics in all cases, with the occurrence of two main phases: they will be denoted as fast and slow volumetric polymerization phases owing to their respective characteristic times.

4.1 Fast volumetric polymerization

Typical results are shown for a glue mixture ($C_G = 50\%$) in contact with an 8% BSA ionic solution (IS-BSA8). As soon as the glue mixture is in contact with the proteinaceous solution, it darkens: this means that the glue becomes denser and thus that polymerization is occurring. The polymerization front propagates upwards within the glue mixture (Figure 4.1a). When the front has travelled a certain distance (~ 2 mm in this case), the polymerization propagation stops and the boundary between the polymerized and liquid glue mixture remains stable. The

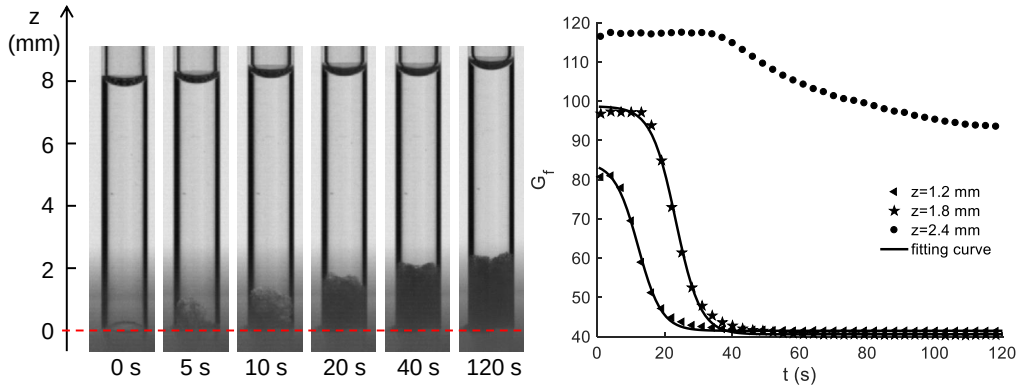

(a) (b)

Fig. 4.1 Change in opacity observed in the glue mixture ($C_G = 50\%$) in contact with IS-BSA8. (a) The darkening of the tube bottom indicates the polymerization of the G-L mixture. The polymerization front stops at $z = z_f$ for time $t = t_f$. (b) Time evolution of the relative grey levels at different vertical positions. The full line corresponds to the sigmoidal fit.

time evolution of the grey level $G_f(z,t)$ within the darkening column is shown as a function of time at different locations $z \leq 2.4$ mm. At a given location z, the grey level $G_f(z,t)$ decreases from the initial value $G_f(z,0)$ towards an asymptotic value $G_f(z,\infty)$ within one or two minutes. Note that the initial value of grey level $G_f(z,0)$ varies with z, due to the shade cast by the cup.

The low value of $G_f(z,\infty)$, which corresponds to a dark grey level close to black, indicates that the glue column is dense. This has been proven by observing the surface of the polymerized glue mixture with a scanning electron microscope (QUANTA FEG 250, FEI, US). The glue exhibits a complex network of connected polymerized structures (Figure 4.2a), with interstices filled with oil (see insert in Figure 4.2a). Qualitatively, the resulting structure is hard and resists compression.

For a given value of z, the curve $G_f(z,t)$ can be fitted with a sigmoid:

$$G_f(z,t) = G_f(z,0) - \frac{G_f(z,0) - G_f(z,\infty)}{1 + \exp\left(-\dfrac{t - t_{1/2}(z)}{\tau_v}\right)}, \tag{4.1}$$

where $t_{1/2}(z)$ is the half time, such that $G_f(t_{1/2}) = [G_f(z,0) + G_f(z,\infty)]/2$. The progression of the polymerization front is thus characterized by $t_{1/2}(z)$. The time τ_v corresponds to a measure of the time that it takes the polymerization to be completed at position z (based on the grey level in the fluid). Indeed, it takes about $5.9\tau_v$ for the grey level at z to drop from $G_f(z,0) - 0.05[G_f(z,0) - G_f(z,\infty)]$ to $G_f(z,0) - 0.95[G_f(z,0) - G_f(z,\infty)]$.

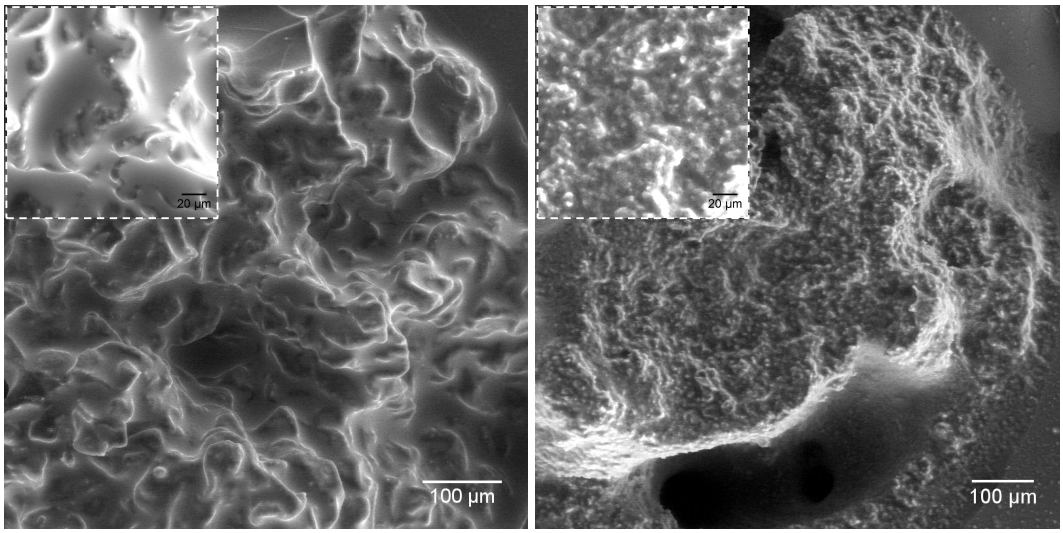

(a) (b)

Fig. 4.2 Scanning electron micrography of the polymerized glue mixture ($C_G = 50\%$) after contact with IS-BSA8: (a) fast polymerization; (b) slow polymerization. Inserts: zoom on the cross-section at a higher magnification.

We face the issue that the polymerization process is fast and occurs over a limited distance, which makes it very difficult to evaluate the propagation kinetics of the polymerization front. We have consequently studied the fast volumetric polymerization reaction by rather determining the height z_f of the front at the final time t_f of the fast polymerization phase. Before explaining how the height z_f is determined from the grey level evolution, one must first note that the final grey level has the same value $G_f(z,\infty)$ at different z locations: for example, in Figure 4.1b, $G_f(z,\infty) \sim 42$ for $z \leq 1.8$ mm. An increase of $G_f(z,\infty)$ means that the glue is less dark (and thus less dense) in the measuring box about point z. Starting from $z = 0$ and increasing z, we look for the two successive measurement points z_1 and $z_2 > z_1$ such that

$$G_f(z_2,\infty) - G_f(z_1,\infty) \geq 0.1 G_f(z_1,\infty). \tag{4.2}$$

We deduce that the boundary of the dark polymerized glue is located somewhere between z_1 and z_2 and take the position of the polymerized front to be $z_f = (z_1 + z_2)/2$. The position z_f is thus determined with an error ± 0.25 mm. Correspondingly, the end of the fast polymerization is defined by

$$t_f = [t_{12}(z_1) + 3\tau_v(z_1) + t_{12}(z_2) + 3\tau_v(z_2)]/2. \tag{4.3}$$

The duration t_f of the fast polymerization is plotted as a function of the propagation distance z_f in Figure 4.3. Not surprisingly, we note that t_f increases with z_f, but that there is not a large dispersion of the results between two experiments: for the 8% BSA ionic solution,

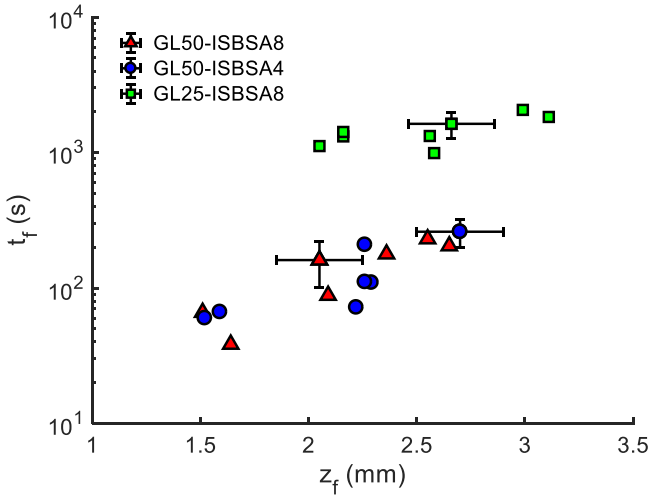

Fig. 4.3 Time t_f necessary to polymerize a distance z_f during the fast polymerization reaction for a G-L mixture ($C_G = 50\%$) upon contact with different solutions.

the polymerization altogether propagates over a distance $z_f = 2.4 \pm 0.3$ mm over a time $t_f = 162 \pm 42$ s.

4.2 Slow volumetric polymerization

Tens of minutes after the fast polymerization has stopped, a new slow polymerization takes place and propagates upwards from $z = z_f$: after about an hour from the beginning of the experiment, the front reaches the top of the glue mixture column (Figure 4.4a). The time evolution of the grey level at different positions for $z > z_f$ is shown in Figure 4.4b. The grey level decreases from the initial value $G_s(z,0) \sim 132$ to the asymptotic value $G_s(z,\infty) \sim 105$, which is much higher than the grey level $G_f(z,\infty) \sim 42$ measured at the end of the fast volumetric polymerization ($z \sim z_f$). The new polymerized solid bulk is much less opaque, which indicates that the polymerization reaction is different from the fast one. On the SEM picture of a section of the polymerized column shown in Figure 4.2b, we note that the structure is very different from the one observed for the fast polymerization: micron size grains appear, which are micro droplets encapsulated by polymerized glue. The same type of structure had also been observed when the glue is undergoing pure anionic polymerization after contact with IS [55]. Qualitatively, the column is still a hard solid that resists compression, like in the bottom region where the slow polymerization takes place.

For every value of z, the curve $G_s(z,t)$ can also be fitted with a sigmoid. As the polymerization is slow, we have enough measurement points to compute the propagation velocity V_p

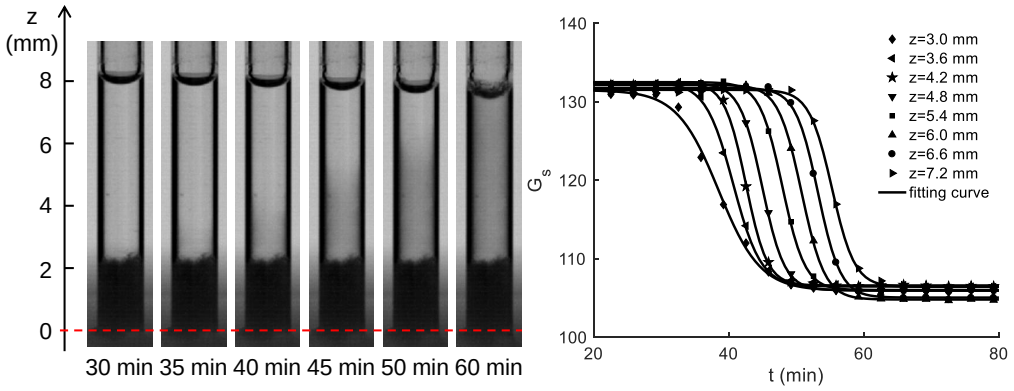

(a) (b)

Fig. 4.4 Change in opacity observed in the G-L mixture ($C_G = 50\%$). (a) Darkening above the black region revealing a slow polymerization of the G-L mixture. (b) Time evolution of the grey level at different positions above the dark region; the continuous line is the sigmoid fit.

of the front from the half time $t_{1/2}(z)$:

$$V_p = (z - z_f)/[t_{1/2}(z) - t_f]. \tag{4.4}$$

We find that V_p increases slightly with z, which may be due to the fact that the reaction is exothermic (Figure 4.5). The average velocity is of the order of 0.05 mm/min, which is much smaller than the average velocity in the fast polymerization phase ($\sim z_f/t_f \sim 0.9$ mm/min). The V_p values and evolution along the tube axis are comparable with the ones previously obtained for a 50% Glubran-Lipiodol mixture in contact with a pure ionic solution (IS) [55]. This seems to indicate that the slow polymerization is anionic.

4.3 Effect of the BSA concentration on the polymerization process

We now turn to the effect of protein concentration and study the polymerization of a G-L mixture ($C_G = 50\%$) in contact with an ionic solution containing only 4% of BSA (IS-BSA4). We observe again a fast polymerization (Figure 4.6a), with a front which is not as sharply defined as for IS-BSA8. The grey level evolution (Figure 4.6b) allows us to determine the position z_f of the front when the fast polymerization stops at time t_f. As shown in Figure 4.3, there is no significant difference of the values of $t_f(z_f)$ for BSA concentrations of 8% or 4%. A slow polymerization phase is also observed, which starts some 50 min later, with

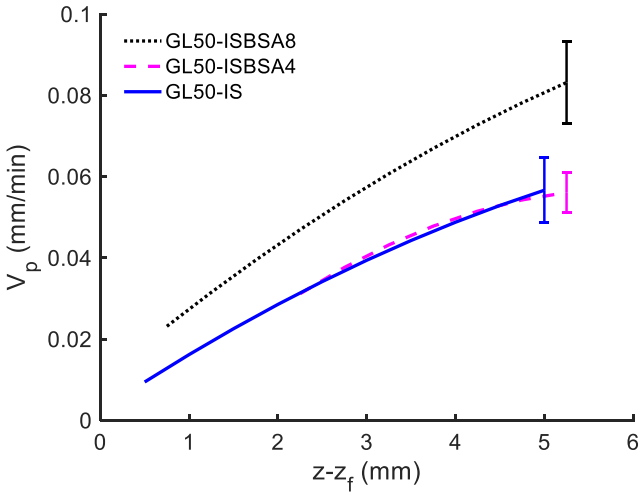

Fig. 4.5 Slow polymerization front for a 50% G-L mixture placed in contact with different solutions: representation of the average front propagation velocity V_p along with the typical error bar for each measurement set. The results are compared to the ones reported in [55] for an ionic solution without protein (IS).

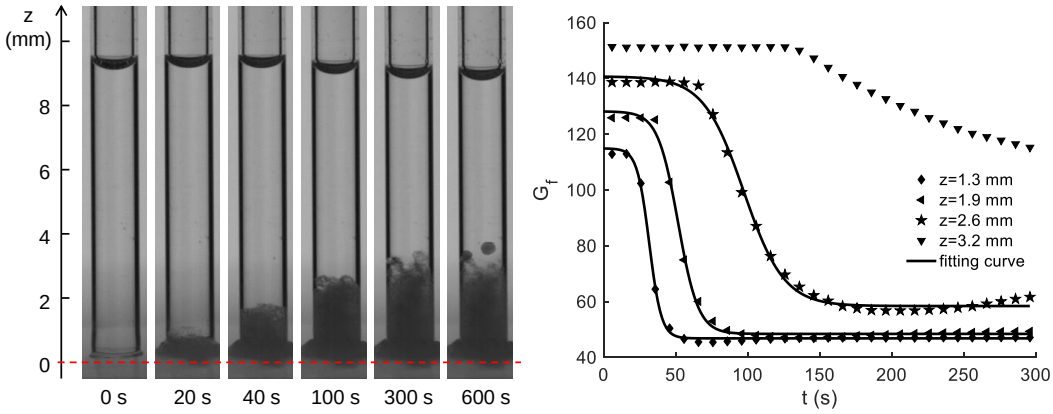

(a) (b)

Fig. 4.6 Change in opacity observed in the glue mixture ($C_G = 50\%$) in contact with IS-BSA4. (a) Darkening of the tube bottom shows the polymerization of the G-L mixture. (b) Time evolution of the relative grey level at different vertical positions. The full line corresponds to the sigmoidal fit.

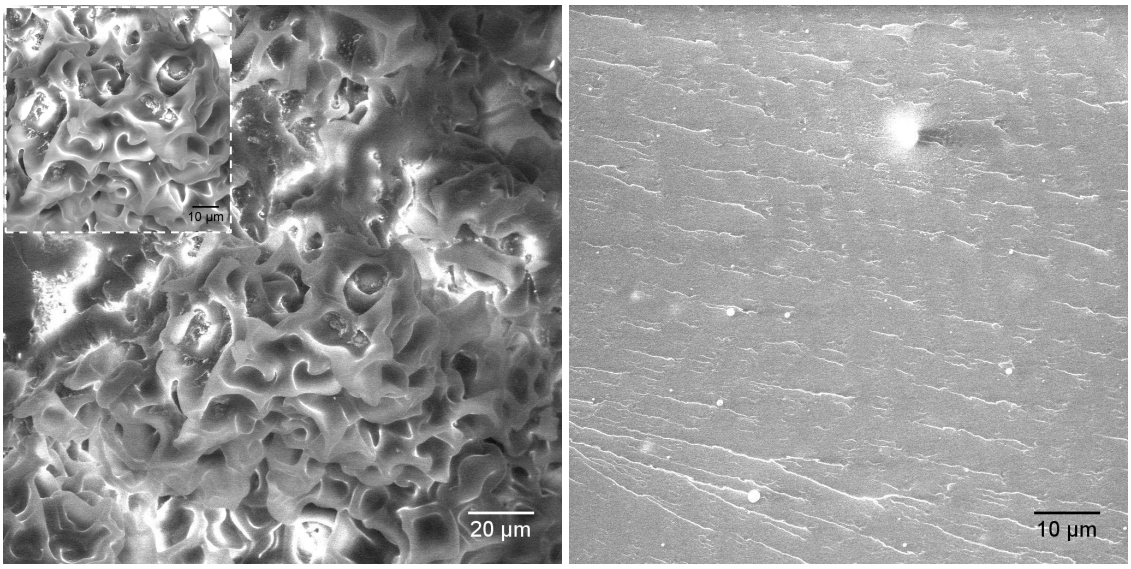

(a) (b)

Fig. 4.7 Scanning electron micrography of the polymerized pure glue ($C_G = 100\%$) after contact with IS-BSA8: (a) fast polymerization; (b) slow polymerization.

a front propagation velocity which is also of the same order as the one observed for a pure ionic solution (Figure 4.5). The SEM observation of the polymerized glue corresponding to both the fast and slow polymerization phases are very similar to the ones shown in Figure 4.2, which would make it redundant to show them. This indicates that an BSA concentration of 4% is quite sufficient to induce the two steps of glue mixture polymerization.

4.4 Effect of the glue-Lipiodol proportion on the polymerization process

We now consider the effect of the glue concentration on the polymerization of a glue-oil mixture in contact with an IS-BSA8 solution. In the case of pure glue ($C_G = 100\%$), the fast polymerization is very fast and extends over a short distance ($z_f \sim 1$ mm, $t_f \sim 5$ s). It stops in the shadow of the cup and is thus difficult to measure with a good precision. The resulting solid glue is organized as a compact network of connected polymer bridges as it appears on SEM images (Figure 4.7a). A slow polymerization follows some 40 min later and propagates fast within the glue column. The high velocity is difficult to measure with precision, because there is little change in grey level for the pure glue during the reaction. From the moment the second polymerization reaction starts, it takes about $\sim 5-10$ min to polymerize the remaining 5 mm of glue column, which is of the same order as what is

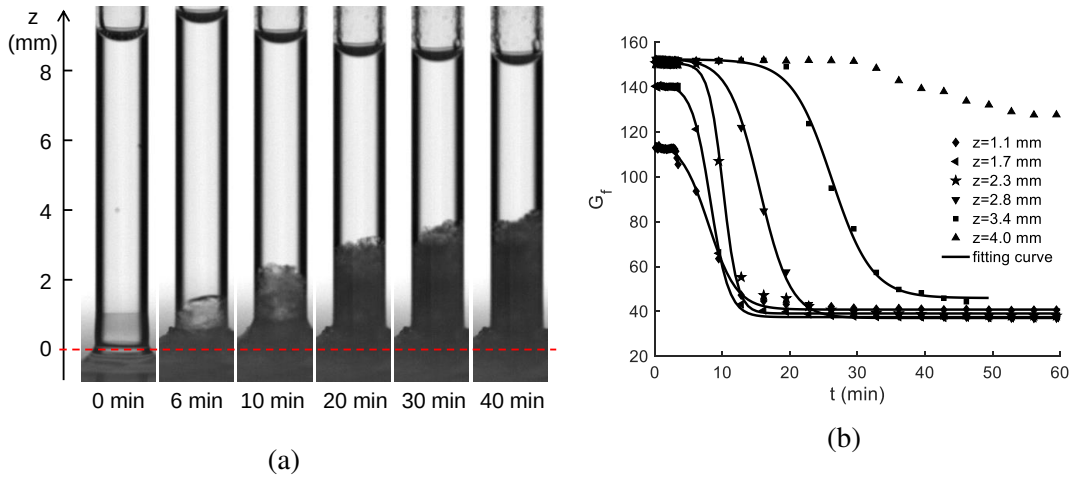

Fig. 4.8 Change in opacity observed in the glue mixture ($C_G = 25\%$) in contact with IS-BSA8. (a) Darkening of the tube bottom shows the polymerization of the G-L mixture. (b) Time evolution of the relative grey level at different vertical positions. Note that the time scale of the phenomenon is greatly increased.

measured for pure Glubran 2 in contact with an ionic solution [55]. The resulting solid glue has a homogeneous structure (Figure 4.7b), which is identical to the one observed for pure glue in contact with an ionic solution containing no protein [55].

Conversely, when the glue concentration of the mixture is reduced to $C_G = 25\%$, the first stage of polymerization occurs over distances z_f and times t_f that are larger than for $C_G = 50\%$, as can be surmised from Figures 4.8 and 4.3. The mean propagation velocity is $V_p \sim 0.11 \pm 0.02$ mm/min, which is an order of magnitude smaller than for $C_G = 50\%$. At the interface with the IS-BSA8 solution, the polymerized glue has a convoluted structure (Figure 4.9a), which is similar, if less compact, to the ones observed for larger values of C_G (Figures 4.2a and 4.7a). However, in the middle of the column (Figure 4.9b), the polymerized glue has a different aspect: there are some polymerized structures, immersed in an emulsion of encapsulated glue droplets in oil. For $z > z_f$ no change occurs in the glue mixture, which remains liquid for days. Note that a 25% G-L mixture does not polymerize at all when it is put in contact with IS [55].

4.5 Discussion and conclusion

The polymerization of cyanoacrylate glue in contact with an ionic solution containing albumin is obviously a complex process. It is clear that two chain reactions occur. One is triggered by the BSA molecules which have about 583 side chains of amino acids, and thus many possible

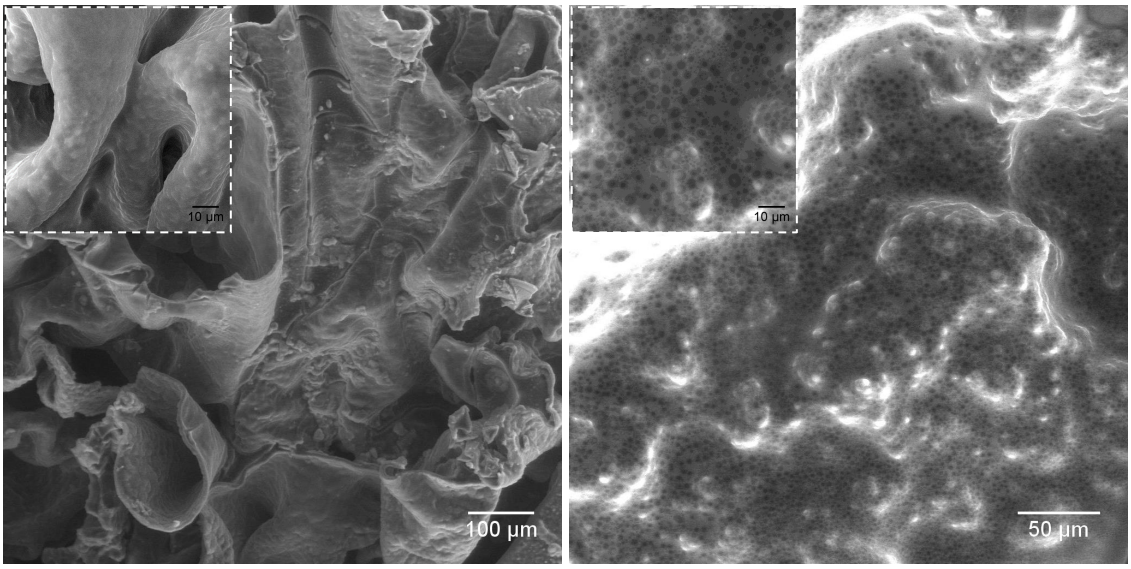

(a) (b)

Fig. 4.9 Scanning electron micrography of a polymerized glue mixture at low concentration ($C_G = 25\%$) on contact with IS-BSA8. (a) Interface between the glue mixture and IS-BSA8; (b) Cut of the polymerized column.

sites for a zwitterionic polymerization as depicted in the chain reaction in Figure 1.7b. This results in the formation of a star polymer, branching out from one BSA molecule [47]. It may be postulated that the reaction stops when the amphiphilic part of a chain branches on the hydrophobic part of another one. This can occur easily because the polymerization occurs in a confined space. Evidence of this process appears on the SEM images of the resulting polymerized glue (Figures 4.2a and 4.7a), in which the same convoluted complex network of polymer structures can be observed. At the same time, an anionic polymerization occurs with a much slower reaction rate, triggered by the hydroxyl ions. This reaction, shown in Figure 1.7a results in linear polymer chains. The two polymerization processes have been observed and used for creating cyanoacrylate nanocapsules [101, 47].

The zwitterionic reaction occurs first and is the prevalent process in what was dubbed the fast polymerization. It is fast because the concentration of BSA molecules is high and thus provides a large number of potential initiation sites. Note that polymerized cyanoacrylate nanoparticles can be obtained with BSA concentrations which are about ten times lower than the ones use here [47]. The variation of the propagation time $t_f(z_f)$ (Figure 4.3) may be attributed to the fact that the propagation/termination process includes some randomness. The values of $t_f(z_f)$ do no depend on the BSA concentration, which is high enough, but depend heavily on the glue/oil concentration C_G, and thus on the availability of glue molecules. For pure glue, z_f and t_f are small (1 mm and 5 s, respectively) and result in a dense polymerized

network with pores of the order of 1 μm or less (Figure 4.7). For $C_G = 50\%$, $t_f(z_f)$ is about 20 times larger resulting in much wider network pores, of order of $10-20$ μm, filled with oil. For $C_G = 25\%$, we also observe a loose network of glue, together with encapsulated glue droplets.

The slow polymerization corresponds to the anionic process, which probably starts at the same time as the zwitterionic reaction. However, the linear polymer chains must first creep upwards out of the dense network to find a reservoir of unpolymerized glue in which the reaction can continue. This process takes time (about 40 min for $C_G \geq 50\%$). Once the unpolymerized glue is reached, the chain polymerization takes place. It is interesting to note that the propagation velocity of the slow polymerization front is then of the same order of magnitude as the one measured for glue-oil mixtures in contact with a pure ionic solution [55], a fact that substantiates the above analysis of an anionic process. The resulting polymerized structures are very similar to the ones observed for glue mixtures in contact with a pure ionic solution. Note that we do not observe any anionic polymerization for $C_G = 25\%$ (except maybe some mixed with the zwitterionic polymerization, from which it is impossible to distinguish), just as was the case when the glue was in contact with IS only [55].

In conclusion, we have designed an experimental setup that allows us to measure the polymerization kinetics of Glubran-Lipiodol mixtures in contact with any triggering solution. This study shows that Glubran-Lipiodol mixtures with concentration larger or equal to 25% polymerize when they are put in contact with an ionic solution containing at least 4% of BSA. The time for the solution of glue to polymerize over a 1 mm thickness varies from 5 s for pure glue to 10 min for $C_G = 25\%$. The final thickness of the polymer depends mostly on the glue concentration. From a practical point of view and specifically for vascular embolization purposes where glue-oil mixture droplets are injected in a vessel, pure glue is never used, as it polymerizes too quickly for the injection process to be safely controlled. The common practice is to use either 50% or 25% Glubran-Lipiodol mixtures. The advantage of a 25% mixture is that the polymerization is slow to develop, which can be a disadvantage because the mixture droplets can be convected away before they have started to solidify. Another disadvantage is the absence of polymerization (and thus solidification) beyond distances of about 4 mm. This limits the amount of glue mixture that ought to be injected at once. Such restriction is especially true under static injection conditions, for which a large amount of glue mixture can be injected at a single location. Under dynamic conditions, the glue mixture will instead be ejected from the catheter in the form of drops, the radius of which is typically smaller than 4 mm [83]. A 50% mixture may offer the good compromise between reaction time and injection control. Note though, that a droplet with a radius larger than 3 mm will take some time to solidify to the core.

Chapter 5

Polymerization kinetics of glue mixtures in dynamic conditions

When vessels are embolized by glue injection, two primary physical phenomena predominate: one is the fluid dynamics of the injection of a fluid into another non-miscible co-flowing fluid, the other is the polymerization kinetics of the embolic glue. In this chapter, we first study the drop formation process in a liquid-to-liquid system by neglecting the polymerization reaction. We then study the injection of glue mixtures into a flow of ionic solution and characterize the polymerization kinetics in dynamic conditions.

5.1 Drop formation of co-flow injections

The experiments of co-flow injection of non-ractive liquids have been conducted under conditions similar to the physiological ones of the portal vein embolization (Table 2.6). All the values of the non-dimensional parameters chosen for the *in vitro* experiments are indicated in Table 2.7. The Weber number varies between 0.9 and 11 and the capillary number assumes 3 possible numbers: 0.9×10^{-3}, 1.8×10^{-3} and 2.7×10^{-3}. With these controlling parameters, we have observed the dripping and the jetting regimes as well as the dripping-to-jetting transition.

5.1.1 Flow regimes and transition

Dripping regime

The dripping regime occurs at low flow rates ($We_i < 3$), which is characterized by the periodic formation of drops and pinch-off from the tip of the injection tube. The emerging liquid from

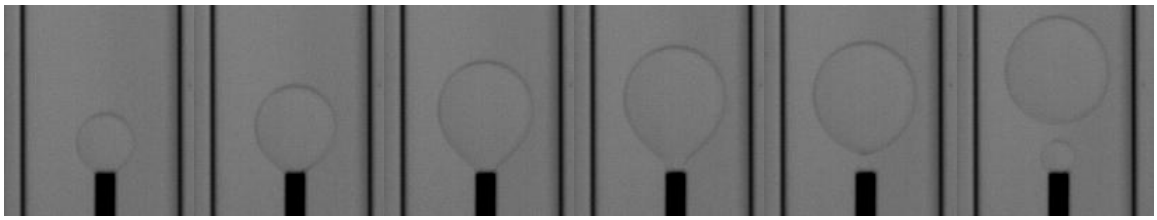

Fig. 5.1 Drop formation in the dripping regime at different instants of time.

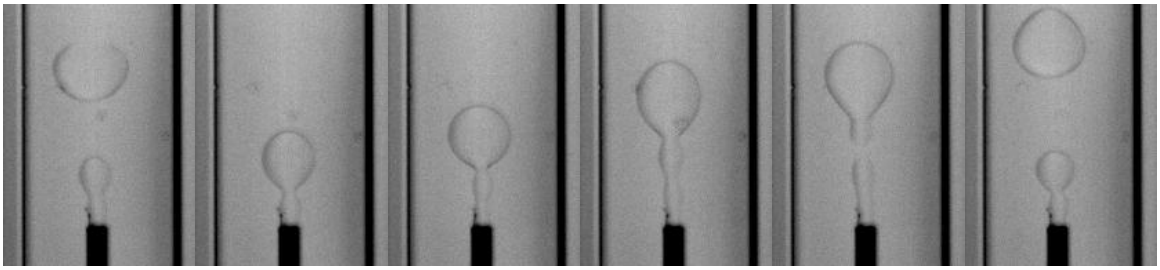

Fig. 5.2 Drop formation in the jetting regime at different instants of time.

the injection of the inner fluid exits and accumulates at the end of the tube forming a drop (Figure 5.1a-5.1d). When the drop reaches a critical volume, it grows and moves slightly under the effect of the buoyant force inertia, external friction and surface tension force. The liquid neck, which connects the drop to the tip of the tube, thinnens until it breaks up leading to the formation of the drop. (Figure 5.1e). After the detachment of the drop, part of the liquid neck retracts and a new drop begins to form following the same process (Figure 5.1f).

Jetting regime

At high flow velocity ($We_i > 10$), the jetting regime occurs which is characterized by the formation of a jet away from the capillary tip. In the jetting regime, the drop formation begins with the formation of a jet (Figure 5.2a), which lengthens and rapidly destabilizes (Figure 5.2b-5.2e), eventually leading to the formation of drops further downstream (Figure 5.2f).

Dripping-to-jetting transition

During the dripping-to-jetting transition, two different patterns of drop formation have been observed depending on the inner flow rate. The first pattern is similar to that of the dripping regime (Figure 5.2). The only difference is that the drop breaks up at the tip of a jet. Occasionally, we observe the formation of a satellite drop (Figure 5.3), which is smaller

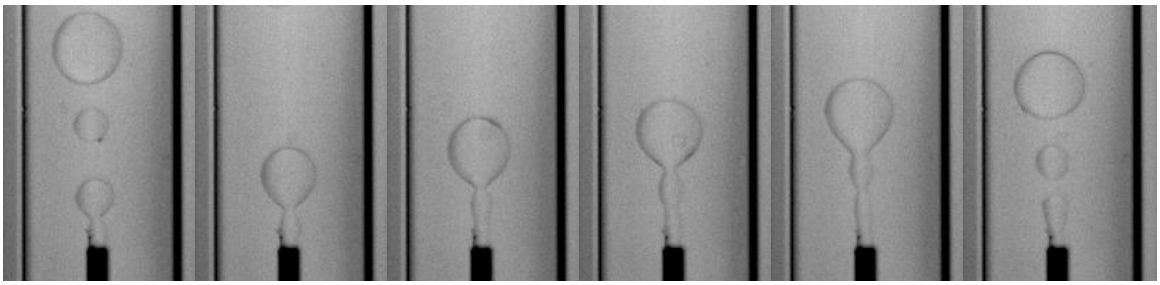

Fig. 5.3 Satellite drop formation in the dripping-to-jetting transition at different instants of time.

in size than the main drop. This second pattern resembles the jetting regime, where the jet instability induces the periodic formation of drops with a single size.

A state diagram of transition from dripping to jetting is shown in Figure 5.4. It is plotted as a function of the Weber number of the inner flow We_i and the capillary number of the outer flow Ca_o. Variations of We_i and Ca_o are obtained by varying Q_i and Q_o, respectively. We find that the dripping regime occurs for low values of We_i, when the surface tension force dominates the inertial forces of the inner flow. The transition from dripping to jetting is governed by the Weber number of the inner phase, which occurs around the value $We_i = 3.1 \pm 0.9$.

5.1.2 Drop size measurement with the image processing

The drop size is measured automatically by the image processing technique described in section 2.6.3. Figures 5.5-5.6 show the resulting images after different steps of image processing in different fluid regimes. When a drop forms in the dripping regime, two clear edges corresponding to the drop boundary are obtained. When a drop forms in the dripping-to-jetting transition, the formed drop is usually followed by a satellite drop. In this case, only the boundary of the parent drop can be successfully detected (Figure 5.6). When there is no satellite drop, the boundary can also be well detected. However in the jetting regime, it is difficult to get a good edge detection because of the small drop size and short interval between two consecutive drops. In this case, the drop size is measured manually from the recording images.

Figure 5.8 shows the measurements of the major axis L_h, minor axis L_v and equivalent diameter d_d in the test1_2. A total of 201 images with good drop boundary are obtained from the 5000 recording images. All the measurements of drop sizes are listed in Table 5.1.

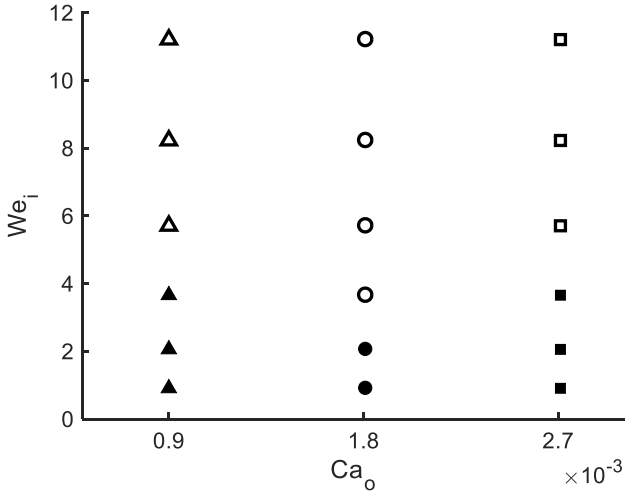

Fig. 5.4 State diagram of transition from dripping (solid symbols) to jetting (open symbols) in the co-flow injection as a function of We_i and Ca_o. Triangle (▲, △), circle (●, ○) and square (■, □) symbols correspond to $Ca_o = 0.9 \times 10^{-3}$, $Ca_o = 1.8 \times 10^{-3}$ and $Ca_o = 2.7 \times 10^{-3}$, respectively.

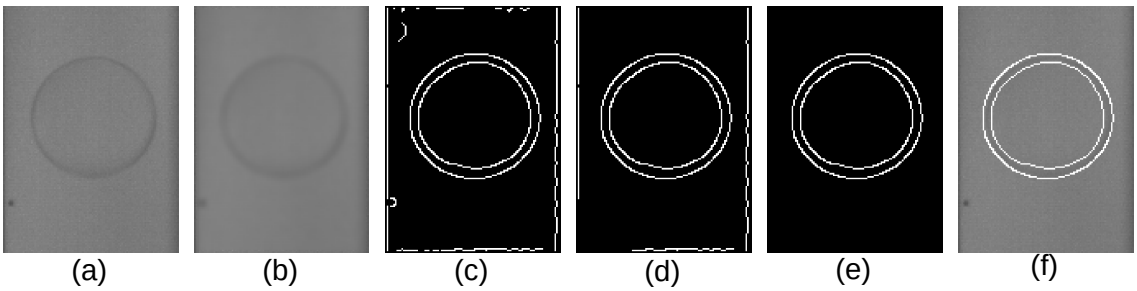

Fig. 5.5 Resulting images after each step of image processing in the dripping regime.(a) original image in the observation window, (b) grayscale image after Wiener filtering, (c) binary image after the edge detection, (d) binary image after removing small objects, (e) binary image after circle detection, (f) overlapping image of (a) and (e).

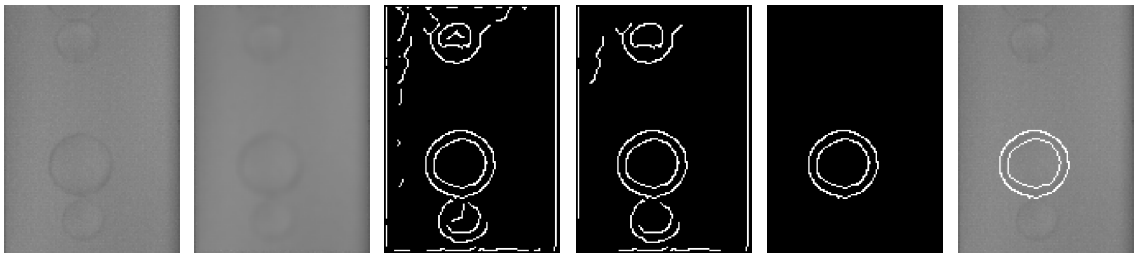

Fig. 5.6 Resulting images after each step of image processing in the transition.(a) original image in the observation window, (b) grayscale image after Wiener filtering, (c) binary image after the edge detection, (d) binary image after removing small objects, (e) binary image after circle detection, (f) overlapping image of (a) and (e).

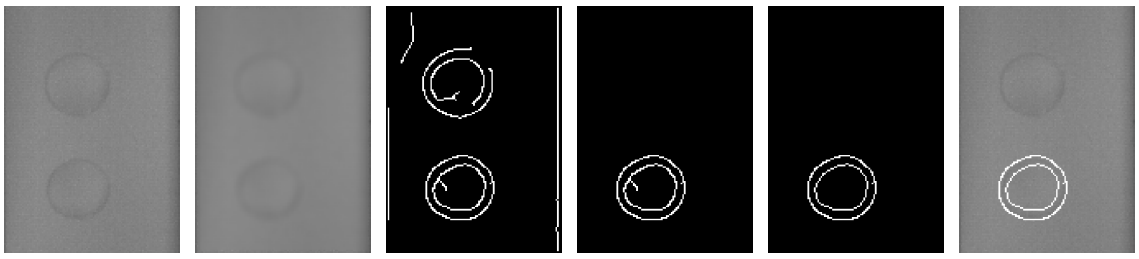

Fig. 5.7 Resulting images after each step of image processing in the jetting regime.(a) original image in the observation window, (b) grayscale image after wiener filtering, (c) binary image after the edge detection, (d) binary image after removing small objects, (e) binary image after circle detection, (c) overlapping image of (a) and (e).

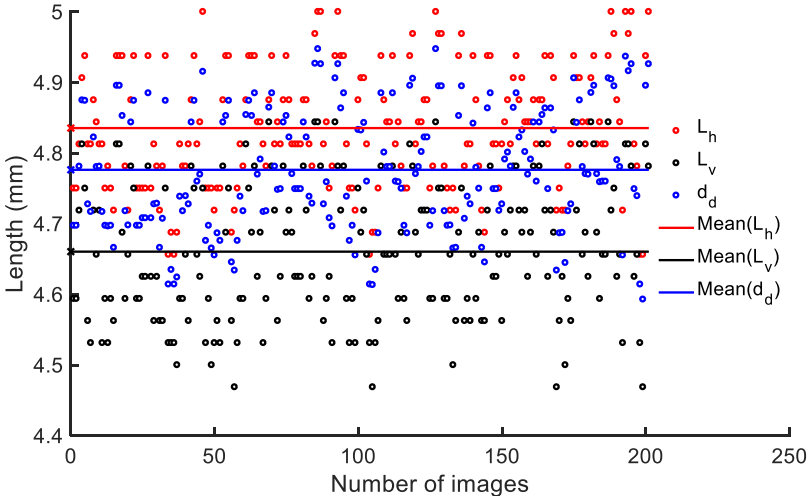

Fig. 5.8 Measurements of major axis L_h, minor axis L_v and equivalent diameter d_d in the test1_2.

Group	Test	N_{good}/N_{total}	$d_d \pm \delta(d_d)$ (mm)	$L_h \pm \delta(L_h)$ (mm)	$L_v \pm \delta(L_v)$ (mm)	$\delta(d_d)/d_d$ (%)
Group 1	Test1_1	141/4500	4.58 ± 0.08	4.64 ± 0.08	4.46 ± 0.08	1.7
	Test1_2	201/5000	4.78 ± 0.09	4.84 ± 0.09	4.66 ± 0.10	1.8
	Test1_3	281/5000	4.58 ± 0.09	4.64 ± 0.10	4.47 ± 0.10	2.0
	Test1_4	279/5000	3.85 ± 0.18	3.89 ± 0.18	3.76 ± 0.18	4.7
	Test1_5	113/4500	2.33 ± 0.10	2.37 ± 0.10	2.26 ± 0.11	4.3
	Test1_6	66	1.56 ± 0.03	1.57 ± 0.04	1.53 ± 0.04	2.0
Group 2	Test2_1	169/5500	4.11 ± 0.06	4.14 ± 0.06	4.04 ± 0.06	1.5
	Test2_2	589/5500	3.81 ± 0.06	3.83 ± 0.07	3.76 ± 0.11	1.5
	Test2_3	39/5000	4.05 ± 0.05	3.98 ± 0.04	4.19 ± 0.10	1.1
	Test2_4	279/5000	3.32 ± 0.08	3.33 ± 0.08	3.30 ± 0.08	2.4
	Test2_5	40	2.51 ± 0.21	2.51 ± 0.21	2.49 ± 0.22	8.1
	Test2_6	56	1.62 ± 0.05	1.64 ± 0.05	1.60 ± 0.06	3.0
Group 3	Test3_1	166/5500	3.57 ± 0.04	3.60 ± 0.04	3.5 ± 0.06	1.2
	Test3_2	212/5000	3.43 ± 0.05	3.46 ± 0.05	3.36 ± 0.05	1.3
	Test3_3	475/5000	3.27 ± 0.05	3.30 ± 0.05	3.20 ± 0.05	1.4
	Test3_4	777/5000	2.89 ± 0.29	2.90 ± 0.29	2.88 ± 0.30	9.9
	Test3_5	62	1.75 ± 0.10	1.76 ± 0.10	1.74 ± 0.10	5.8
	Test3_6	62	1.44 ± 0.03	1.44 ± 0.03	1.43 ± 0.04	2.0

Table 5.1 Drop size measurements in the three groups of experiments. Tests noted in italic are measured manually.

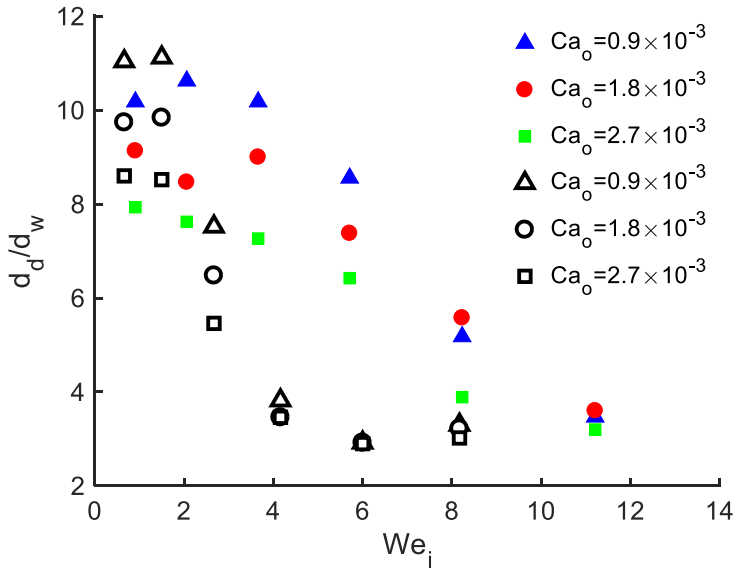

Fig. 5.9 Evolution of the drop size as a function of We_i and Ca_o. Results in open symbols are from reference [83].

In order to non-dimensionalize the drop diameter d_d, the natural choice is to use the wetted diameter of the capillary tube d_w. This diameter is chosen as reference based on the wetting phenomenon which influences the mechanism of drop formation. In this study, the wetted diameter d_w is equal to $d_i = 0.45$ mm as the inner liquid presently used (silicone oil) does not wet the injection tube. The evolution of the drop size ratio d_d/d_w is shown in Figure 5.9, and is plotted as a function of the Weber number We_i for different values of Ca_o. The results are compared with those of Sandulache *et al.* [83].

For a constant value of the outer capillary number Ca_o, the drop size ratio d_d/d_w changes slightly in the dripping regime ($We_i < 3$). When We_i is increased, the drop size ratio decreases slowly until it reaches an asymptotic value for $We_i > 10$ (jetting regime). In the jetting regime, the drop size ratio is independent of Ca_o, which only depends on the width of the jet. For a constant value of the inner Weber number We_i, the drop size ratio d_d/d_w decreases with the increase in the outer capillary number Ca_o. This phenomenon is particularly marked in the dripping regime. The influence of Ca_o on the drop size ratio diminishes as We_i is increased. No influence is observed in the jetting regime for $We_i > 10$. The drop size is around 3 times of the wetted diameter, which is consistent with that in Sandulache *et al.* [83].

Both the inner Weber number We_i and the outer capillary number Ca_o play important roles on the drop formation. The inner Weber number We_i determines the transition from the dripping regime to the jetting regime. The outer capillary number Ca_o mainly affects the drop size especially in the dripping regime.

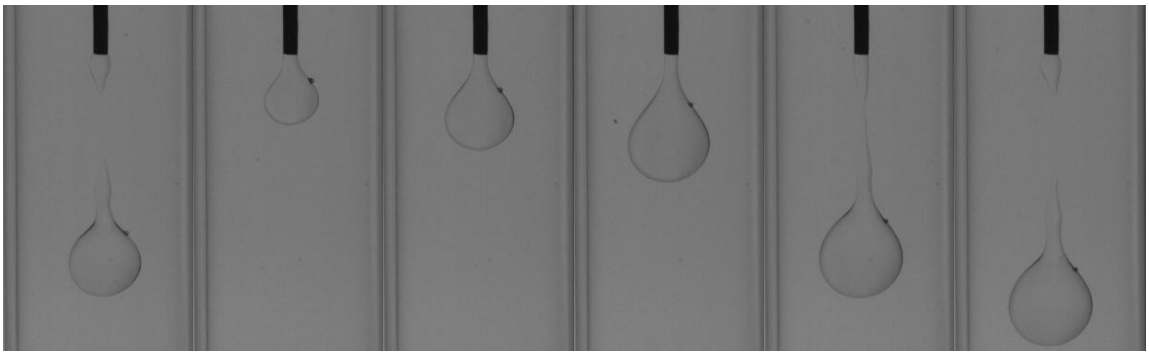

Fig. 5.10 Drop formation of the G-L mixture (C_G = 25%) injected into the flowing ionic solution.

5.2 Injection of a glue mixture into a flowing ionic solution

The G-L mixture (C_G = 25%) is injected into the flowing ionic solution with the controlling parameters indicated in Table 2.8. The drop formation begins from the retracted liquid neck that formed as the previous drop detached. It leads to the formation of a small quasi-conical drop at the capillary tip (Figure 5.10a). The continuously injected mixture accumulates in the drop and elongates the neck owing to the increasing gravitational force (Figure 5.10a-5.10c), which is similar that was observed for the co-flow injection of non-reactive liquids (Figure 5.1). When the drop grows to a critical volume, its neck lengthens quickly and thinnens out until it breaks up into a drop with a tail. The presence of the tail is due to the rapid interfacial polymerization of the drop interface, which leads to the adherence of the drop to the catheter tip and affects the shape of the formed drops. The occurrence of the interfacial polymerization can be proven by the fixed drop shape when the drop detaches (Figure 5.10f). During the injection process, an interfacial polymerization is quickly initiated on the drop surface, which plays an essential role on the conformation of the formed drops. In contrast, no slow volumetric polymerization inside the drop ever seems to occur, the core of the drop being still liquid days after the experiment. This result is consistent with those found on the G-L mixture (C_G = 25%) upon contact with the ionic solution. The shapes and sizes of the formed drops are not uniform (Figure 5.11). A majority of drops have tails and a diameter in the range $\sim$3-6 mm. The volume of deposited drops varies in the range of 10-90 μl.

Figure 5.12 shows the collected polymerized drops. The drop surface is observed to be wrinkled when placed under the microscope. It encapsulates the liquid mixture inside, which is still liquid days after the experiment.

Fig. 5.11 Different shapes of drops during the injection of the G-L mixture (C_G = 25%) into the flowing ionic solution.

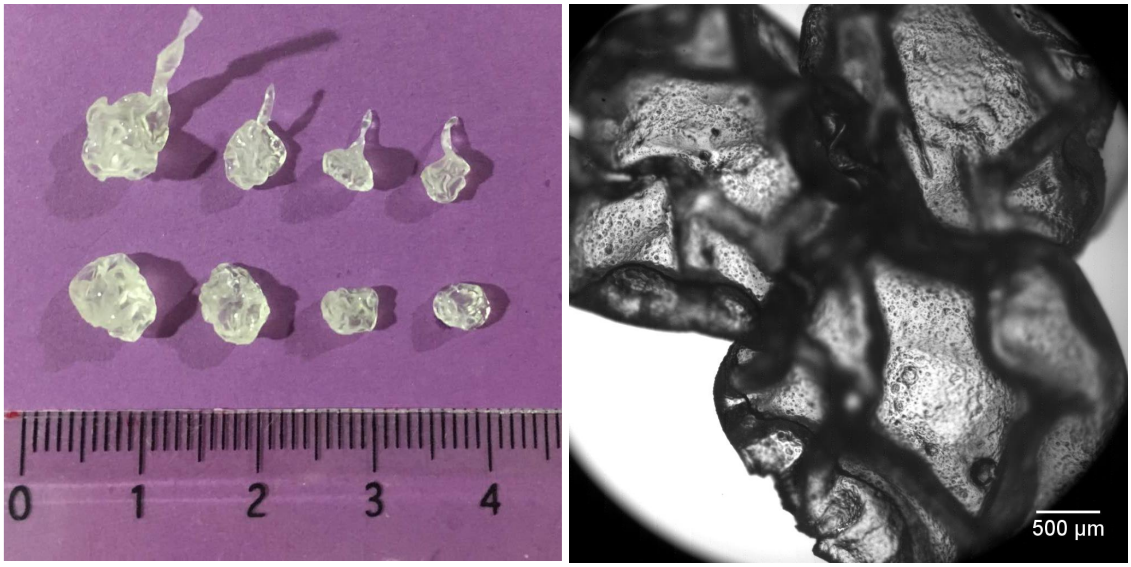

(a) (b)

Fig. 5.12 Collected drops formed by injection of G-L mixture (C_G = 25%) into flowing ionic solution. (a) a picture of polymerized drops, (b) a microscopic image of polymerized drops.

5.3 Discussion and conclusion

In this chapter, we have first investigated the liquid injection in a confined co-flow system by neglecting the polymerization of glue. In order to better understand the injection dynamics that are at stake during the embolization, we have conducted *in vitro* experiments under conditions that are similar to the physiological ones encountered during PVE. The outer flow has thus been assumed to be steady as the blood flow has a low pulsatility in the portal vein. More investigations on the influence of pulsatility would to be done in order to extend the results to the embolization of arteries.

We have made three groups of experiments by taking account the influence of both the Weber number of the inner flow We_i and capillary number of the outer flow Ca_o. All the values chosen for the *in vitro* experiments are based on the physiological parameters of PVE (Table 2.6). A wide range of We_i has been selected to investigate the influence of inner flow rates on the injection dynamics. From the results, different fluid regimes have been observed: dripping regimes, dripping-to-jetting transitions and jetting regimes. The Weber number of the inner flow We_i is the main parameter that governs the dripping-to-jetting transition. When We_i is small, surface tension dominates over the inertial forces of the inner flow and drops are formed at the tip of the injection tube. In contrast, when the inertial forces are large enough to overcome surface tension, the forming drop is convected downstream, favoring the formation of a liquid jet. Our results are consistent with those reported by Utada *et al.* [99]. The capillary number of the outer fluid Ca_o mainly affects the drop size especially in the dripping regime.

We have seen that *in vivo* injection is usually performed at Weber number $We_i \leq 2$ (Table 2.6). Glue injection is therefore mainly carried out in the dripping regime. In the dripping regime, the diameter of the drops is independent of We_i and mainly depends on the capillary number of the blood flow Ca_o. Clinically, Ca_o is determined by the blood flow rate and the diameter of the vessels (see Eq. 2.3). It can only be controlled by interventional radiologists in flow-controlled embolization performed with the detachable balloon. In the general case radiologists can only act on the Weber number We_i to alter the drop size by regulating the diameter of the injection tube d_i and the flow rate Q_i. Although We_i has no significant effect on the drop size in the dripping regime, the drop size can be modified by converting the fluid regime into the transition or jetting regime. In the jetting regime ($We_i > 10$), neither the inner flow rate nor the outer flow rate affect the size of the drops. The drop size only depends on the diameter of the jet, which is determined by the catheter tube diameter. Injecting in the jetting regime may seem like a great solution to embolize small distal vessels, as small calibrated glue drops are produced. However it may be difficult in clinical practice, as interventional

radiologists would have to choose a very small injection tube diameter d_i and a high injection flow rate Q_i.

We have then performed the injection of glue mixture (C_G = 25%) into the flowing ionic solution by using the experimental setup described in the section 2.7. We have recreated the similar conditions as those of the physiological case indicated in Table 2.9. With the chosen Weber number $We_i = 1$, the flow regime of the formation of a drop of glue mixture corresponds to the dripping regime. We have seen that the formation of drops during glue injection (Figure 5.10) is different from that for the co-flow injection of non-reactive liquids (Figure 5.1). The difference is caused by the rapid interfacial polymerization at the drop surface. The reaction leads to the adherence of the drop to the catheter tip and affects its conformation. The sizes and conformations of the drops are not uniform, which may explain the difficulty encountered by the radiologists during the injection of glue mixture clinically. For the injection of glue mixture at low concentration (C_G = 25%), we can observe that only the interfacial polymerization occurs and that no slow volumetric polymerization takes place inside the drop. Even days after, there is still liquid glue mixture encapsuled within a solid film. This is due to the fact that the external liquid only contains ions. *In vivo*, other nucleophiles will be present within blood (e.g. proteins) or on the cell membranes. The present results have only been conducted for the glue concentration of C_G = 25%. More complete investigations will be needed to provide a better understanding of the injection dynamics as a function of the parameters used for the embolization.

Chapter 6

Conclusion and perspectives

6.1 Conclusion

Vascular embolization with cyanoacrylate-based embolic glue is a commonly applied surgical procedure used to selectively reduce or stop the blood supply to specific parts of the body. It is carried out by introducing glue mixtures, which rapidly polymerize upon contact with the blood, into the circulation to occlude the vessels. The motivation of the thesis is initiated by the lack of knowledge of the polymerization kinetics of glue mixture and of the injection dynamics of a polymerizing mixture into the blood flow. We have thus carried out an *in vitro* study for a better understanding of these two processes.

The polymerization kinetics of glue mixture is systematically characterized with a newly designed experimental setup (Figure 2.5), which allows to rigorously investigate the polymerization of glue mixtures upon contact with ionic solutions, analogous to blood. The principle of the technique relies on the formation of a well-defined interface between the two liquids and on an objective measurement of the progression of the polymerization reaction by means of a high-speed imaging system, which measures the opacity change due to the polymerization reaction in the system. With the experimental setup, both the volumetric polymerization within the mixture column and the initiation of the polymerization process (the interfacial polymerization) can be studied simultaneously in the same system.

The polymerization kinetic of glue mixture have been studied in static conditions by neglecting the motion of fluids. When a glue mixture comes in contact with an ionic solution, we observe that the whole polymerization process includes two phases: an interfacial polymerization that takes place at the interface as soon as the two liquids are in contact with a characteristic time scale of the order of the minute; a volumetric polymerization during which a reaction front propagates within the mixture bulk with a characteristic time scale of

the order of tens of minutes. The polymerization rate, front propagation speed and volume reduction increase with the glue concentrations.

When an ionic solution containing albumin is used to initiate the polymerization of a glue mixture, a complex polymerization process has been observed. The process is decomposed into two chain reactions: a fast zwitterionic polymerization triggered by the BSA molecules and a slow anionic polymerization induced by the ions. The reaction speed and extent of the solidification region mostly depend on the glue concentration.

The injection dynamics of a glue mixture in blood flow is quantitatively investigated in the physiological conditions of PVE. But the results are transferable to other clinical uses of vascular embolization. From the co-flow injection of non-active liquids, we have found that the behavior of drop formation depends on both the capillary number of the outer fluid Ca_o and the Weber number of the inner fluid We_i. The transition from dripping to jetting is governed by the Weber number of the inner flow We_i. The capillary number of the outer fluid Ca_o mainly affects the drop size especially in the dripping regime. When a glue mixture is injected into flowing ionic solution, the conformation of formed drops depends on the joint influence of polymerization and hydrodynamics.

The present study not only systematically characterizes the polymerization kinetics of glue mixture, but also quantitatively analyzes the governing parameters of the injection process in the physiological conditions. The results can provide crucial information to interventional radiologists, that will help them understand and control the glue behavior after injection to achieve a safe and permanent obliteration of the vessels.

6.2 Perspectives

In this present study, we have designed new experimental setups (Figure 2.5 and 2.7) to study the polymerization of glue mixtures upon contact with ionic solutions or proteinaceous solutions. They present various advantages in characterization of polymerization of glue mixtures: both the initiation of polymerization and the propagation of polymerization can be visualized. However the principle of the technique is based on the change in opacity owing to polymerization reaction. In practice, there are also advanced technologies can be used to determine the polymerization kinetics, such as NMR and FTIR. These techniques can provide information of the polymerization at the molecular level, which could be used to study the polymerization of glue mixtures.

In this study, we have not taken into account the influence of temperature on the polymerization of glue-Lipiodol mixtures. The ionic or proteinaceous solutions used have a constant temperature of 21 °C. While *in vivo*, glue mixtures are injected into the blood flow at the

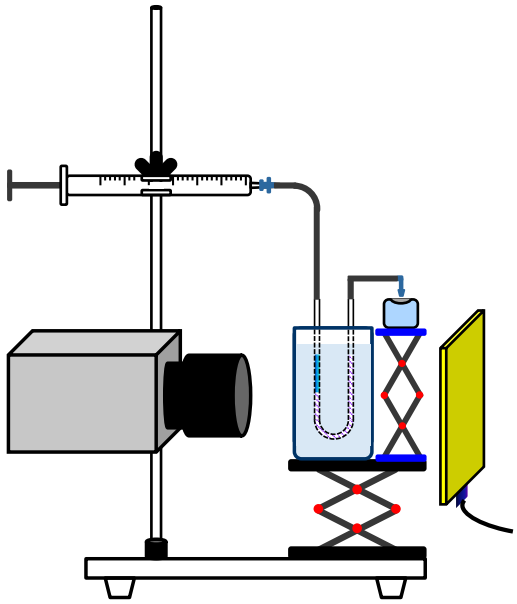

Fig. 6.1 Experimental setup used for investigating influence of temperature on polymerization of glue-Lipiodol mixtures.A U-shaped capillary tube is immersed in a water bath.

body temperature ∼37 °C. The higher body temperature may influence the initiation and also the progress of the polymerization reaction. An experimental setup shown in figure 6.1 is proposed to study the influence of temperature on the polymerization of glue-Lipiodol mixtures. A U-shaped capillary tube is used to create an interface between the glue mixture and a substitute solution of blood. It is immersed in a transparent water bath which is used to control the temperature. A problem of the use of a U-shaped tube is that the tube cannot be cleaned or reused. To solve this problem, we can use two straight capillary tubes connected with a silicone tube to replace a U-shaped tube.

For better understanding the injection dynamics of the glue mixture into the blood flow, more investigations are needed. The experimental setup indicated in figure 2.9 can be used to conduct experiments with various flow rates and at different glue concentrations. The confinement effect can also be investigated by varying diameters of the outer tube and the injection catheter. We assumed that the blood flow is a steady flow (flow rate of the outer flow is constant) in the present study, but the blood flow *in vivo* is a pulsating flow. One investigation on the influence of pulsatility on the injection dynamics is required for the application in vascular embolization. The present results have shown that protein plays an essential role on the polymerization of glue-Lipiodol mixture. For better modeling the blood *in vitro*, the effect of blood protein should thus be taken account.

References

[1] M. Atai, D. C. Watts, and Z. Atai. Shrinkage strain-rates of dental resin-monomer and composite systems. *Biomaterials*, 26:5015 – 5020, 2005.

[2] F. Baltacioğlu, N. C. Cimşit, K. Bostanci, M. Yüksel, and N. Kodalli. Transarterial microcatheter glue embolization of the bronchial artery for life-threatening hemoptysis: Technical and clinical results. *European Journal of Radiology*, 73:380 – 384, 2010.

[3] N. Behana, C. Birkinshawa, and N. Clarkeb. Poly n-butyl cyanoacrylate nanoparticles: a mechanistic study of polymerisation and particle formation. *Biomaterials*, 22: 1335–1344, 2001.

[4] N. Bekkedahl. Volume dilatometry. *Journal of Research of the National Buteau of Standards*, 43:145–156, 1949.

[5] C. A. Binkert. Embolization tools and techniques. *Applied Radiology*, 31:55 – 64, 2002.

[6] S. Bracard, J. M. Macho-Fernández, X. Wang, R. Anxionnat, and L. Picard. Influence of temperature on embolisation with cyanoacrylate. *Interventional neuroradiology*, 4: 301 – 305, 1998.

[7] F. Brassel and D. Meila. Evolution of embolic agents in interventional neuroradiology. *Clinical Neuroradiology*, 25:333–339, 2015.

[8] F. P. Bretherton. The motion of long bubbles in tubes. *Journal of Fluid Mechanics*, 10:166 – 188, 1961.

[9] A. Bright. Minimum drop volume in liquid jet breakup. *Chemical Engineering Research & Design*, 63:59–66, 1985.

[10] B. Brooks. The treatment of traumatic arteriovenous fistula. *Southern Medical Journal*, 23:100–106, 1930.

[11] M. F. Brother, J. C. E. Kaufmann, A. J. Fox, and J. P. Deveikis. n-butyl 2-cyanoacrylate–substitute for ibca in interventional neuroradiology: histopathologic and polymerization time studies. *American Journal of Neuroradiology*, 10:777 – 786, 1989.

[12] Cambridge Polymer Group Inc. Determination of the kinetics of curing of cyanoacrylate-based adhesives with fourier transform infrared spectroscopy. *Application Notes*, #001, 2004.

[13] P. Chabrot, V. Vidal, and L. Boyer. *Embolization*. Springer-Verlag, 2014.

[14] M. Chanda. *Introduction to Polymer Science and Chemistry : A Problem-Solving Approach, Second Edition*. CRC Press, 2013.

[15] A. Chiriac, J. Baldof, N. Dobrin, and I. Poeata. Embolic materials for cerebral endovascular theraphy. *Romanian Neurosurgery*, 2:171–181, 2010.

[16] M. L. Cordero, F. Gallaire, and C. N. Baroud. Quantitative analysis of the dripping and jetting regimes in co-flowing capillary jets. *Physical of Fluids*, 23:094111, 2011.

[17] G. Costa, J. P. Cronin, D. C. Pepper, and C. Loonan. Termination and transfer by acids in the pyridine-initiated polymerization of butyl cyanoacrylate. *European Polymer Journal*, 19:939–945, 1983.

[18] P. Couvreur, B. Kante, M. Roland, P. Guiot, P. BAuduin, and P. Speiser. Polycyanoacrylate nanocapsules as potential lysosomotropic carriers: preparation, morphological and sorptive properties. *Journal of Pharmacy and Pharmacology*, 31:331–332, 1979.

[19] C. Cramer, P. Fischer, and E. Windhab. Drop formation in a co-flowing fluid. *Chemical Engineering Science*, 52:3045–3058, 2004.

[20] L. D. Cromwell and C. W. Kerber. Modification of cyanoacrylate for therapeutic embolization: preliminary experience. *American Journal of Roentgenology*, 132:799 – 801, 1979.

[21] T. K. Das. Prediction of jet breakup length in liquid-liquid systems using the rayleigh-tomotika analysis. *Atomization and Sprays*, 7:549–559, 1997.

[22] R. H. M. Dawbarn. The starvation operation for malignancy in the external carotid area. *The Journal of the American Medical Association*, 12:792–795, 1904.

[23] H. A. Desal, F. Toulgoat, S. Raoul, B. Guillon, R. Al Hammad Ibrahim, E. Auffray-Calvier, and A. DE Kersaint-Gilly. Brain arteriovenous malformations technical note of endovascular treatment with glubran. *Interventional Neuroradiology*, 11:125 – 130, 2005.

[24] J. E. Dion. Embolic agents: Now & future. *Journal of Vascular and Interventional Radiology*, 11:149–152, 2000.

[25] R. Djindjian, R. Houdart, J. Cophignon, M. Hurth, and J. Comoy. 1st trials of embolization by the femoral route with muscle fragments in a case of medullary angioma and a case of angioma supplied by the external carotid. *Revue Reurologique (Paris)*, 125:119–130, 1971.

[26] E. F. Donnelly, D. S. Johnston, D. C. Pepper, and D. J. Dunn. Ionic and zwitterionic polymerization of n-alkyl 2-cyanoacrylates. *Journal of Polymer Science: Polymer Letters Edition*, 15:399 – 405, 1977.

[27] J. L. Doppman, G. Di Chiro, and A. Ommaya. Obliteration of spinal-cord arteriovenous malformation by percutaneous embolisation. *The Lancet*, 291:477, 1968.

[28] S. J. Douglas, L. Illum, S. S. Davis, and J. Kreuter. Particle size and size distribution of poly(butyl-2-cyanoacrylate) nanoparticles. *Journal of Colloid and Interface Science*, 101:149–158, 1984.

[29] H. G. M. Edwards and J. S. Day. Fourier transform raman spectroscopic studies of the curing of cyanoacrylate glue. *Journal of Raman Spectroscopy*, 35:555–560, 2004.

[30] I. C. Eromosele and D. C. Pepper. Anionic polymerization of butyl cyanoacrylate by tetrabutylammonium salts, 1. initiation processes. *Micromolecular Chemistry and Physics*, 190:3085 – 3094, 1989.

[31] I. C. Eromosele and D. C. Pepper. Anionic polymerization of butyl cyanoacrylate by tetrabutylammonium salts, 2. propagation rate constants. *Micromolecular Chemistry and Physics*, 190:3095 – 3103, 1989.

[32] N. A. K. Fallouh, L. Roblot-Treupel, H. Fessi, J. Devissaguet, and F. Puisieux. Development of a new process for the manufacture of polyisobutylcyanoacrylate nanocapsules. *International Journal of Pharmaceutics*, 28:125 – 132, 1986.

[33] A. Gabelmann, J. Görich, and E. M. Merkle. Endovascular treatment of visceral artery aneurysms. *Journal of Endovascular Therapy*, 9:38 – 47, 2002.

[34] M. J. Gounis, B. B. Lieber, A. K. Wakhloo, R. Siekmann, and L. N. Hopkins. Effect of glacial acetic acid and ethiodized oil concentration on embolization with n-butyl 2-cyanoacrylate: an in vivo investigation. *American Journal of Neuroradiology*, 23: 938 – 944, 2002.

[35] P. Guillot, A. Colin, A. S. Utada, and A. Ajdari. Stability of a jet in confined pressure-driven biphasic flows at low reynolds numbers. *Physical Review Letters*, 99:104502, 2007.

[36] P. Guillot, A. Colin, and A. Ajdari. Stability of a jet in confined pressure-driven biphasic flows at low reynolds number in various geometries. *Physical Review E*, 78: 016307, 2008.

[37] P. Guillot, A. Ajdarib, J. Goyona, M. Joanicota, and A. Colin. Droplets and jets in microfluidic devices. *Comptes Rendus Chimie*, 12:247–257, 2009.

[38] A. Heifetz, L. R. Ritter, W. E. Olmstead, and V. A. Volpert. A numerical analysis of initiation of polymerization waves. *Mathematical and Computer Modelling*, 41:271 – 285, 2005.

[39] J. M. Idée and B. Guiu. Use of lipiodol as a drug-delivery system for transcatheter arterial chemoembolization of hepatocellular carcinoma: a review. *Critical Reviews in Oncology/Hematology*, 88:530 – 549, 2013.

[40] J. E. Jackson, A. O. Mansfield, and D. J. Allison. Treatment of high-flow vascular malformations by venous embolization aided by flow occlusion techniques. *Cardio Vascular and Interventional Radiology*, 19:323 – 328, 1996.

[41] R. Jahan, Y. Murayama, Y. P. Gobin, G. R. Duckwiler, H. V. Vinters, and F. Viñuela. Embolization of arteriovenous malformations with onyx: Clinicopathological experience in 23 patients. *Neurosurgery*, 48:984–997, 2001.

[42] T. P. Jiang, L. Z. Wang, X. Li, J. Song, X. P. Wu, T. Z. An, and S. Zhou. Experimental research of fuaile medical adhesive for portal vein embolization in white rabbit models. *Oncology Letters*, 9:2609–2616, 2015.

[43] D. S. Johnston and D. C. Pepper. Polymerisation via macrozwitterions, 3. ethyl and butyl cyanoacrylates polymerised by benzyldimethyl, triethyl and tribenzylamines. *Macromolecular Chemistry and Physics*, 182:421–435, 1981.

[44] D. Katti and N. Krishnamurti. Anionic polymerization of alkyl cyanoacrylates: In vitro model studies for in vivo applications. *Journal of Applied Polymer*, 74:336–344, 1999.

[45] N. Kawai, M. Sato, H. Minamiguchi, A. Ikoma, H. Sanda, K. Nakata, F. Tanaka, M. Nakai, and T. Sonomura. Basic study of a mixture of n-butyl cyanoacrylate, ethanol, and lipiodol as a new embolic material. *Journal of Vascular and Interventional Radiology*, 23:1516 – 1521, 2012.

[46] B. S. Kim, H. M. Do, and M. Razavi. N-butyl cyanoacrylate glue embolization of splenic artery aneurysms. *Journal of Vascular and Interventional Radiology*, 15:91 – 94, 2004.

[47] S. Kim, K. Evans, and A. Biswas. Production of bsa-poly(ethyl cyanoacrylate) nanoparticles as a coating material that improves wetting property. *Colloids and Surfaces B: Biointerfaces*, 107:68–75, 2013.

[48] Y. Kitamura, H. Mishima, and T. Takahashi. Stability of jets in liquid-liquid systems. *The Canadian Journal of Chemical Engineering*, 60:723–731, 1982.

[49] P. Klemarczyk. The isolation of a zwitterionic initiating species for ethyl cyanoacrylate (eca) polymerization and the identification of the reaction products between 1, 2, and 3 amines with eca. *Polymer*, 42:2837–2848, 2001.

[50] I. I. Kricheff, M. Madayag, and P. Braunstein. Transfemoral catheter embolization of cerebral and posterior fossa arteriovenous malformations. *Radiology*, 103:107–111, 1972.

[51] F. Leonard. The n-alkylalphacyanoacrylate tissue adhesives. *Annals of the New York Academy of Sciences*, 146:203–213, 1968.

[52] M. Leonardi, C. Barbara, L. Simonetti, R. Giardino, N. N. Aldini, M. Fini, L. Martini, L. Masetti, M. Joechler, and F. Roncaroli. Glubran 2: a new acrylic glue for neuroradiological endovascular use: experimental study on animals. *Interventional Neuroradiology*, 8:245 – 250, 2002.

[53] M. Leonardi, P. Cenni, L. Simonetti, A. Bozzao, A. Romano, M. Bonamini, L. M. Fantozzi, and G. Fini. Glubran 2: a new acrylic glue for neuroradiological endovascular use: a complementary histological study. *Interventional Neuroradiology*, 9:249 – 254, 2003.

[54] O. Levrier, C. Mekkaoui, P. H. Rolland, K. Murphy, P. Cabrol, G. Moulin, J. M. Bartoli, and C. Raybaud. Efficacy and low vascular toxicity of embolization with radical versus anionic polymerization of n-butyl-2-cyanoacrylate (NBCA). an experimental study in the swine. *Journal of Neuroradiology*, 30:95 – 102, 2003.

[55] Y. J. Li, D. Barthès-Biesel, and A.-V. Salsac. Polymerization kinetics of n-butyl cyanoacrylate glues used for vascular embolization. *Journal of the Mechanical Behavior of Biomedical Materials*, 12:307–317, 2017.

[56] Y. J. Li, D. Barthès-Biesel, and A.-V. Salsac. Polymerization kinetics of a mixture of Lipiodol and Glubran 2 cyanoacrylate glue upon contact with a proteinaceous solution. *Journal of the Mechanical Behavior of Biomedical Materials*, 2017.

[57] C. Limouzin, A. Caviggia, F. Ganachaud, and P. Hémery. Anionic polymerization of n-butyl cyanoacrylate in emulsion and miniemulsion. *Micromolecules*, 36:667 – 674, 2003.

[58] M. Lubarsky, C. E. Ray, and B. Funaki. Embolization agents-which one should be used when? part 1: Large-vessel embolization. *Seminars in Interventional Radiology*, 26:352–357, 2009.

[59] M. Lubarsky, C. E. Ray, and B. Funaki. Embolization agents-which one should be used when? part 2: Small-vessel embolization. *Seminars in Interventional Radiology*, 27:99–104, 2010.

[60] A. J. Luessenhop and W. T. Spence. Artificial embolization of cerebral arteries. report of use in a case of arteriovenous malformation. *The Journal of the American Medical Association*, 172:1153–1155, 1960.

[61] T. S. Matalon, C. A. Athanasoulis, M. N. Margolies, A. C. Waltman, R. A. Novelline, A. J. Greenfield, and S. E. Miller. Hemorrhage with pelvic fractures: efficacy of transcatheter embolization. *American Journal of Roentgenology*, 133:859–864, 1979.

[62] B. Meister and G. Scheele. Generalized solution of the tomotika stability analysis for a cylindrical jet. *AIChE Journal*, 13:682–688, 1967.

[63] B. Meister and G. Scheele. Prediction of jet length in immiscible liquid systems. *AIChE Journal*, 15:689–699, 1969.

[64] B. Meister and G. Scheele. Drop formation from cylindrical jets in immiscible liquid systems. *AIChE Journal*, 15:700–706, 1969.

[65] L. Montanaro, C. R. Arciola, E. Cenni, G. Ciapetti, F. Savioli, F. Filippini, and L. A. Barsanti. Cytotoxicity, blood compatibility and antimicrobial activity of two cyanoacrylate glues for surgical use. *Biomaterials*, 22:59 – 66, 2001.

[66] K. Murphy and F. Robertson, editors. *Interventional Neuroradiology*. Springer-Verlag, London, 2014.

[67] J. Nicolas and P. Couvreur. Synthesis of poly(alkyl cyanoacrylate)-based colloidal nanomedicines. *Wiley Interdisciplinary Reviews: Nanomedicine and Nanobiotechnology*, 1:111 – 127, 2009.

[68] K. Osuga, N. Maeda, H. Higashihara, S. Hori, T. Nakazawa, K. Tanaka, M. Nakamura, K. Kishimoto, Y. Ono, and N. Tomiyama. Current status of embolic agents for liver tumor embolization. *International Journal of Clinical Oncology*, 17:306–315, 2012.

[69] G. Pascual, S. Sotomayor, M. Rodríguez, B. Pérez-Këhler, A. Kühnhardt, M. Fernández-Gutiérrez, J. S. Román, and J. M.l Bellón. Cytotoxicity of cyanoacrylate-based tissue adhesives and short-term preclinical in vivo biocompatibility in abdominal hernia repair. *PLoS One*, 11:e0157920, 2016.

[70] D. C. Pepper. Kinetics and mechanisms of zwitterionic polymerizations of alkyl cyanoacrylates. *Polymer Journal*, 12:629–637, 1980.

[71] D. C. Pepper and B. Ryan. Kinetics of polymerization of alkyl cyanoacrylates by tertiary amines and phosphines. *Macromolecular Chemistry and Physics*, 184:395–410, 1983.

[72] J. Plateau. *Acad. Sci. Bruxelles Mém*, 23:5, 1849.

[73] J. Plateau. *Statique expérimentale et théorique des liquides soumis aux seules forces moléculaires*. Gauthier-Villars, Paris, 1873.

[74] J. S. Pollak and R. I. White. The use of cyanoacrylate adhesives in peripheral embolization. *Journal of Vascular and Interventional Radiology*, 12:907 – 913, 2001.

[75] L. Rayleigh. On the instability of jets. *Procedings of the Royal Society of Londan*, s1-10:4–13, 1878.

[76] L. Rayleigh. On the capillary phenomena of jets. *Procedings of the Royal Society of Londan*, 29:71–97, 1879.

[77] I. Repa, G. P. Moradian, L. P. Dehner, S. M. Tadavarthy, D. W. Hunter, W. R. Castañeda-Zúñiga, G. B. Wright, H. Katkov, P. Johnson, and B. Chrenka. Mortalities associated with use of a commercial suspension of polyvinyl alcohol. *Radiology*, 170:395–399, 1989.

[78] J. Rösch, C. T. Dotter, and M. J. Brown. Selective arterial embolization. a new method for control of acute gastrointestinal bleeding. *Radiology*, 102:303–306, 1972.

[79] J. Rösch, F. S. Keller, and J. A. Kaufman. The birth, early years, and future of interventional radiology. *Journal of Vascular and Interventional Radiology*, 14:841 – 853, 2003.

[80] R. J. Rosen and S. Contractor. The use of cyanoacrylate adhesives in the management of congenital vascular malformations. *Seminars in Interventional Radiology*, 21:59 – 66, 2004.

[81] L. C. Rubens and R. E. Skochdopole. Continuous measurement of polymerization rates over the entire conversion range with a recording dilatometer. *Journal of Applied Polymer Science*, 9:1487–1497, 1965.

[82] M. C. Sandulache. *Caractérisation in vitro de la technique endovasculaire d'embolisation par colle chirurgicale*. PhD thesis, Université de Technologie de Compiègne, 2011.

[83] M. C. Sandulache, P. Paullier, R. Bouzerar, T. Yzet, O. Balédent, and A. V. Salsac. Liquid injection in confined coflow: application to portal vein embolization by glue injection. *Physics of Fluids*, 24:081902, 2012.

[84] F. Savart. Mémoire sur la constitution des veines liquides lancées par des orifices circulaires en mince paroi. *Annales de Chimie et de Physique*, 53:337, 1833.

[85] L. Simonetti, L. Raffi, P. Cenni, A. Andreoli, F. Calbucci, and M. Leonardi. Presurgical embolization of intracranial extra-axial tumours using glubran 2(r): Our experience in 14 patients. *The Neuroradiology Journal*, 17:645–658, 2004.

[86] C. A. Spade and V. A. Volpert. On the steady-state approximation in thermal free radical frontal polymerization. *Chemical Engineering Science*, 55:641 – 654, 2000.

[87] S. M. Spiegel, F. Viñuela, J. M. Goldwasser, A. J. Fox, and D. M. Pelz. Adjusting the polymerization time of isobutyl-2 cyanoacrylate. *American Journal of Neuroradiology*, 7:109 – 112, 1986.

[88] K. J. Stebe and D. Barthès-Biesel. Marangoni effects of adsorption-desorption controlled surfactants on the leading end of an infinitely long bubble in a capillary. *Journal of Fluid Mechanics*, 286:25 – 48, 1995.

[89] F. Stolesslein, G. Ditscherlein, and P. A. Romaniuk. Experimental studies on new liquid embolization mixtures (histoacryl-lipiodol, histoacryl-panthopaque). *Cardiovascular Interventional Radiology*, 5:264 – 267, 1982.

[90] H. A. Stone. Dynamics of drop formation and breakup in viscous fluids. *Annual Review of Fluid Mechanics*, 26:65–102, 1994.

[91] D. C. Suh, H. B. Shi, S. S. Park, M. S. Lee, and H. Y. Choi. Change of spontaneous reaction of glue and lipiodol mixture during embolization after the addition of tungsten powder: in vitro study. *American Journal of Neuroradiology*, 21:1277–1279, 2000.

[92] I. Szanka, A. Szanka, and J. P. Kennedy. Rubbery wound closure adhesives. ii. initiators for and initiation of 2-octyl cyanoacrylate polymerization. *Polymer Chemistry*, 53: 1652–1659, 2015.

[93] C. Takasawa, K. Seiji, K. Matsunaga, T. Matsuhashi, M. Ohta, S. Shida, K. Takase, and S. Takahashi. Properties of n-butyl cyanoacrylate-iodized oil mixtures for arterial embolization: in vitro and in vivo experiments. *Journal of Vascular and Interventional Radiology*, 23:1215 – 1221, 2012.

[94] S. K. Tomlinson, O. R. Ghita, R. M. Hooper, and K. E. Evans. The use of near-infrared spectroscopy for the cure monitoring of an ethyl cyanoacrylate adhesive. *Vibrational Spectroscopy*, 40:133–141, 2006.

[95] S. Tomotika. On the stability of a cylindrical thread of a viscous liquid surrounded by another viscous liquid. *Procedings of the Royal Society A, Methematical, Physical and Engineering Science*, 150:322–337, 1935.

[96] D. M. Toriumi, W. F. Raslan, M. Friedman, and M. E. Tardy. Histotoxicity of cyanoacrylate tissue adhesives: a comparative study. *Otolaryngology Head and Neck Surgery*, 116:546 – 550, 1990.

[97] E. Tyler. Instability of liquid jets. *Philosophical Magazine*, 16:504–518, 1933.

[98] A. Utada, A. Fernandez-Nieves, J. Gordillo, and D. Weitz. Absolute instability of a liquid jet in a co-flowing stream. *Physical Review Letters*, 100:014502, 2008.

[99] A. S. Utada, A. Fernandez-Nieves, H. A. Stone, and D. A. Weitz. Dripping to jetting transitions in coflowing liquid streams. *Physical Review Letters*, 99:094502, 2007.

[100] S. Vaidya, K. R. Tozer, and J. Chen. An overview of embolic agents. *Seminars in Interventional Radiology*, 25:204 – 215, 2008.

[101] C. Vauthier, C. Dubernet, E. Fattal, H. Pinto-Alphandary, and P. Couvreur. Poly(alkylcyanoacrylates) as biodegradable materials for biomedical applications. *Advanced Drug Delivery Reviews*, 55:519–548, 2003.

[102] G. L. Velat, J. F. Reavey-Cantwell, C. Sistrom, D. Smullen, G. L. Fautheree, J. Whiting, S. B. Lewis, R. A. Mericle, C. S. Firment, and B. L. Hoh. Comparison of n-butyl cyanoacrylate and onyx for the embolization of intracranial arteriovenous malformations: analysis of fluoroscopy and procedure times. *Neurosurgery*, 63:ONS73 – 78, 2008.

[103] S. P. Wargacki, L. A. Lewis, and M. D. Dadmun. Understanding the chemistry of the development of latent fingerprints by superglue fuming. *Journal of Forensic Science*, 52:1057–1062, 2007.

[104] D. M. Widlus, G. K. Lammert, A. Brant, T. Tsue, M. A. Samphillipo, C. Magee, F. L. Starr, J. H. Anderson, and R. I. White. In vivo evaluation of iophendylate-cyanoacrylate mixtures. *Radiology*, 185:269–273, 1992.